Monthly Scientific-Technical and Production Journal

The Paton WELDING JOURNAL

March 2001 # 3

English translation of the monthly «Avtomaticheskaya Svarka» journal published in Russian since 1948

The National Academy of Sciences of Ukraine
The E.O. Paton Electric Welding Institute of the NAS of Ukraine
International Association «Welding»

«The Paton Welding Journal»
is published monthly by the
International Association «Welding»

Promotion group:
V.N.Lipodaev, V.I.Lokteva
A.T.Zelnichenko (Exec. director)
Translators:
S.A.Fomina, I.N.Kutianova,
T.K.Vasilenko

Editorial and advertising offices
are located at PWI,
International Association «Welding»,
11, Bozhenko str., 03680,
Kyiv, Ukraine
Tel.: (38044) 227 67 57
Fax: (38044) 268 04 86
E-mail: tomik@mac.relc.com
E-mail: office@paton.kiev.ua

State Registration Certificate
KV 4790 of 09.01.2001

Subscriptions:
$460, 12 issues, postage included

«The Paton Welding Journal» Website:
http://www.nas.gov.ua/pwj

CONTENTS

MODEL OF EVAPORATION OF METAL IN ARC, LASER AND LASER-ARC WELDING

I.V. KRIVTSUN
The E.O. Paton Electric Welding Institute, NASU, Kyiv, Ukraine

ABSTRACT

The model of multicomponent plasma formed near the metal surface in gas-shielded arc, laser and laser-arc welding is suggested. The model is based on the system of balance relationships for flows of heavy particles, their momentum and energy in the Knudsen layer near the surface of metal evaporating into the plasma of external gas. Expressions derived for density of electron and ion currents flowing to the metal surface and for distribution of potential in the multicomponent near-surface plasma (arc, laser or combined) are given.

Key words: *laser welding, arc welding, laser-arc (combined) welding, near-surface plasma, Knudsen layer, metal, surface, evaporation, investigations*

Main factors which determine metal penetration in arc, laser or laser-arc (combined) welding are the thermal and dynamic effects of a heat source used on the weld pool surface. Therefore, the knowledge of principles of interaction of the electric arc and laser beam with metal is a necessary condition for substantiated prediction and control of the respective welding processes.

High-power density heat sources (electric arc, laser beam or their combination) affecting the metal surface may result in its heating to temperatures comparable with boiling temperatures and higher. Such heating causes a marked evaporation of metal into the environment, as a result of which the latter becomes multicomponent, i.e. containing particles of the metal vapours, in addition to particles of the external gas. As long as the partial pressure of the vapour is lower than that of the environment, metal atoms diffuse into it (diffusion mode of evaporation) and pressure on the metal surface is almost equal to the external pressure. With further increase in temperature of the metal surface the pressure of the vapour becomes higher than the external one, which induces scatter of the vapour (convective mode of evaporation) accompanied by formation of the reactive force affecting the metal surface. In this case the pressure on the weld pool, which determines dynamics of motion of its surface and, eventually, metal penetration, can be much in excess of the pressure of the external medium [1], and the energy of sublimation of atoms removed with the vapour flow from the metal surface contributes substantially to the energy balance of this surface [2].

An important factor which affects metal evaporation processes in the case of the welding methods under consideration is that the medium which is external with respect to the metal is ionized to a considerable extent, i.e. contains both neutral particles (gas atoms and molecules, metal atoms) and charged particles (electrons and ions of different kinds and charges). Physical phenomena occurring in such a multicomponent plasma (energy release due to flow of the electric current; absorption and refraction of the laser beam; heat, mass and electric transfer between plasma and metal) determine in many respects characteristics of the thermal and dynamic effects of the heat sources under consideration on the weld pool surface. On this basis, the purpose of the work described in this article was a detailed theoretical investigation of processes occurring in the multicomponent near-surface plasma in gas-shielded arc, laser and laser-arc welding.

Model of the near-surface plasma. To describe processes occurring in the arc, laser and combined plasma adjoining the metal surface (Figure 1), we use a unified approach [3 – 5] within which the near-surface plasma layer is conditionally divided into three zones.

The first zone which directly adjoins the surface is the space charge layer. It is in this layer that the condition of quasi-neutrality of the plasma is disturbed and the main drop of potential between plasma and metal is formed. This layer is assumed to be collisionless, as at a pressure close to the atmospheric one and values of the electron temperature, $T_e \cong 1 - 2$ eV, characteristic of the welding methods under consideration, thickness of this layer $\bar{x}$ commensurable with the Debye radius $r_D \leq 10^{-5}$ cm* is much less than the characteristic lengths of the free path of the plasma particles, $l \cong 10^{-2} - 10^{-4}$ cm.

The second zone is the ionization region of the quasi-neutral plasma (or presheath), where an intensive generation of the charged particles occurs due to ionization of the gas atoms desorbed from the surface and the evaporating metal atoms by the plasma electrons. Ions formed here are accelerated to the metal surface and recombine near it under the effect of the electric field induced by more mobile electrons. Therefore, conditions of local ionization equilibrium are disturbed and a marked change in the plasma potential

*Here and below all estimates of orders of magnitudes apply to the atmospheric-pressure argon plasma.

occurs within the ionization region of the plasma, the change in the plasma potential (Figure 1) being commensurable with the potential drop in the space charge layer.

Boundary of the Knudsen layer L_K thick is at a distance of several lengths of the free path of heavy particles from the metal surface. Outside this layer there lies the third zone, i.e. the hydrodynamic region of the plasma, where local thermodynamic equilibrium is established both by translational and internal degrees of freedom of the particles. As thickness of the Knudsen layer $L_K \leq 10^{-2}$ cm is much less than the characteristic transverse sizes of the zone of contact of the plasma with the metal surface and radius of curvature of this surface, $a \cong 10^{-1}$ cm, the Knudsen layer, and especially the presheath and the space charge layer, can further on be considered flat and quasi-unidimensional. The latter implies that space changes in characteristics of the plasma along the layer interface can be ignored, as compared with their changes across each layer.

According to this approach, the near-surface plasma consists actually of two main regions — non-equilibrium ($x < L_K$) and hydrodynamic ($x > L_K$), for which the first region is a discontinuity surface. It should be noted that, because of a small value of L_K, as compared with characteristic sizes of the hydrodynamic region of the plasma, conditional overlap of the Knudsen layer on the metal surface is a sufficiently good approximation for description of the hydrodynamic processes. Parameters of the plasma at this boundary (concentration and temperature of particles, velocity and pressure of plasma), which play the role of boundary conditions for determination of respective values in the hydrodynamic region, can be calculated providing that the distribution functions of the plasma particles by velocities are known. In a general case, to determine them it is necessary to solve a complicated system of kinetic equations with respect to the distribution functions of particles of all kinds by allowing for interaction of the charged particles with the electric field in the presheath and in the space charge layer, as well as for inelastic processes in the ionization region (ionization, recombination, re-charging, etc.). No precise solution is available so far for this problem. Therefore, we suggest using an approximate approach based on making some assumptions with respect to the kind of the distribution functions at boundaries of the layers and deriving balance relationships for the flows of particles, their momentum and energy. A similar approach was used earlier for description of the Knudsen layer formed near the surface of metal evaporating under the effect of a high-power laser radiation into vacuum [6] and gas with back pressure [1], as well as evaporation of metal into plasma at the cathode spot of the vacuum electric arc [7, 8].

Prior to realization of the approach suggested, consider in more detail the processes which occur in the Knudsen layer, formed near the surface of the metal

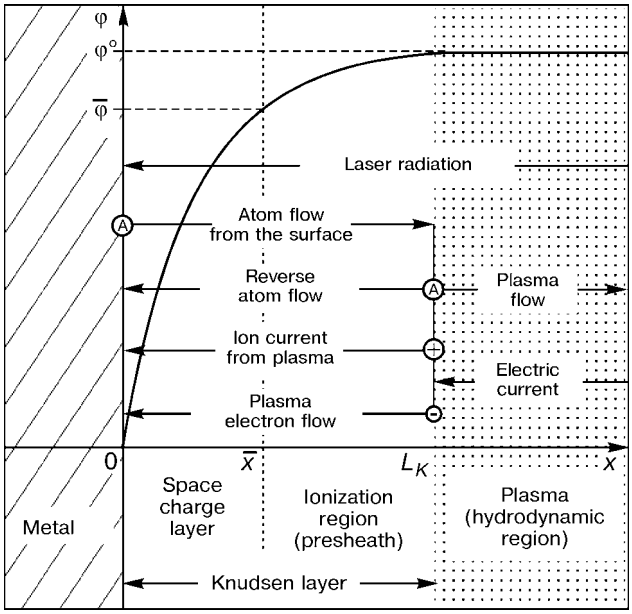

Figure 1. Structure of the near-surface plasma, flows of particles and distribution of potential in the Knudsen layer: φ^0, $\bar{\varphi}$ are the values of potential at the external boundary of the Knudsen layer and the space charge layer, respectively; A — atoms; + — ions; - — electrons

evaporating into the plasma of the atmospheric pressure external gas. Assume that there is a flow of the electric current between the plasma and this metal (in arc or combined welding). Besides, further on we will consider only the case where metal serves as the arc anode. As far as laser welding is concerned, in this case the electric current between the plasma and surface will be assumed to be equal to zero.

Current transfer and distribution of potential in the Knudsen layer. Assume that plasma at the external boundary of the Knudsen layer is characterized by the following parameters: n_e^0 — concentration of electrons, $n_{\alpha 0}^0$ — concentration of atoms, $n_{\alpha Z}^0$ — concentration of ions ($\alpha = g$ — for external gas particles, $\alpha = m$ — for metal particles, Z — charge number), Ze — ion charge, e — elementary charge, T_e — electron temperature, T — temperature of heavy particles, which is assumed to be the same for all kinds of atoms and ions but other than T_e (two-temperature plasma model), m_e — electron mass, M_α — mass of heavy particles (atoms and ions) of gas and metal, j — component of density of the electric current in the near-surface plasma normal to the metal surface. As noted above, under an external gas pressure close to the atmospheric one, the Knudsen layer can be considered thin and quasi-unidimensional. Therefore, values of n_e^0, $n_{\alpha 0}^0$, $n_{\alpha Z}^0$, T_e, T and j can be regarded as local parameters corresponding to a certain point of the metal surface characterized by a local value of temperature of its surface, T_{ms}.

Assume that the electric current transfer in the Knudsen layer is realized only by electrons and ions coming from the plasma (it is assumed that all ions which come to the metal surface recombine there and come back to the plasma in the form of atoms and

that there are no flows of electrons reflected from the surface and emitted by metal). Then the total density of the electric current, j, flowing from the plasma to the surface (in the case of a laser plasma $j = 0$) can be represented as follows:

$$j = j_e - j_i, \tag{1}$$

where j_e is the density of the electron current onto the metal surface;

$$j_i = \sum_{\alpha;\ Z \geq 1} j_{\alpha Z}$$

is the total density of the ion current (for ions of all kinds and charges), the direction of movement of electrons being taken as the direction of the electric current in the plasma.

Numerical estimates show that for conditions under consideration the characteristic lengths of the free path of electrons, $l_{ea} \cong 10^{-2}$ cm, are commensurable with L_K. Therefore, the electron component of the plasma within the Knudsen layer can be considered collisionless with a sufficient degree of accuracy, and the electron temperature can be considered constant through thickness of this layer. In addition, as potential of the plasma is as a rule higher than potential of the metal surface, which is true up to $j \cong$ $\cong 10^5$ A/cm^2, movement of electrons is inhibited by the electric current and that of ions is accelerated towards the surface. In this case the distribution of concentration of electrons in the Knudsen layer can be regarded as the Boltzmann distribution:

$$n_e(x) = n_e^0 \exp\left\{-\frac{e[\varphi^0 - \varphi(x)]}{k_B T_e}\right\}, \tag{2}$$

where φ^0 is the potential of the plasma with regard to the metal surface ($\varphi^0 > 0$); $\varphi(x)$ is the distribution of potential in this layer (see Figure 1); and k_B is the Boltzmann constant. Then the current density of electrons which reach the surface can be determined using the following relationship:

$$j_e = \frac{1}{4} e n_e^0 v_{T_e} \exp\left(-\frac{e\varphi^0}{k_B T_e}\right), \tag{3}$$

where $v_{T_e} = \sqrt{\dfrac{8k_B T_e}{\pi m_e}}$ is the thermal velocity of electrons at the external boundary of the layer.

To calculate values of the ions currents flowing onto the metal surface, it is necessary to consider processes taking place in the ionization region, where the intensive generation of ions and their acceleration to the surface occur. For this we use an approach suggested in [9, 10]. It is based on an assumption that the length of the free path of ions relative to the Coulomb collisions between each other, l_{ii}, is much shorter than the corresponding length for elastic collisions of ions with atoms, l_{ia}, and the length of the free path of atoms with respect to the ionization events, l_{ion}. Characteristic values of the above parameters for conditions under consideration are as follows: $l_{ii} \cong 10^{-5}$ cm, $l_{ia} \cong 10^{-2}$ cm and $l_{ion} \cong 10^{-2}$ cm. In this case it can be considered that ions in the presheath of the plasma are intensively transformed into Maxwellian ones and acquire a common velocity of the directed movement $V_i(x)$, which can be determined by using the equation of motion of the «ion fluid» as a unit:

$$\sum_{\alpha;\ Z \geq 1} M_\alpha n_{\alpha Z} V_i \frac{dV_i}{dx} + \frac{dp_i}{dx} + \sum_{\alpha;\ Z \geq 1} Z e n_{\alpha Z} \frac{d\varphi}{dx} = 0, \tag{4}$$

where $p_i(x) = \sum_{\alpha;\ Z \geq 1} n_{\alpha Z}(x) k_B T$ is the total ion pressure (temperature of heavy components is assumed to be constant through thickness of the presheath). As it is supposed that all ion components are accelerated as a unit, allowing for quasi-neutrality of the plasma in the ionization region and using dependence $n_e(x)$ determined from formula (2) in the explicit form, solution for this equation can be written as follows:

$$V_i^2(x) = \frac{\sum_{\alpha;\ Z \geq 1} 2\left(Z + \dfrac{T}{T_e}\right) e n_{\alpha Z}^0}{\sum_{\alpha;\ Z \geq 1} M_\alpha n_{\alpha Z}^0} [\varphi^0 - \varphi(x)], \tag{5}$$

where the initial velocity of ions at the external boundary of the presheath is assumed to be negligibly small.

To find concentrations of the charged particles at the boundary of the space charge layer, we use the equation of continuity for each ion component. Multiplying these equations by a corresponding value of Z, and summing them up for all kinds and charges of ions allowing for the condition of quasi-neutrality of the plasma in the ionization regions yield

$$\frac{d(n_e V_i)}{dx} = \sum_{\alpha;\ Z \geq 1} Z \dot{n}_{\alpha Z} \neq 0, \tag{6}$$

where $\dot{n}_{\alpha Z}$ is the rate of changes in the concentrations of the corresponding ions related to the inelastic processes. Concentration of the charged particles at the boundary of the presheath and the space charge layer can be solved directly without solving the above equation. By selecting such a value of $\bar{x}^*$ for the above boundary, at which the condition of quasi-neutrality of the plasma is disturbed, i.e. $\left.\dfrac{dn_e}{dx}\right|_{x=\bar{x}} = \infty$ [11], and using (6), we find that

*Here and below the bar over a letter means that the value refers to the external boundary of the space charge layer.

$$\bar{n}_e = n_e^0 \exp\left(-\frac{1}{2}\right), \quad \bar{n}_{\alpha Z} = n_{\alpha Z}^0 \exp\left(-\frac{1}{2}\right), \quad \alpha = m, g;\ Z \geq 1, \tag{7}$$

and, according to (2),

$$\bar{\varphi} = \varphi^0 - \frac{1}{2}\frac{k_B T_e}{e}. \tag{8}$$

By substituting (8) to (5) we obtain an expression which determines the velocity of ions at the boundary of the space charge layer

$$\bar{V}_i = \sqrt{k_B T_e \frac{\sum\limits_{\alpha;\ Z\geq 1}\left(Z + \frac{T}{T_e}\right)n_{\alpha Z}^0}{\sum\limits_{\alpha;\ Z\geq 1} M_\alpha n_{\alpha Z}^0}}. \tag{9}$$

Using (7), we can write densities of the ion currents at the metal surface in the following form:

$$j_{\alpha Z} = Z e n_{\alpha Z}^0 \exp\left(-\frac{1}{2}\right)\bar{V}_i, \quad \alpha = m, g;\ Z \geq 1. \tag{10}$$

By determining the electron and ion components of the electric current flowing from the plasma to the surface, we can find potential of the plasma relative to metal. Substituting (3) and (10) to (1) yields

$$\varphi^0 = \frac{k_B T_e}{e} \ln\left(\frac{e n_e^0 v_{T_e}}{4\left[j + \sum\limits_{\alpha;\ Z\geq 1} Z e n_{\alpha Z}^0 \exp\left(-\frac{1}{2}\right)\bar{V}_i\right]}\right). \tag{11}$$

It should be emphasized that the velocity of ions at the presheath boundary given by expression (9) should meet criterion of formation of the space charge layer (Bohm criterion [12]). In the case of the multicomponent plasma under consideration, the said criterion is determined by an approach described in [11]. Assume that all ions are «cold» and have common velocity $\bar{V}_i$ in a direction to the surface. Considering that electrons are distributed following the Boltzmann criterion and that there are no flows of the charged particles from the metal surface, for a collisionless layer of the space charge the Poisson's equation can be written as follows:

$$\frac{d^2\varphi}{dx^2} = 4\pi e\left\{\bar{n}_e \exp\left[-\frac{e(\bar{\varphi} - \varphi)}{k_B T_e}\right]\right\} - 4\pi e\left\{\sum_{\alpha;\ Z\geq 1} \frac{Z\bar{n}_{\alpha Z}}{\sqrt{1 + \frac{2Ze(\bar{\varphi} - \varphi)}{M_\alpha \bar{V}_i^2}}}\right\}. \tag{12}$$

Condition of existence of the solution for this equation at $x \leq \bar{x}$ can be found by multiplying it by $d\varphi/dx$, integrating between $\bar{x}$ and x and assuming that (see [11])

$$\frac{d\varphi}{dx}\Big|_{x=\bar{x}} \approx 0.$$

Expanding the solution obtained into a series near point $x = \bar{x}$ ($\varphi \approx \bar{\varphi}$) and using condition of non-quasineutrality of the plasma at the boundary of the layers yield generalization of the Bohm criterion for a case of the non-magnetized plasma containing ions of differing masses and charges:

$$\bar{V}_i \geq \sqrt{k_B T_e \sum_{\alpha;\ Z\geq 1} \frac{Z^2 \bar{n}_{\alpha Z}}{\bar{n}_e M_\alpha}}, \tag{13}$$

which is in agreement with (9).

Finally, solution of the Poisson's equation (12) for the space charge layer allows the intensity of the electric field at the metal surface to be found:

$$E_s = -\frac{d\varphi}{dx}\Big|_{x=0}.$$

This is necessary for determination of the emission current and estimation of its contribution to the current transfer between the plasma and metal. By assuming in the first integral of this equation that $x = 0$ ($\varphi = 0$), we can show that for conditions under consideration $E_s \leq 10^6$ V/cm and that characteristic values of the thermionic emission current density, e.g. for iron, at $T_{ms} \cong 3000$ K do not exceed 10 A/cm^2 (for comparison, $j_i \cong 10^3$ A/cm^2). Therefore, neglecting the emission current in writing expression (1) is a sufficiently good approximation.

Metal evaporation into plasma with back pressure. Consider metal evaporation into the plasma of a surrounding gas having pressure p^0. Upon entering the plasma, some of the evaporated atoms are ionized. As a result, under a pressure of the ionized vapour lower than p^0 the near-surface plasma contains atoms and ions of the external gas (further on the gas is assumed to be atomic), in addition to electrons, and atoms and ions of metal, i.e. it is two-component. As the pressure of the vapour increases to a value in excess of p^0, it starts pressing out the external gas plasma to form a flow of the ionized metal vapour (one-component plasma) from the metal surface.

In both cases, to find characteristics of the plasma at the external boundary of the Knudsen layer, we will use a unified approach similar to that described in [1], allowing for the fact that the external medium with respect to the metal is ionized [7, 8] and can be one- or two-component. The point of the approach suggested is as follows. In transition over the Knudsen layer the flows of heavy particles (atoms and ions), flows of their momentum and the total energy flow for a translational motion of all heavy particles should persist but separately for gas and metal components of the plasma (it is assumed that the external gas is inert and does not enter into chemical reactions with metal atoms). As the heavy components of the plasma in a hydrodynamic region may have different velocities (e.g. in a diffusion mode of evaporation) but are

assumed to have the same temperature, the balance relationships for the flow of momentum are written separately for each of the components and those for the total energy flow are written as a sum. In addition, to write these relationships it is necessary to account for the corresponding contributions of ions from the electric field in the bulk of the Knudsen layer into the flows of momentum and energy. All of the balance relationships obtained should be regarded as locally unidimensional, similar to conventional gas-dynamic discontinuities [13].

Following [1], set an explicit form of the functions of distribution of heavy particles in velocities at the Knudsen layer boundaries. Considering that at the external boundary of the layer there is an equilibrium in the translational degrees of freedom of heavy particles, the corresponding distribution functions at $x = L_K$ can be set in the form of the locally Maxwellian distributions:

$$f_{mZ}(\vec{v}) = n^0_{mZ}\left(\frac{M_m}{2\pi k_B T}\right)^{3/2} \times \exp\left\{-\frac{M_m}{2k_B T}[(v_x - u)^2 + v_\parallel^2]\right\}, \quad Z \geq 0; \tag{14}$$

$$f_{gZ}(\vec{v}) = n^0_{gZ}\left(\frac{M_g}{2\pi k_B T}\right)^{3/2} \times \exp\left\{-\frac{M_g}{2k_B T}[v_x^2 + v_\parallel^2]\right\}, \quad Z \geq 0, \tag{15}$$

where u is the mean velocity of metal particles ($u \geq 0$) and $v_\parallel^2 = v_y^2 + v_z^2$. The allowance is made in writing (15) that the mean velocity of the heavy particles of gas is equal to zero, i.e. the flows of gas atoms and ions to the metal surface are compensated for by the flow of gas atoms emitted from this surface, as it is suggested that the gas particles do not penetrate deep into the metal and are not accumulated at its surface.

As the second boundary for deriving the balance relationships, instead of the metal surface we can select the external boundary of the space charge layer, which is thin ($\bar{x} << L_K$) and collisionless under the conditions considered. This selection is based on the fact that at this boundary the concentrations and velocities of ions have been already determined and the atom distribution functions can be considered constant within the space charge layer. Then, the following can be assumed for the metal atoms at $x = \bar{x}$ [1]:

$$f_{m0}(\vec{v}) = \begin{cases} n_{ms}\left(\frac{M_m}{2\pi k_B T_{ms}}\right)^{3/2} \exp\left\{-\frac{M_m}{2k_B T_{ms}}[v_x^2 + v_\parallel^2]\right\}, & v_x > 0, \\ \beta_{m0} n^0_{m0}\left(\frac{M_m}{2\pi k_B T}\right)^{3/2} \exp\left\{-\frac{M_m}{2k_B T}[(v_x - u)^2 + v_\parallel^2]\right\}, & v_x < 0. \end{cases} \tag{16}$$

Here β_{m0} is the proportionality coefficient which determines which part of the evaporated atoms actually comes back to the surface; n_{ms} is the concentration of atoms of a saturated vapour near the metal surface [6], corresponding to a given local value of temperature of this surface, T_{ms},

$$n_{ms} = \left(\frac{2\pi M_m \nu_0^{*2}}{k_B T_{ms}}\right)^{3/2} \exp\left(-\frac{\lambda_v}{k_B T_{ms}} - 1\right), \tag{17}$$

where ν_0^* is the effective Debye frequency of oscillations of atoms in metal and λ_v is the electronic work function of the melt. As to the part of the distribution function which describes behaviour of the metal atoms coming back to the surface ($v_x < 0$), according to [1] it is assumed to be proportional to the distribution function of atoms at an external boundary of the Knudsen layer (14).

Allowing for the above assumption that all metal ions coming to the surface recombine near it, are absorbed by the surface and emitted only in the form of atoms, it can be written for the metal ions at $x = \bar{x}$ that

$$f_{mZ}(\vec{v}) = \begin{cases} 0, & v_x > 0; \\ \beta_{mi} n^0_{mZ}\left(\frac{M_m}{2\pi k_B T}\right)^{3/2} \exp\left\{-\frac{M_m}{2k_B T}[(v_x - u_{mi})^2 + v_\parallel^2]\right\}, & v_x < 0, \ Z \geq 1. \end{cases} \tag{18}$$

Here the β_{mi} coefficient allows for variations in the concentration of metal ions at the boundary of the space charge layer, as compared with their concentration at the external boundary of the Knudsen layer, while addition of the $u_{mi} \neq u$ ($u_{mi} < 0$) parameter makes it possible to account for the velocity of ions coming back to the surface, which they acquire in the presheath of the plasma.

By an analogy with (16) and (18), the following can be written for heavy gas particles at $x = \bar{x}$

$$f_{g0}(\vec{v}) = \begin{cases} n_{gs}\left(\frac{M_g}{2\pi k_B T_{ms}}\right)^{3/2} \exp\left\{-\frac{M_g}{2k_B T_{ms}}[v_x^2 + v_\parallel^2]\right\}, & v_x > 0, \\ \beta_{g0} n^0_{g0}\left(\frac{M_g}{2\pi k_B T}\right)^{3/2} \exp\left\{-\frac{M_g}{2k_B T}[v_x^2 + v_\parallel^2]\right\}, & v_x < 0 \end{cases} \tag{19}$$

and

$$f_{gZ}(\vec{v}) = \begin{cases} 0, & v_x > 0; \\ \beta_{gi} n^0_{gZ}\left(\frac{M_g}{2\pi k_B T}\right)^{3/2} \exp\left\{-\frac{M_g}{2k_B T}[(v_x - u_{gi})^2 + v_\parallel^2]\right\}, & v_x < 0, \ Z \geq 1, \end{cases} \tag{20}$$

where parameters of the distribution functions for the heavy gas particles, β_{g0}, β_{gi} and u_{gi}, have the same implication as for the metal particles.

Parameters of the distribution functions for ions, $\beta_{\alpha i}$ and $u_{\alpha i}$ ($\alpha = m, g$), can be determined as follows. Using (18) and (20), calculate the concentration of ions of all kinds and their velocities, which are assumed to be identical, at the external boundary of the space charge layer:

$$\bar{n}_{\alpha Z} = \int f_{\alpha Z}(\vec{v})\mathrm{d}\vec{v}, \quad \bar{V}_i = \frac{1}{\bar{n}_{\alpha Z}} \int v_x f_{\alpha Z}(\vec{v})\mathrm{d}\vec{v}, \tag{21}$$

$$\alpha = m, g; \quad Z \geq 1.$$

And set the results obtained equal to expressions (7) and (9), respectively. This will result in the following:

$$\beta_{\alpha i} = \frac{2\exp\left(-\frac{1}{2}\right)}{1 - \Phi(\gamma_{\alpha i})}, \quad w_{\alpha i} \equiv \overline{V}_i \left(\frac{2\pi M_\alpha}{k_B T}\right)^{1/2} = \tag{22}$$

$$= \frac{2\left\{\exp(-\gamma_{\alpha i}^2) - \gamma_{\alpha i}\sqrt{\pi}[1 - \Phi(\gamma_{\alpha i})]\right\}}{1 - \Phi(\gamma_{\alpha i})}, \ \alpha = m, g,$$

here

$$\gamma_{\alpha i} = -\left(\frac{M_\alpha u_{\alpha i}^2}{2k_B T}\right), \quad \alpha = m, g; \tag{23}$$

$w_{\alpha i}$ is the dimensionless velocity of ions coming back to the metal surface and $\Phi(x) = 2/\sqrt{\pi}\int_0^x \exp \times (-\xi^2)d\xi$ is the probability integral. For comparison, it should be noted that in [7, 8] the velocity of ions calculated at the external boundary of the Knudsen layer was set equal to u_{mi}, which generally speaking is not valid for the half-Maxwellian distribution functions of the type of (18).

By setting the explicit kind of the distribution functions for heavy particles at the ionization region boundaries, it is not difficult to obtain the desired balance relationships by equating results of calculations of the corresponding flows at $x = L_K$ and $x = \overline{x}$. Besides, the flows of momentum and energy at $x = \overline{x}$ should be calculated with allowance for the inflow of momentum and energy of ions from the electric field in the bulk of this region. Thus, allowing for (22) and (23) and adding designation of the dimensionless velocity of vapour at the Knudsen layer boundary

$$\gamma_m = \left(\frac{M_m u^2}{2k_B T}\right)^{1/2} \tag{24}$$

(here u is the velocity of the metal vapour at the external boundary of the Knudsen layer), the balance relationships to be determined can be written as follows:

for the flows of particles:

$$n_{ms}T_{ms}^{1/2} = n_{m0}^0[2\gamma_m\sqrt{\pi} + \beta_{m0}\{\exp(-\gamma_m^2) - \gamma_m\sqrt{\pi}[1 - \Phi(\gamma_m)]\}]\,T^{1/2} +$$

$$+ \sum_{Z \geq 1} n_{mZ}^0\left[2\gamma_m\sqrt{\pi} + \exp\left(-\frac{1}{2}\right)w_{mi}\right]T^{1/2}, \tag{25}$$

$$n_{gs}T_{ms}^{1/2} = \left(n_{g0}^0\beta_{g0} + \sum_{Z \geq 1} n_{gZ}^0 \exp\left(-\frac{1}{2}\right)w_{gi}\right)T^{1/2}; \tag{26}$$

for the flows of momentum:

$$n_{ms}T_{ms} = n_{m0}^0\left[2(1 + 2\gamma_m^2) + \beta_{m0}\left\{\frac{2\gamma_m}{\sqrt{\pi}}\exp(-\gamma_m^2) - (1 + 2\gamma_m^2)[1 - \Phi(\gamma_m)]\right\}\right]T + \tag{27}$$

$$+ \sum_{Z \geq 1} n_{mZ}^0 2\left[(1 + 2\gamma_m^2) - \exp\left(-\frac{1}{2}\right)\left(1 - \frac{w_{mi}^2}{2\pi} - \frac{\gamma_{mi}w_{mi}}{\sqrt{\pi}}\right)\right]T,$$

$$n_{gs}T_{ms} = \left(n_{g0}^0(2 - \beta_{g0}) + \sum_{Z \geq 1} n_{gZ}^0 2\left[1 - \exp\left(-\frac{1}{2}\right)\left(1 - \frac{w_{gi}^2}{2\pi} - \frac{\gamma_{gi}w_{gi}}{\sqrt{\pi}}\right)\right]\right)T; \tag{28}$$

for flows of energy:

$$\left(\frac{n_{ms}}{\sqrt{M_m}} + \frac{n_{gs}}{\sqrt{M_g}}\right)T_{ms}^{3/2} = \frac{n_{m0}^0}{\sqrt{M_m}} \times$$

$$\times\left[\gamma_m\left(\frac{5}{2} + \gamma_m^2\right)\sqrt{\pi} + \beta_{m0}\left\{\left(1 + \frac{\gamma_m^2}{2}\right)\exp(-\gamma_m^2) - \frac{\gamma_m}{2}\left(\frac{5}{2} + \gamma_m^2\right)\sqrt{\pi}\,[1 - \Phi(\gamma_m)]\right\}\right]T^{3/2} + \tag{29}$$

$$+ \sum_{Z \geq 1} \frac{n_{mZ}^0}{\sqrt{M_m}}\left[\gamma_m\left(\frac{5}{2} + \gamma_m^2\right)\sqrt{\pi} + \exp\left(-\frac{1}{2}\right)\left\{\left(1 - \frac{w_{mi}^2}{8\pi} + \frac{\gamma_{mi}^2}{2}\right)w_{mi} - \frac{\gamma_{mi}\sqrt{\pi}}{2}\right\}\right]T^{3/2} +$$

$$+ \left(\frac{n_{g0}^0}{\sqrt{M_g}}\beta_{g0} + \sum_{Z \geq 1} \frac{n_{gZ}^0}{\sqrt{M_g}}\exp\left(-\frac{1}{2}\right)\left[\left(1 - \frac{w_{gi}^2}{8\pi} + \frac{\gamma_{gi}^2}{2}\right)w_{gi} - \frac{\gamma_{gi}\sqrt{\pi}}{2}\right]\right)T^{3/2}.$$

Therefore, we have a system of five equations (25) to (29) to determine n_{m0}^0, n_{gs}, β_{m0}, β_{g0} and T. The rest of the $n_{\alpha Z}^0$ ($\alpha = m, g$) parameters, which are part of this system of equations, are found from conditions of the ionization equilibrium in the hydrodynamic region of the plasma. The concentration of atoms of the saturated vapour, n_{ms}, is determined from relationship (17). The surface temperature T_{ms} and the dimensionless velocity of the vapour at the boundary of the Knudsen layer, γ_m, are the external parameters.

As noted above, in a case where the ionized vapour pressure is in excess of the external pressure

$$n_e^0 k_B T_e + \sum_{Z \geq 1} n_{mZ}^0 k_B T > p^0$$

evaporation is of a convective mode and the near-surface plasma becomes one-component. In this case the system of the balance relationships is simplified and reduced to three equations (25), (27) and (29) at $n_{gs} = n_{gZ}^0 = 0$ ($Z \geq 0$)with respect to the unknown values of n_{m0}^0, β_{m0} and T.

In the absence of ionization ($n_{\alpha Z}^0 = 0$; $\alpha = m, g$; $Z \geq 0$), the complete system of equations (25) through (29) generalizes results of [1] obtained for a case of rapid surface evaporation into a gas with back pressure (convective mode) and for a case of diffusion evaporation where the external medium is multi-component. In the convective mode of evaporation into the external gas without ionization ($n_{m0}^0 k_B T > p^0$) this system has the known analytical solution [1], whereas in the diffusion mode ($n_{m0}^0 k_B T \leq p^0$), assuming that the rate of diffusion of the vapour atoms into the external gas is negligibly low ($\gamma_m \approx 0$), this solution in an approximate form can be written as follows:

$$n_{m0}^0 = n_{ms}, \quad n_{gs} = n_{g0}^0 = \frac{p^0}{k_B T} - n_{m0}^0,$$
$$\beta_{m0} = \beta_{g0} = 1, \quad T = T_{ms}. \tag{30}$$

The solutions given can be used, for example, for calculation of the mass Q_M and energy Q_E flows from the melt surface, as well as pressure P acting on this surface during laser treatment of metals without formation of the near-surface plasma. By calculating the respective flows we find [2] that

$$Q_M = M_m n^0_{m0} \mathrm{M} s,$$
$$Q_E = \frac{5}{2} n^0_{m0} k_\mathrm{B} T \mathrm{M} s \left(1 + \frac{1}{3}\mathrm{M}^2\right) + \frac{\lambda_v}{M_m} Q_M, \qquad (31)$$
$$P = n^0_{m0} k_\mathrm{B} T \left(1 + \frac{5}{3}\mathrm{M}^2\right) + n^0_{g0} k_\mathrm{B} T,$$

where $\mathrm{M} \equiv u/s$ is the Mach number for the vapour flow at the external boundary of the Knudsen layer; $s = \sqrt{5 k_\mathrm{B} T / 3 M_m}$ is the local velocity of sound (the vapour is assumed to be an ideal one-atomic gas). It follows from relationships (30) and (31) that in the diffusion mode of evaporation ($\mathrm{M} \approx 0$) the resulting mass and energy flows from the metal surface are almost equal to zero and pressure applied to the surface is equal to an ambient pressure (i.e. the vapour under such conditions can be regarded as saturated).

Analysis of the Knudsen layer of the plasma does now allow calculation of the M value for the vapour flow at the external boundary of the layer. In other words, the velocity of scatter of the vapour can be set arbitrarily without violation of the laws of conservation of mass, momentum and energy in transition over the Knudsen layer. This result is not extraordinary, as this is true also for the Renkin-Hugoniot conditions for shock waves [13]. The values of u (or M) can be determined from the state of the plasma flow in the hydrodynamic region and the requirement that the Knudsen layer remain adjacent to the metal surface [1].

Ionization processes and plasma composition outside the Knudsen layer. To complete the above system of the balance relationships, it is necessary to determine concentrations of all charged particles at the external boundary of the Knudsen layer. As it is supposed that plasma in the hydrodynamic region is quasi-neutral and ionization-equilibrium, composition of such a multi-component plasma can be determined using the following system of equations:

Sach's equation, with allowance for non-ideality of the plasma [14]

$$\frac{n^0_e n^0_{\alpha Z+1}}{n^0_{\alpha Z}} = \left(\frac{2\pi m_e k_\mathrm{B} T_e}{h^2}\right)^{3/2} \times \qquad (32)$$
$$\times \frac{2\theta_{\alpha Z+1}}{\theta_{\alpha Z}} \exp\left[-\frac{e\,(U_{\alpha Z} - \Delta U_Z)}{k_\mathrm{B} T_e}\right], \quad \alpha = m, g; \quad Z \geq 0$$

(here h is the Planck's constant; $\theta_{\alpha Z}$ are the statistical sums for heavy particles of the kind of αZ; $U_{\alpha Z}$ are their ionization potentials for transition of particles of the kind of α from charged state Z into $Z + 1$; $\Delta U_Z = e(Z + 1)/r_\mathrm{D}$ is the decrease in the respective ionization potentials caused by interaction of the charged particles in the plasma);

Debye radius

$$r_D = \left[\frac{k_\mathrm{B} T_e}{\sum\limits_{\alpha;\ Z \geq 1} n^0_{\alpha Z} (Ze)^2}\right]^{1/2};$$

condition of quasi-neutrality of the plasma

$$n^0_e = \sum_{\alpha;\ Z \geq 1} n^0_{\alpha Z} Z, \quad \alpha = m, g; \qquad (33)$$

law of partial pressures which determines the overall gas-static pressure of the plasma (allowing for the electron pressure) at the external boundary of the Knudsen layer

$$p = n^0_e k_\mathrm{B} T_e + \sum_{Z \geq 0} n^0_{mZ} k_\mathrm{B} T + \sum_{Z \geq 0} n^0_{gZ} k_\mathrm{B} T, \qquad (34)$$

where

$$p = \begin{cases} p^0, \ n^0_e k_\mathrm{B} T_e + \sum\limits_{Z \geq 0} n^0_{mZ} k_\mathrm{B} T \leq p^0; \\ n^0_e k_\mathrm{B} T_e + \sum\limits_{Z \geq 0} n^0_{mZ} k_\mathrm{B} T, \ \ n^0_e k_\mathrm{B} T_e + \sum\limits_{Z \geq 0} n^0_{mZ} k_\mathrm{B} T > p^0, \end{cases} \qquad (35)$$

and a decrease in pressure due to non-ideality of the plasma is ignored.

Equations (32) through (35) complete the system of equations describing the Knudsen layer formed near the surface of the metal at its evaporation into the external gas plasma. Besides, they include one more external parameter T_e, i.e. the electron temperature. Therefore, the Knudsen layer can be comprehensively studied by setting only three external parameters: T_{ms}, u and T_e, which can be determined by using the equation of thermal conductivity in the bulk of metal, equation of motion of the plasma in the hydrodynamic region and equation of the energy balance for plasma electrons. It should be noted here that within the frames of the model of the near-surface plasma under consideration the density of the current, j, flowing from the plasma to the metal surface is not an independent external parameter which determines the evaporation process, as it is expressly included neither in the balance relationships nor in the equations for determination of the ionization composition of the plasma.

Analyse the above relationships to find pressure of the plasma which determines its motion into the hydrodynamic region. As it follows from (35), pressure at the external boundary of the Knudsen layer remains constant ($p = p^0$) as long as the surface temperature is such that the corresponding value of the partial pressure of the ionized vapour is lower than or equal to the ambient pressure, and starts growing (other conditions being equal) with further increase in T_{ms}. Growth of pressure is accompanied by the acceleration of the vapour and a corresponding increase in pressure onto the melt surface, which deter-

mines dynamics of its motion under the effect of the laser beam, electric arc or their combination. The role of the boundary temperature of the surface, at which the acceleration of the vapour into the external medium with an atmospheric pressure starts at the absence of ionization, is played by the boiling temperature T_b, at which the pressure of the saturated vapour is equal to the atmospheric one. The effect of the electron pressure determined by the concentration and temperature of electrons on the said boundary temperature can be illustrated by a plot shown in Figure 2. The Figure shows dependence of the iron surface temperature, at which

$$n_e^0 k_B T_e + \sum_{Z \geq 0} n_m^0 Z k_B T_{ms} = p^0 = 1 \cdot 10^5 \text{ Pa},$$

upon the electron plasma temperature calculated on the basis of simplified relationships (30) with further allowance for ionization from (32) and quasi-neutrality of the plasma (33). As it follows from Figure 2, the surface temperature, above which pressure onto the surface starts growing to exceed the atmospheric one, is much lower than T_b at the presence of ionization, and decreases with an increase in T_e. Therefore, in heating metals using a low-power laser beam (not leading to formation of the natural laser plasma) the use of an extra external ionizer, such as the electric arc, enables a substantial decrease in a threshold temperature of the surface for transition from the thermal conductivity mode of metal penetration to a more efficient mode of deep penetration. In addition to an extra arc heating of the metal surface, this is one of the main causes of an increase in the efficiency of laser-arc welding, as compared with laser welding using low- and medium-power lasers.

CONCLUSIONS

1. The general system of equations for description of the multicomponent plasma formed near the evaporating metal surface in gas-shielded arc, laser or combined welding was obtained.

2. This system of equations allows determination of composition of the multicomponent near-surface plasma, temperature of heavy particles, values of electron and ion currents flowing from the plasma to the surface, as well as potential distribution in the Knudsen layer depending upon the local values of the metal surface temperature, the electron plasma component temperature, velocity of scatter of the vapour and current density at the external boundary of the Knudsen layer.

3. The equations derived make the basis for calculation of characteristics of the thermal and dynamic

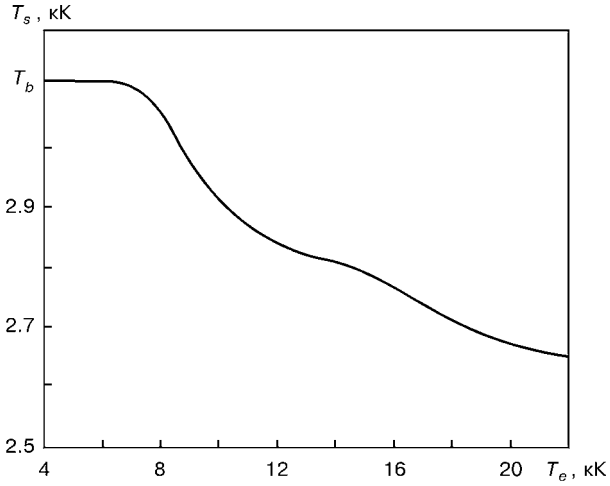

Figure 2. Dependence of the iron surface temperature T_s, at which pressure of the ionized vapour is equal to the atmospheric pressure, upon electron temperature T_e of the plasma

effect of the arc, laser or combined plasma on the weld pool surface in the respective gas-shielded welding methods.

The author is grateful to Yu.L. Vasenin for his participation in discussion of the data given in this article.

REFERENCES

1. Knight, Ch.J. (1979) Theoretical modeling of rapid surface vaporization with back pressure. *AIAA J.*, **5**, 519 – 523.
2. Arutyunyan, R.V., Baranov, V.Yu., Bolshov, L.A. *et al.* (1989) *Effect of laser radiation on materials*. Moscow: Nauka.
3. Bejlis, I.I., Lyubimov, G.A., Rakhovsky, V.I. (1972) Diffusion model of the near-cathode region of a high-current arc discharge. *Doklady AN SSSR*, **1**, 71 – 74.
4. Zhukov, M.F., Kozlov, N.P., Pustogarov, A.V. *et al.* (1982) *Near-electrode processes in arc discharges*. Novosibirsk: Nauka.
5. Dyuzhev, G.A., Nemchinsky, V.A., Shkolnik, S.M. *et al.* (1983) Anode processes in the high-current arc discharge. *Khimiya Plazmy*, **10**, 169 – 209.
6. Anisimov, S.I., Imas, Ya.A., Khodyko, G.S. *et al.* (1970) *Effect of high-power radiation on metals*. Moscow: Nauka.
7. Bejlis, I.I. (1982) On the theory of erosion processes in the arc discharge cathode plasma. *Doklady AN SSSR*, **6**, 1356 – 1361.
8. Bejlis, I.I. (1986) Flow of the near-cathode arc plasma in the Knudsen layer. *Teplofizika Vysokikh Temperatur*, **3**, 437 – 444.
9. Baksht, F.G., Dyuzhev, G.A., Mitrofanov, N.K. *et al.* (1973) Probe measurements of the low-temperature plasma at high degrees of ionization. *Zhurnal Tekhn. Fiziki*, **12**, 2574 – 2583.
10. Zharinov, A.V., Sanochkin, Yu.V. (1983) Dynamics of heavy particles near the negatively charged wall in the dense ionized plasma. *Fizika Plazmy*, **2**, 397 – 400.
11. Chen, F. (1967) Electrical probes. In: *Diagnostics of plasma*. Ed. by R. Haddlstone, S. Leonard. Moscow: Mir.
12. Bohm, D. (1949) *The characteristics of electrical discharge in magnetic fields*. Ed. by A. Guthrie, R.K. Wakerling. New York: McGraw-Hill.
13. Landau, L.D., Lifshits, E.M. (1986) *Hydrodynamics*. Moscow: Nauka.
14. Granovsky, V.L. (1971) *Electric current in gas. Established current*. Moscow: Nauka.

AXIAL DISTRIBUTION OF TEMPERATURE IN ARC IN GTA WELDING OF TITANIUM*

L.E. EROSHENKO, V.P. PRILUTSKY, V.Yu. BELOUS and **V.N. ZAMKOV**
The E.O. Paton Electric Welding Institute, NASU, Kyiv, Ukraine

ABSTRACT

The spectral method was used to investigate the real GTA welding arc burning between a non-consumable tungsten electrode and a consumable titanium and non-consumable copper water-cooled anodes. Experimental data were obtained on distribution of temperature in the arc column along the arc radius near the anode. It is shown that axial distribution of temperature in the arc column depends upon the state of the anode. In a region adjoining the anode the arc temperature is higher in the vicinity of the consumable anode.

Key words: *welding arc, spectrum, arc temperature, titanium anode, non-consumable anode, tungsten electrode*

Temperature of the welding arc is one of the main parameters which determine its technological characteristics and physical-chemical processes occurring in the welding zone. Therefore, the data on values of the temperature and its distribution in a real welding arc are needed both for estimation of the efficiency of the methods employed for increasing the technological capabilities of the arc and for checking the directivity and kinetics of the metallurgical processes.

However, no data obtained directly during the welding process are available in the literature. The majority of papers describe investigations which involve a non-consumable (usually copper water-cooled) anode [1 – 6]. At the same time, conditions of the experiments involving a consumable anode [1, 7 – 14] differ greatly from the actual welding conditions. In the reported cases Fe-based alloys were as a rule used as the anode. We are not aware of any literature sources giving the data on the temperature in the arc burning at a consumable titanium anode. Besides, in investigations of the temperature in the arcs burning at a consumable steel anode there were cases characterized by some procedural inaccuracies. They include, for example, processing of the results of spectral studies [1, 9 – 11, 13, 14] which is not always correct for a selected spectrograph slit [15], using unreliable values of probabilities of transition of spectral lines [14], etc. In addition, the publications give no data on the errors in establishing the distance from the plane of the anode to the plane of cross section of the column of the arc in which the spectrum was taken. It should also be noted that all of the investigations were conducted at the arc which was fixed relative to the anode (unlike actual welding conditions).

It is very likely that the above procedural errors affected results of determination of temperature at the arc axis [9 – 13]. For example, as it follows from the references, an increase of 20 times in the welding arc (from 20 to 400 A) is accompanied by an increase of only 600 K in the arc temperature. Besides, it is difficult to agree with the results given in [14], where the argon arc was investigated using a tungsten cathode and anodes made from Cr–Ni steel and aluminium. The average temperature in the bulk of the arc column was determined by a relative intensity of glow of spectral lines ArI, ArII and CrI. Despite the fact that the intensive glow of the atomic lines of argon can be observed only at a temperature of more than 6000 K [16], the values of the temperature calculated by the authors of [14] from spectral lines ArI were not in excess of 4000 K at I_w = 50 A. The cause of a decrease in the arc temperature determined from spectral lines ArII, i.e. 13300 – 10900 (steel anode) and 15400 – 14300 K (aluminium anode), with an increase in the current from 25 to 85 A is not clear either. It is likely that it is the procedural errors made in taking the spectra and their processing that resulted in the data obtained in [1]. They suggest that the arc temperature (other conditions being equal) does not depend in the least upon the state of the anode. Along the entire length of the column of the arc burning at a copper water-cooled and consumable steel anodes the values of the temperature determined were similar — about 11000 K near the cathode and about 8000 K near the anode (I_w = 100 A, arc length = 2 mm). The above values of the temperature near the anode are much lower than those given in [17, 18]. As it follows from these references, the arc temperature near the anode made from Cr–Ni steel, which was calculated from the relative intensity of glow of spectral lines of the vapours, i.e. CaI and CaII, was about 5600 K (at I_w = = 250 A), and that calculated from the intensity of continuum was about 14100 K (at I_w = 70 A). In some references [19 – 24] a conclusion of the presence of the anode vapours in the arc column is made only from the presence of their spectral lines in spectra of radiation of the arc. On this basis, the authors made theoretical calculations for two- and three-component plasma and estimated the effect of the anode vapours on characteristics of the arc [23, 24]. Since it is experimentally established [7, 8, 17, 18, 25] that the

*The work performed was supported by the State Fundamental Research Fund, Project No.4.04/578.

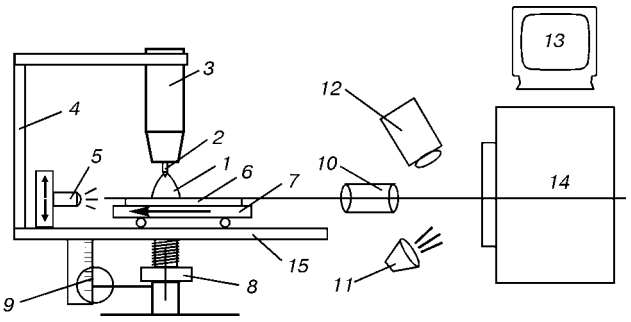

Figure 1. Schematic of the experimental setup for investigation of the arc: *1* — arc; *2* — tungsten electrode; *3* — torch; *4* — frame; *5* — laser emitter; *6* — anode; *7* — table; *8* — mechanism for axial movement of the anode; *9* — optical distance gauge; *10* — optical system; *11* — illuminator; *12* — TV camera; *13* — monitor; *14* — spectrograph; *15* — bed

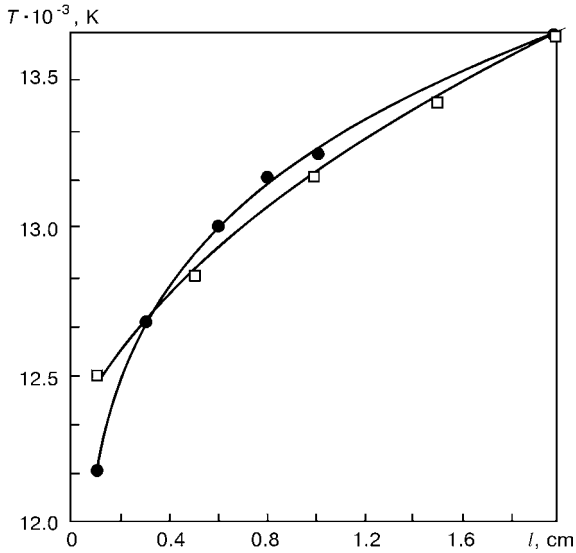

Figure 2. Axial distribution of temperature in the arc column: ❐ — titanium anode; ● — copper anode; l — distance from the anode

anode material vapours do not penetrate into central regions of the arc column, the temperature calculated from their glow can correspond only to the peripheral region of the arc gap. Therefore, the procedure for determination of the temperature of the column of the arc burning at a consumable anode based on the glow of spectral lines of the anode material vapours should be considered incorrect.

Of notice also is a rather large scatter of the values of the arc temperature determined from spectral lines ArI and ArII [1, 14, 26], which can be attributed to errors in the experimental procedures.

To increase the accuracy of measurements in determination of the axial distribution of temperature in the arc burning at a consumable titanium anode, we modified the experimental procedure, as compared to that described in [7, 8]. This allowed us to register spectrum of radiation of the real welding arc. In the experimental setup shown in Figure 1, welding torch *3* with cathode *2* was rigidly fixed at bed *15* using frame *4*. Welding table *7* with anode *6* (consumable titanium or non-consumable copper water-cooled) placed on it was moved over bed *15*. Laser emitter *5* illuminated the end of anode *6*, and the anode plane was aligned with the edge of the slit of spectrograph *14*. This was done using mechanism for the axial movement of the anode *8* and optical system *10*. Picture of the anode plane and spectrograph slit was displayed at a ×10 magnification by TV camera *12* on monitor *13* equipped with a coordinate grid. Illuminator *11* was used for tuning to increase contrast of the picture of the spectrograph slit. Filming of spectrum of arc column *1* at a preset section was done during the welding process by controlling the distance from the anode plane to the preset section at an accuracy of up to 0.1 mm using optical distance gauge *9*. The welding speed was 8 m/h.

Transverse spectra of the arc were photographed at regions located at a spacing of 0.5 mm along the arc length using the spectrograph with a slit width of 0.28 mm. The arc temperature was determined from radiation of continuum, as this method is less susceptible to random errors. The use was made of a radiation of continuum with a wave length of λ = 431.5 nm, which falls within a range of λ = 430 – 480 nm, where the intensity of continuum of the argon plasma is constant and does not depend upon the radiation frequency [27]. The emissivity for a continuum in this range of frequencies can be written as follows [2]:

$$\varepsilon_\nu = 6.36 \cdot 10^{-54}\, \xi(\nu, T) n_e n_i / (kT)^{1/2}\ [\mathrm{W}/(\mathrm{cm}^3 \cdot \mathrm{sr} \cdot \mathrm{s}^{-1})],$$

where $\xi(\nu, T)$ is the function which allows for the deviation of a given atom from the hydrogen model; n_e and n_i are the concentrations of electrons and ions, respectively; T is the temperature of the arc plasma and k is the Boltzmann constant. For argon the $\xi(\nu, T)$ dependence upon the temperature is very small and can be ignored [27]. In the above range of the spectrum frequencies $\xi(\nu, T) \approx$ const. The absolute value of this parameter, according to [2, 27], can be considered equal to 2.3. To investigate the distribution of temperature in the arc from the above expression, we plotted a theoretical dependence of the emissivity of continuum upon the temperature. Composition of the argon plasma (n_e, n_i) depending upon the temperature with the most complete allowance for the energy levels was calculated in the work described in [28]. The argon arc burning at a copper water-cooled anode [3, 4] was used as a radiation reference for the experimental determination of the emissivity of continuum and then for the calculation of the arc temperature from the theoretically calculated dependence $\varepsilon(T)$. Heterogeneity of the arc discharge was allowed for by numerical solution of the Abel equation [2] to determine local parameters of the plasma along the radius of the arc. Conversion of the observed distributions of $\varepsilon_\nu(x)$ from the centre to periphery of the arc column (at each of its sections) into radial emissivity was done on the basis of 20 points using tables taken from [29]. Conversion of the radial distributions of the continuum emissivity to the radial distribution of temperature was performed using computer data processing.

Along with taking the arc spectra using the spectrograph, the arc was synchronously filmed using a video camera by the method described in [30]. Then the video film was watched and photographs of the image were made from the monitor screen.

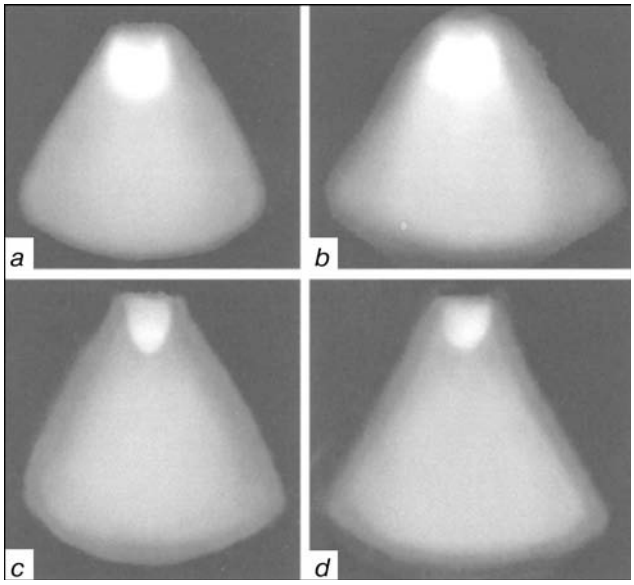

Figure 3. Argon arc 5 mm long, burning at copper water-cooled (*a, c*) and consumable titanium (*b, d*) anodes at I_w = 100 A: *a, b* — light filter at λ_{max} = 421 nm; *c, d* — same at λ_{max} = 650 nm

The same conditions as in [3, 4, 6] were selected for investigation of temperature of the arc burning at the consumable anode 100 × 50 × 4 mm in size made from commercial titanium of the VT1-0 grade. The above references describe investigations of the distribution of temperature in the arc burning at a copper water-cooled anode under the following conditions: I_w = 100 A, arc gap length — 5 mm, diameter of the tungsten cathode — 3 mm and its pointing angle — 30°. This allowed comparison of the axial distribution of temperature in the arcs burning at the consumable titanium and copper water-cooled anodes (Figure 2), as well as of structures of these arcs (Figure 3). As it can be seen from Figure 2, the values of temperature along the length of the arc from cathode to anode coincide for both types of the anodes up to a distance of 1 mm from the anode. In the near-anode region the temperature of the arc burning at the consumable titanium anode is higher, which seems to be caused by a higher temperature in the active spot of the consumable titanium anode. At the same time, both arcs have the identical structure. This can be seen from photographs of the arcs made by using a light filter which transmits radiation of spectral lines ArI, ArII and continuum (Figure 3, *a, b*), as well as only the continuum radiation of the argon plasma (Figure 3, *c, d*). In the first case a bright core is observed near the end of the cathode, which is caused by an enhanced glow of the lines of argon [5]. In the second case the end of the cathode immersed in plasma is seen.

The results obtained (allowing for the data of works in [7, 8]), make it possible to conclude that the axial distribution of temperature in the welding argon arc with a tungsten cathode depends upon the state of the anode. In a region adjoining the anode the arc temperature is higher in the case of using a consumable anode. For the titanium anode this temperature is 12600 K. At the same time, the arc structure does not depend upon the state of the anode.

REFERENCES

1. Glickstein, S.S. (1976) Temperature measurements in a free burning arc. *Welding J.*, **8**, 222 – 229.
2. Mechev, V.S., Eroshenko, L.E. (1970) Determination of temperature of the arc discharge plasma in argon. *Avtomaticheskaya Svarka*, **8**, 1 – 6.
3. Mechev, V.S., Eroshenko, L.E. (1975) Radial distribution of temperature of the electric arc in argon. *Ibid.*, **3**, 6 – 9.
4. Mechev, V.S., Eroshenko, L.E. (1975) Axial distribution of temperature of the electric arc in argon. *Ibid.*, **6**, 14 – 17.
5. Mechhev, V.S., Eroshenko, L.E. (1972) Investigation of the spectrum of radiation of the argon plasma near electrodes. *Ibid.*, **8**, 1 – 5.
6. Mechev, V.S., Eroshenko, L.E. (1972) Parameters of the arc discharge plasma near evaporating electrodes. *Teplofizika Vysokikh Temperatur*, **5**, 926 – 930.
7. Mechev, V.S., Eroshenko, L.E. (1984) Parameters of the arc column in argon near a workpiece in non-consumable electrode welding. *Avtomaticheskaya Svarka*, **1**, 25 – 30.
8. Eroshenko, L.E., Mechev, V.S., Demianchuk, A.S. (1979) Investigation of the near-electrode region of the argon arc at an evaporating anode. *Zhurnal Prikladnoj Spektroskopii*, **30**, 7 – 10.
9. Lapin, I.L. (1966) Determination of temperature of the welding arc by atomic lines of copper. *Svarochnoye Proizvodstvo*, **8**, 1 – 3.
10. Lapin, I.L. (1968) Optical study of the high-current Fe-arc. *Ibid.*, **1**, 3 – 5.
11. Lapin, I.L. (1971) Optical study of radial distribution of temperature and electrical conductivity of plasma in the high-current Fe-arc. *Ibid.*, **4**, 5 – 6.
12. Lapin, I.L., Turkin, P.S., Samsonov, V.I. (1978) Effect of fluorspar on structure of the arc burning in the air atmosphere. *Ibid.*, **4**, 1 – 2.
13. Lapin, I.L., Turkin, P.S., Samsonov, V.I. (1983) Effect of fluorspar on radial distribution of temperature and electrical conductivity of the electric arc burning in air. *Ibid.*, **4**, 8 – 10.
14. Shaw, C.B. (1975) Diagnostic studies of the GTAW arc. *Welding J.*, **2**, 33 – 44.
15. Eroshenko, L.E. (1977) Width of the spectrograph slit in determination of the arc discharge temperature. In: *Spectroscopy, spectral analysis and technical-and-economic effect of their application*. Kyiv: Znaniye.
16. Mechev, V.S., Eroshenko, L.E. (1974) Electrical conductivity of the electric arc in argon. *Avtomaticheskaya Svarka*, **7**, 13 – 16.
17. Belov, Yu.M., Blokhina, T.A., Goldfarb, V.M. *et al.* (1970) Properties of the short argon arc and its interaction with consumable anode. In: *Physics, engineering and application of the low-temperature plasma*. Alma-Ata.
18. Belov, Yu.M., Goldfarb, V.M., Iliina, E.V. (1972) Characteristic of the short argon arc with consumable steel anode. *Fizika i Khimiya Obrab. Materialov*, **5**, 127 – 130.
19. Dunn, G.J., Allemand, C.D., Eager, T.W. (1986) Metal vapors in gas tungsten arcs. Part 1, Spectroscopy and monochromatic photography. *Metallurgical Transact. A*, **7 – 12**, 1851 – 1863.
20. Metcale, J.C., Quigley, B.C. (1977) Arc and pool instability in GTA welding. *Welding J.*, **5**, 133 – 139.
21. Mills, G.S. (1979) Fundamental mechanisms of penetration in GTA welding. *Ibid.*, **1**, 21 – 24.
22. Glickstein, S.S. (1980) *Arc physics and weld pool behaviour*. Cambridge: TWI.
23. Dunn, G.J., Eager, T.W. (1986) Metal vapors in gas tungsten arcs. Part 2, Theoretical calculations of transport properties. *Metallurgical Transact. A*, **7 – 12**, 1865 – 1871.
24. Romanenkov, E.I., Vinogradov, V.A., Guma, V.V. *et al.* (1975) Calculation of composition of the two-component equilibrium plasma. *Avtomaticheskaya Svarka*, **4**, 27 – 29.
25. Eroshenko, L.E., Prilutsky, V.P., Zamkov, V.N. (1997) Investigation of glow of the anode vapours in the arc in GTA welding of titanium over the flux layer. *Ibid.*, **11**, 11 – 13.
26. Lyubavsky, K.V., Sidelnikov, Yu.V., Starchenko, E.G. (1969) Spectral investigation of the welding arc in argon. *Fizika i Khimiya Obrab. Materialov*, **6**, 133 – 135.
27. Asinovsky, E.I., Batenin, V.M. (1965) Experimental study of the continuous spectrum of the argon plasma. *Teplofizika Vysokikh Temperatur*, **4**, 539 – 535.
28. Drellishak, K.S., Knopp, C.F., Camnel, A.B. (1963) Practition functions and thermodynamic properties of argon plasma. *Physics of Fluid*, **9**, 1280 – 1288.
29. Bielski, A., Kaczmarek, W., Kybrycht, J. *et al.* (1968) On the determination of the radial intensity distribution of radiation in cylindric plasma. *Acta Phys. Pol.*, **5**, 701 – 709.
30. Eroshenko, L.E., Prilutsky, V.P., Zamkov, V.N. (1994) Video spectral method for investigation of the welding arc in argon. *Avtomaticheskaya Svarka*, **7/8**, 6 – 8, 14.

SOFTENING OF HIGH-STRENGTH ALUMINIUM ALLOYS IN DIFFERENT FUSION WELDING PROCESSES

A.V. LOZOVSKAYA, A.A. CHAJKA, A.A. BONDAREV, A.G. POKLYATSKY and **Andr.A. BONDAREV**
The E.O. Paton Electric Welding Institute, NASU, Kyiv, Ukraine

ABSTRACT

Base metal softening in the HAZ in EBW and argon-arc welding (AAW) of work- and heat-hardened aluminium alloys (AMg6, 1420, 1201, 1460) was studied. It is found that in EBW the extent of the softening zone is 4 – 5 times smaller than in AAW. After artificial ageing the greatest hardness of the HAZ metal is observed in alloy 1420 and the lowest — in alloy 1201.

Key words: *aluminium alloys, heat hardening, electron beam welding, argon-arc welding, heat-affected zone, hardness, microstructure*

Metal softening and structure in any point of the HAZ are dependent on the initial structure of the base metal and the thermal cycle of welding [1, 2]. The base metal microstructure can be different, depending on the previous heat or thermomechanical treatment. Materials in the heat- or work-hardened conditions are mostly used in welded structures [3]. In welding of such materials individual zones of the HAZ are heated to different temperatures. The degree of HAZ metal softening in each concrete zone depends on the nature of transformations in the solid solution. HAZ section with the maximal softening is the weakest link of the welded joint that is responsible for its strength.

The aim of this work was to study the features of metal softening in the HAZ of high-strength aluminium alloys in EBW and AAW with different heat inputs.

The influence of the welding process on base metal softening in the HAZ was studied on work- and heat-hardened aluminium alloys. A not heat-hardenable alloy AMg6 was welded in the work-hardened condition (AMg6NPP after work hardening); and heat-hardenable alloys 1420 (Al–Mg–Li), 1201 (Al–Cu) and 1460 (Al–Cu–Li) after quenching and artificial ageing (Table).

Plates 6 mm thick were joined by EBW and AAW in one pass in optimal modes, without applying filler wire. The following mode was selected for EBW: v_w = = 60 m/h, accelerating voltage of 30 kV, beam current of 75 mA; for AAW: v_w = 12 m/h, I_w = 280 – 300 A.

As there exists a certain correlation between the metal strength and hardness, softening of the alloys in welding was studied by hardness measurement in the points located at different distances from the weld axis or the fusion line. The hardness was measured with Rockwell instrument at 600 N load.

The nature of base metal softening in the HAZ is illustrated by the curves of variation of welded joint hardness (Figure 1). It is found that the degree of metal softening in each point of the HAZ depends on the type of base metal strengthening and thermal cycle of welding. Under the influence of the welding arc heat, the work-hardened (wrought) alloy AMg6 in the HAZ in non-consumable electrode AAW, is softened to the level characteristic of the metal in the annealed condition (*HRB* 83). The extent of the softening zone, including the weld, is 60 mm, the degree of softening being 15 – 20 % (Figure 1, *a*). A much smaller softening of this alloy is found in EBW. The extent of the softening zone is reduced to 20 mm, the degree of softening does not exceed 10 % (Figure 1, *b*).

A characteristic feature of heat-hardenable alloys is the fact that metal softening in the HAZ can be due both to the processes of dissolution of the strengthening phases and their further precipitation from the solid solution. These are opposite processes that proceed simultaneously. The dynamics of development of each of them depends on the maximal tem-

Composition of welded alloys

Alloy	*Element content, wt.%*				
	Mg	*Cu*	*Li*	*Mn*	*Other elements*
AMg6	6.2	–	–	0.6	Ti = 0.1; Fe = 0.4; Si = 0.4
1420	5.5	–	1.95	–	Zr = 0.1; Fe ≤ 0.3; Si = 0.2
1201	–	6.5	–	0.35	Ti = 0.1; Zr = 0.2; Mg < 0.2
1460	–	2.9	2.0	–	Zr = 0.1; Ti = 0.12; Sc = 0.08 – 0.12

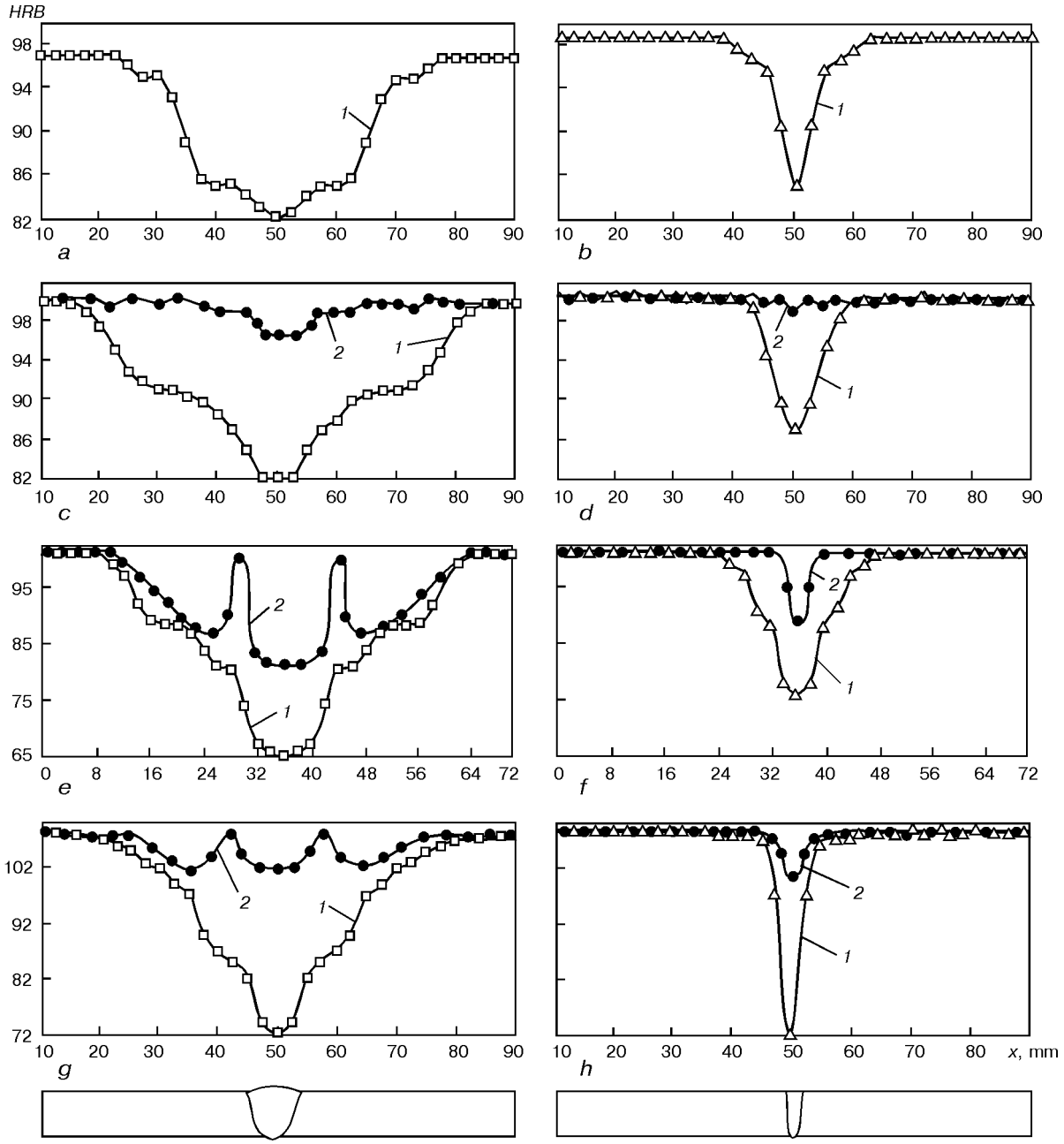

Figure 1. Hardness profiles of welded joint metal in argon-arc (*a*, *c*, *e*, *g*) and electron beam (*b*, *d*, *f*, *h*) processes of fusion welding of the following aluminium alloys: *a*, *b* — AMg6NPP; *c*, *d* — 1420; *e*, *f* — 1201; *g*, *h* — 1460; *1* — results obtained after welding (❐ — AAW; Δ — EBW); *2* — after artificial ageing (● — for any welding process)

perature achievable in each point of the HAZ, and the duration of staying in each temperature interval.

Hardness profiles of welded joints metal (Figure 1, *c* – *h*) have plateaux symmetrical relative to the weld that correspond to the hardness level lowering.

It is found that hardness levels close in their value, can be achieved both at the stage of high-temperature recovery of the quenched condition and partial annealing. The derived data are indicative of the fact that the nature of softening of alloys 1420, 1460 and 1201 in as-welded condition is practically the same. In AAW the extent of the softening zone, including the weld, is ≈ 55 – 60 mm; in EBW it is reduced to 15 – 20 mm. With both welding processes the weld metal has the lowest hardness.

In the case of EBW, the level of weld metal hardness is by 3 – 5 units higher than with AAW, except for alloy 1460. In alloy 1460 with both welding processes, the weld metal hardness is approximately the same, being equal to *HRB* 72. The level of weld metal hardness in alloys AMg6 and 1420 is higher (*HRB* 82 at AAW and *HRB* 85 – 87 in EBW), than in alloys 1201 and 1460 (*HRB* 65 – 72 and 72 – 75, respectively).

Artificial ageing of welded joints was used for identification of the processes, proceeding in different points of the HAZ. The same samples that were used for hardness measurement after welding, were subjected to artificial ageing in the optimal production mode, different for each of the alloys. The artificial ageing operation is admissible for certain weldments.

It allows evaluation of the nature of structural transformations and the condition of the solid solution in each point of the HAZ at the moment of welding. The presence or absence of softening at artificial ageing is directly related to the condition of the solid solution, i.e. the processes of low- and high-temperature recovery and annealing.

Comparison of the derived curves of hardness variation directly after welding and subsequent artificial ageing, allowed determination of the limits of high-temperature recovery of the annealed condition, degree of annealing, presence of low-temperature recovery for each of the studied alloys (see Figure 1, curves *1*). Alloy 1420, as a rule, is not subjected to annealing in welding, as after artificial ageing the softening zone is practically absent in it. The weld metal hardness is restored to the level of base metal hardness in the welded joints produced by EBW process and in AAW the softening zone of this alloy is significantly reduced (from 60 to 15 mm).

After artificial ageing of welded joints of alloys 1201 and 1460 produced by EBW, a considerable increase of the HAZ metal hardness to the base metal hardness level is found. This is attributable to the processes of temperature recovery and absence of annealing due to a short-term impact of the EBW thermal cycle.

Weld metal hardness is considerably increased (by 25 units in alloy 1201 and 30 units in alloy 1460), this being, probably, due to formation of solid solution of the main alloying elements, namely copper and lithium, in aluminium during the weld metal solidification in cooling.

In artificial ageing of welded joints of these alloys produced by AAW, the HAZ metal hardness profiles have sections of high- and low-temperature recovery, as well as a partial or complete annealing. In the sections of high-temperature recovery of the quenched state, directly adjacent to the fusion line, the hardness after artificial ageing increases by 20 units for both alloys and reaches the base metal hardness values in as-welded + artificial ageing condition.

At 10 mm distance from the fusion line the hardness profiles show the presence of «dips» symmetrical relative to the weld, considerable in alloy 1201 and less pronounced in alloy 1460, this being indicative of different degrees of HAZ metal annealing during welding (see Figure 1, *e, g*). At a greater distance from the fusion line, a certain increase in the base metal hardness is found that is indicative of a low-temperature recovery. Thus, in AAW of alloys of Al–Cu–Li and Al–Cu systems a weak annealing of alloy 1460 and a more significant annealing of alloy 1201 are found.

Comparison of hardness profiles for alloys 1201 and 1460 after their artificial ageing leads to the conclusion that despite the fact that the extent of the softening zone in both alloys is practically the same, the degree of softening is much greater (about 19 %) in alloy 1201, compared to Li-bearing alloy 1460. It is not more than 6 % for the latter.

Lithium presence in Al–Cu system alloy is also favourable for increasing the weld metal hardness after artificial ageing. So, in alloy 1460, it is increased by 30 units and reaches *HRB* 102, in alloy 1201 it increases by 17 units to the level of *HRB* 83.

The HAZ metal structure forms under complex non-equilibrium conditions. The HAZ metal near the fusion line is characterised by that in addition to solid solution transformations, it undergoes overheating due to partial melting of structural components, and recrystallization processes become well-developed. Three levels of overheating can be conditionally singled out: strong — almost all the grain boundaries are thickened, triple junctions are observed, phase inclusions are partially melted; medium — individual boundary thickening appears, junctions, individual inclusions or «peripheral» zone of inclusions are partially melted; weak — a polyhedral structure is formed. All the three stages of overheating, gradually going over from one to another, are characteristic for EBW, in AAW the fusion zone can be characterised as a zone with a weak, or, at the utmost, medium overheating.

Overheating of the metal in high-temperature recovery section of the HAZ is characterised by that under the influence of heating up to the non-equilibrium solidus temperature, partial melting of structural components occurs with liquid inclusions formation in the solid metal bulk. The closer to the fusion zone, the greater the degree of partial melting. In this case, continuous interlayers of a low-melting eutectic, form instead of individual partially melted inclusions. Appearance of liquid interlayers in the solid metal bulk, leads to redistribution of the alloying, impurity elements, and gases, as a result of the difference in the coefficients of diffusion in the solid and liquid states. Figure 2 shows the microstructure of three zones of a welded joint, produced in AAW of alloy 1201, that characterises the structural changes in the section of a high-temperature recovery of the quenched condition, annealing section and base metal. In other alloys it is difficult to single out the annealing zone in an optical microscope, especially in EBW.

The greatest extent of the zone of partially melted structural components is found in AAW of alloys 1201 and 1460 and is equal to 2.15 – 3.00 and 2.00 – 2.25 mm, respectively (Figures 3, *a* and 4, *a*). In alloys AMg6 and 1420 partial melting takes place in a section 0.6 mm long from the fusion line. In individual areas of welded joint of alloy 1420, the extent of this zone can be 1.5 mm. In EBW the length of the zone of partially melted structural components is reduced by 5 – 10 times and does not exceed 0.5 mm in alloy 1201 and 0.2 mm in alloy 1460, while in alloys AMg6 and 1420, this zone is practically absent (less than 0.1 mm).

The nature of partial melting in EBW is more local than in AAW. So, for instance, in EBW alloy

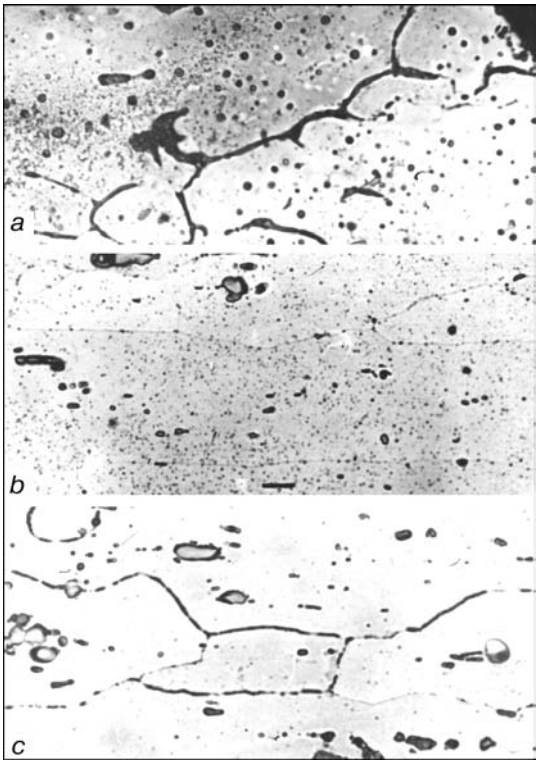

Figure 2. Microstructure of the HAZ metal (*a*, *b*) and base metal (*c*) in non-consumable electrode AAW of 1201 alloy sheets (6 mm thick): *a* — high-temperature recovery zone; *b* — annealing zone; *c* — base metal (×500) (reduced by 4/5)

1201 demonstrates partial melting of the grain boundaries, but the thickness of partially melted interlayers and their length are much smaller than in AAW. Partial melting of individual intermetallics proceeds directly at the fusion boundary (Figure 3, *b*). In EBW of alloy 1460, the partially melted zones are individual local areas (Figure 4, *b*).

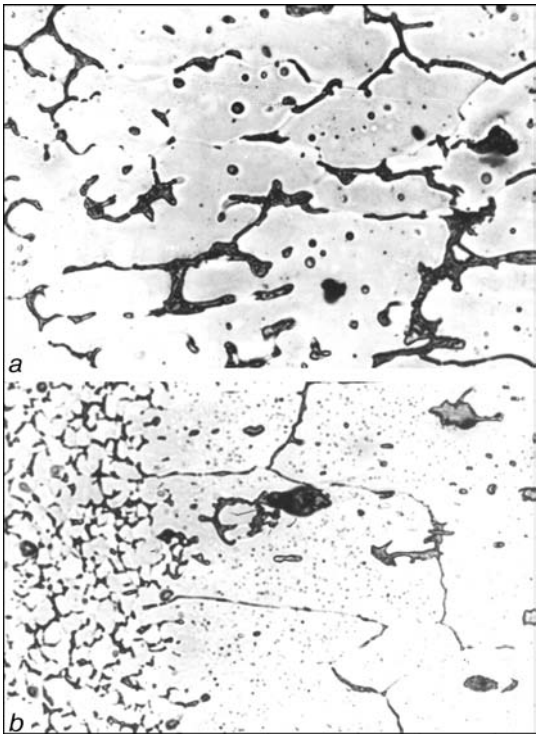

Figure 3. Mictrostructure of the fusion zone metal in AAW (*a*) and EBW (*b*) of 1201 alloy sheets 6 mm thick (×500) (reduced by 4/5)

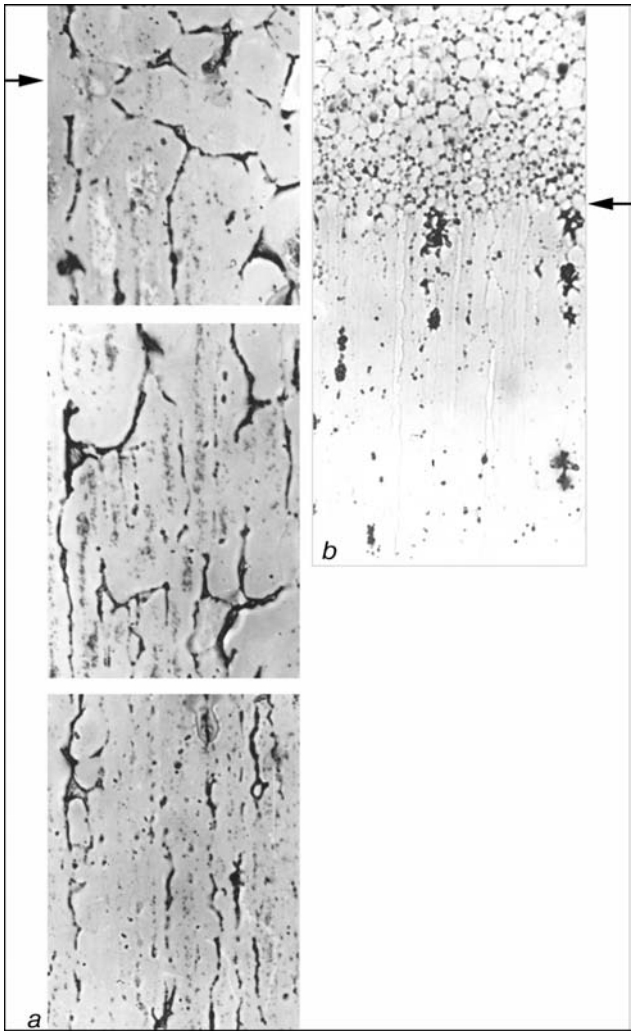

Figure 4. Mictrostructure of the HAZ metal produced in AAW (*a*) and EBW (*b*) of alloy 1460 (arrows shows the fusion boundaries) (×500) (reduced by 4/5)

Development of recrystallization processes also depends on the welding process. The smallest recrystallization zone is found in welded joints of alloy 1460, in AAW its length is 0.55 mm, in EBW — 0.12 mm. In alloys AMg6 and 1420, its length is almost the same and does not exceed 2 mm in AAW and 0.4 mm in EBW (Figure 5). Alloy 1201 was welded in the recrystallized condition.

Structural transformations related to partial melting of the structural components and recrystallization, proceed within the zone of the high-temperature recovery of the quenched condition.

Analysis of the derived data showed that the properties of the HAZ metal near the fusion line depend on a number of transformations related to dissolution of the strengthening phases and repeated formation of the solid solution, i.e. recovery of the quenched condition, as well as growth of individual coarser particles leading to an increase of ductility and lowering of the metal hardness (strength); partial melting of the structural components and formation of continuous brittle eutectic interlayers along the grain

boundaries, causing the alloy embrittlement; grain recrystallization and growth, lowering the metal strength properties. The strength of individual samples made, close in their composition to the eutectic interlayers, that form along the boundaries of partially melted grains in the HAZ metal in welding of alloy 1201, does not exceed 10 MPa.

Artificial ageing of heat-hardenable aluminium alloys allows increasing the strength (hardness) of the welded joint metal at the expense of additional decomposition of the solid solution newly formed during welding. The structural condition, due to partial melting of the phase components (overheating), cannot be changed by recrystallization or annealing at the expense of low-temperature heat treatment (ageing). In this connection, application of the welding processes with a concentrated heat source, is promising, as it allows the HAZ metal overheating and annealing to be reduced.

CONCLUSIONS

In non-consumable electrode AAW, the work-hardened alloy AMg6 has the HAZ hardness characteristic of annealed metal.

The extent of the softening zone in AAW of 6 mm sheets of heat-hardened alloys 1420, 1460 and 1201 and work-hardened alloy AMg6, is approximately the same and equal to 55 – 60 mm, including the weld. After artificial ageing, the extent of the softening zone in alloy 1420 is reduced to 15 – 20 mm, and practically does not change in alloys 1460 and 1201. The degree of softening after artificial ageing of the welded joints is the smallest (about 2 %) in alloy 1420 and the highest (about 10 – 13 %) in alloy 1201. In alloy 1460 it is smaller than in alloy 1201 and is about 5 %.

In EBW of work- and heat-hardened alloys, the extent of the softening zone is 4 – 5 times smaller than in AAW. After artificial ageing of welded joints on heat-hardened alloys, the HAZ metal hardness is restored to the level of hardness of the metal in the initial condition.

In both fusion welding processes, the lowest hardness is found in the weld metal (in EBW it is higher, than in AAW). After artificial ageing, the weld metal hardness in alloy 1420 rises to the base metal level (*HRB* 100), thus allowing production of a joint of equivalent strength.

Softening in the HAZ in fusion welding of heat-hardened alloys is due to the high- and low-temperature recovery of the quenched condition, as well as partial annealing. Analysis of hardness profiles leads to the conclusion that softening of alloy 1420 is mainly due to high- and low-temperature recovery; in alloy 1460 — to recovery processes and weak annealing; in alloy 1201 — to recovery and considerable annealing.

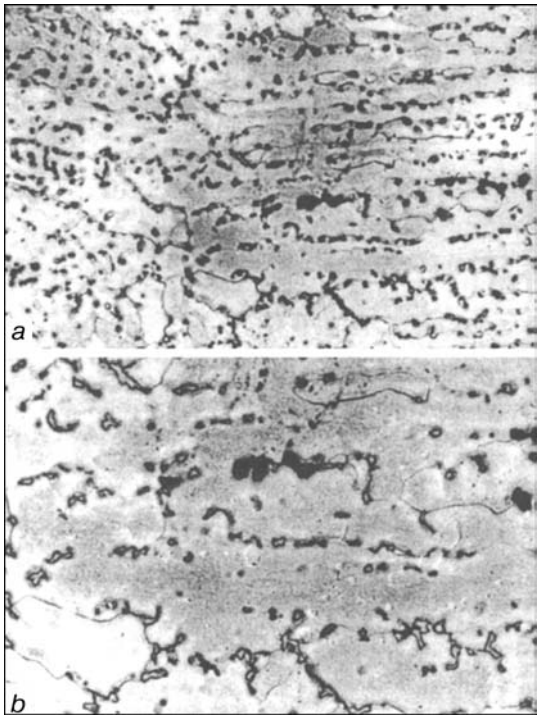

Figure 5. Microstructure of the fusion zone in AAW of 6 mm sheets of alloy 1420: *a* — (×150); *b* — (×500) (reduced by 4/5)

A feature of the HAZ metal near the fusion zone (high-temperature recovery zone) is metal overheating due to partial melting of the structural components and formation of extended low-melting eutectic interlayers along the grain boundaries. In AAW overheating of the HAZ metal has three levels, conditionally described as strong, medium and weak, and in EBW metal overheating reaches only the second level, namely the medium one.

REFERENCES

1. Rabkin, D.M. (1986) *Metallurgy of fusion welding of aluminium and its alloys*. Kyiv: Naukova Dumka.
2. Rabkin, D.M., Lozovskaya, A.V., Sklabinskaya, I.E. (1992) *Metal science of welding aluminium and its alloys*. Kyiv: Naukova Dumka.
3. Golder, Yu.P., Grishina, V.M., Dorokhina, V.E. *et al.* (1978) *Reference book on aluminium alloys*. Moscow: VILS.

LOW-CYCLE FATIGUE OF WELDED BUTT JOINTS MADE FROM ALLOY AMg6 IN INERT ATMOSPHERE

V.A. SHONIN and **A.G. POKLYATSKY**
The E.O. Paton Electric Welding Institute, NASU, Kyiv, Ukraine

ABSTRACT

Results of experimental investigations of a low-cycle fatigue resistance of butt joints made from 6 mm thick AMg6 alloy at axial from-zero loading depending on the geometry of weld convexity, stipulated by the TIG and MIG welding methods, are presented. The feasibility of evaluation of fatigue limit of butt joints by parameter of the convexity height–weld width ratio which has a good correlation with an estimated stress concentration factor at the weld boundaries is proved.

Key words: *aluminium alloys, shielded-gas welding, non-consumable and consumable electrodes, butt joint, fatigue resistance, weld convexity, weld flaws, stress concentration*

One of main factors determining the low values of fatigue resistance of butt welded joints as compared with those of the parent metal, is a stress concentration at the weld boundaries [1 – 6]. It depends mainly on such local parameters of the weld convexity contour as a radius [3] and angle of mating the surfaces of the deposited and parent metal [4]. Control of these parameters in welded joints is a rather labour-intensive operation [7, 8].

External parameters of the contour, a weld width and its convexity height, which are regulated by standards for welded butt joints and controlled in manufacture of structures, influence the weld strength at static loading [1, 2, 4] and are taken into account in evaluating the quality class of the welded joint ([9] and oth.).

Mechanical removing of a convex part of the weld to the level of the parent metal surface to prevent the stress concentration leads to a significant reduction in a static strength and does not always provide the increase in the fatigue resistance of the welded butt joint. This is due to the lower characteristics of the weld metal strength as compared with those of the parent metal, as well as to the presence of flaws [1, 2, 4, 5, 10, 11]. It is evident that in this case the weld convex part is a necessary design element. The selection of the method and conditions of the arc welding, coming from the parameters of weld convexity at which the high values of fatigue resistance and static strength of the joint are provided, is an actual problem.

It is known [12 – 15] that the shape of the butt weld convexity depends, first of all, on the width of the penetration zone, amount of melted parent and filler metal and also on the arc pressure, thermophysical characteristics of the molten metal, gravity force and capillary forces. Effect of these factors on the weld convexity is predetermined by the welding conditions, preparation of edges welded and spatial position of the weld pool.

All the parameters of weld convexity contour, determined by processes of welding are interrelated. Thus, the radius r and angle θ of mating surfaces of weld and parent metal are connected into relation $r = f(1/\theta)$ [12, 13], and the angle θ is directly proportional to the convexity height h and inversely proportional to the weld width b [15]. Here, the relation of parameters h/b is used as a total parameter of the external shape of the weld contour in the butt joint [3]. Taking into account that the stress concentration factor α_σ and ratio h/b are the functions of the same parameters, namely $\alpha_\sigma = f(r, \theta)$ and $h/b = \varphi(r, \theta)$, the value α_σ can be presented as $\alpha_\sigma = f[\varphi_1(h/b)] = F(h/b)$. This relationship can serve a basis in selection of welding technology by parameters of the convexity contour, providing the optimum values of a stress concentration factor and fatigue resistance of the butt joints.

The aim of the present work is to establish the characteristics of fatigue resistance of welded butt joints of the aluminium alloys depending on the geometry of weld convexity at different methods of welding and to prove experimentally the feasibility of using the external parameters of the weld convexity for evaluating the fatigue resistance.

Procedure of investigations. Aluminium alloy AMg6 (Mg — 6.2; Mn — 0.6; Ti — 0.1; Fe — 0.4; Si — 0.4 wt.%) plates of 6 mm thickness were investigated. Two plates of 100×300 mm^2 size were butt welded with a weld of 300 mm length for one pass on a backing, without edge preparation, with 1 – 2 mm gap using non-consumable (TIG) and consumable (MIG) electrodes at six different variants (Table 1). Before welding the butt edges were cleaned by a scraper.

In TIG welding, the argon shielding gas (its consumption was 3.3 m^3/s), 8 mm diameter non-consumable electrode and 2 mm diameter filler wire Sv-AMg6 were used. Welding of the 1st variant was performed by alternating current supplied from arc power source of the UDG-501 type, welding of the 2nd variant — by a pulsed symmetric current, and welding of the 3rd variant — by a pulsed variable-

Table 1. Conditions of single-pass welding of butt joint

No. of variant	*Method of welding*	$U_{o.-c}$, *V*	U_a, *V*	I_w, *A*	v_w, *m/s*	v_{wire}, *m/s*
1	TIG	70	12	360	0.0028	0.026
2	»	70	12	340/340*	0.0031	0.024
3	»	70	12	410/205*	0.0022	0.018
4	MIG	35	30	270	0.0097	0.146
5	»	30 – 32	25 – 26	275 – 300	0.0064	0.179
6	»	36/106**	20 – 21	195	0.0071	0.135

*Values of straight and reversed polarity current.
**Values of open-circuit voltage in a pause and pulse.

polarity asymmetric current of a rectangular shape from the power source of the I-126 type.

In MIG welding, the 1.6 mm diameter wire Sv-AMg6 was used. In case of variants 4 and 5 a DCRP was used from arc power source of the VDU-504 type, while in variant 6 a pulsed current of 100 Hz frequency was used from power source of the IUP-1 type. In variant 4 the mixture of shielding gases 2.5 m^3/s Ar + 7.5 m^3/s He was used, while in variants 5 and 6 only argon was used whose consumption amounted to 2.5 m^3/s.

17 plates of 200 × 300 mm^2 size were welded. After welding the weld convexity from the back side of the joint was subjected to grinding to the level of the parent metal surface. The welded plates were cut by a mechanical method across the weld for the samples of 50 mm width and 200 mm length with a next milling of lateral surfaces in the zone of the welded joint. After milling in 40 mm length the width of the working zone of the sample was 40 mm with a radius R = 30 mm of transition to the clamping areas.

The geometry of the welded joint contour in samples was measured by a roughness indicator having a dial with the 0.01 mm scale factor and a micrometric screw with 0.005 mm scale factor using the procedure described in [8]. Using the computer processing of the measurement data the values of width and height of the weld convexity and also radius and angle of mating the surface of the welded joint with the parent metal were determined.

Coming from the obtained values of parameters of the welded joint contour a stress concentration factor α_σ at the weld boundaries according to the relationship of B.M. Berezovsky and O.A. Bakshi was calculated [16]

$$\alpha_\sigma = 1 + \frac{1}{\left(\frac{r}{h}\operatorname{ctg}\frac{\theta}{2} + 4\frac{r}{s} + 5\frac{r}{b+r}\right)^{2/3}}, \qquad (1)$$

where s is the thickness of metal being welded.

The mean statistic values of stress concentration factors $\overline{\alpha_\sigma}$ and relative convexity $\overline{h/b}$, and also root-mean-square deviations S_α of stress concentration factors and relative convexity $S_{h/b}$ were determined (Table 2). Volume w of metal deposited during welding per linear length 1 m of weld was found from formula

$$w = \frac{\pi d_{wire}^2 v_{wire}}{4 v_w}, \qquad (2)$$

where d_{wire} is the wire diameter; v_{wire} is the speed of wire feeding; v_w is the welding speed.

The fatigue tests of samples were performed for an axial tension under the conditions of a soft loading at 0.05 – 0.07 Hz frequency at from-zero cycle of stresses $R_\sigma = 0$ in a modified test machine UME-10tm. From 5 to 23 samples were tested for each variant.

Test results and their discussion. Results of low-cycle tests are presented by the relationship of a maximum rated stress of cycle from fatigue life to fracture in logarithmic coordinates (Figure 1). In the Figure, the confidence boundaries of position of fatigue curves at 95 % probability are outlined with dash lines and the areas of scattering of experimental data — with thin solid lines. The values of tensile strength and fatigue limit within the range of fatigue life N =

Table 2. Parameters characterizing weld convexity and stress concentration at its boundaries

No. of variant	*Method of welding*	$w \cdot 10^{-4}$, m^3/m	*h, mm*	*b, mm*	$\overline{\alpha_\sigma}$	S_α	$\overline{h/b}$	$S_{h/b}$
1	TIG	0.29	1.12	14.7	1.28	0.140	0.077	0.020
2	»	0.24	1.18	13.4	1.19	0.153	0.089	0.019
3	»	0.26	1.03	14.7	1.14	0.075	0.071	0.018
4	MIG	0.30	1.29	16.5	1.52	0.302	0.082	0.023
5	»	0.56	2.42	18.1	2.11	0.464	0.135	0.024
6	»	0.38	2.72	14.4	2.44	0.593	0.190	0.030

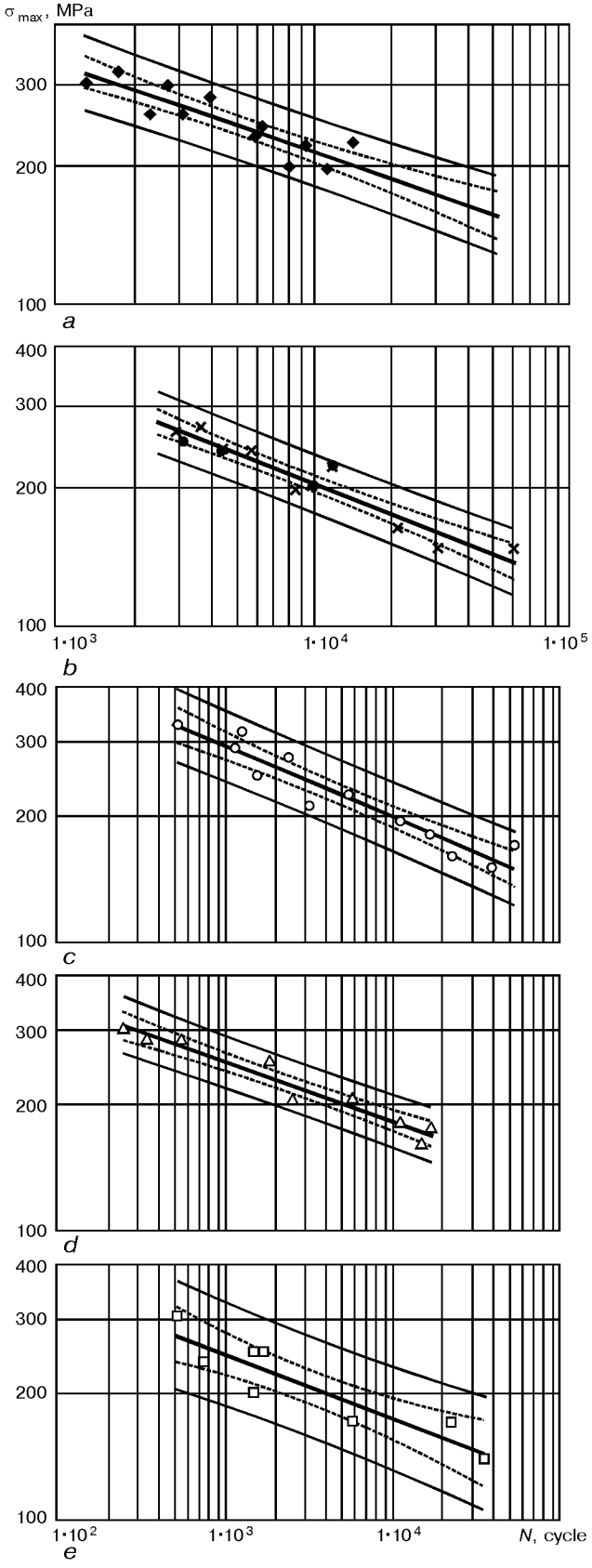

Figure 1. Results of fatigue tests of samples of butt joints welded by different methods: *a* — variant 1 (◆), TIG welding, sinusoidal current; *b* — variant 2 (●), TIG welding, pulsed sinusoidal current; variant 3 (×), TIG welding, pulsed asymmetric current; *c* — variant 4 (○), MIG welding, sinusoidal current; *d* — variant 5 (△), MIG welding, sinusoidal current; *e* — variant 6 (□), MIG welding, pulsed current (argon was used in all the cases, except variant 4; in variant 4 shielding gases Ar + He were used; $R_\sigma = 0$)

$= 2 \cdot 10^3 - 2 \cdot 10^4$ cycles are presented in Table 3. It also contains data of value of root-mean-square deviation S_σ at test base $N = 1 \cdot 10^4$ cycles.

During tests the fatigue crack initiation in samples occurred mainly in the weld boundaries. It was established that the joints made by TIG welding possess the best characteristics of fatigue resistance. Their fatigue life is 1.5 – 3.0 times higher than that of the joints welded by the MIG method. The fatigue limit of welded joints made by variant 5 by the MIG method are by 12 – 22 % lower than that of joints made by variant 1 by the method TIG. The decrease in fatigue limits by 6 – 11 % is provided by MIG welding using shielding gases Ar + He by variant 4. In variant 6 as compared with variant 5 the welding speed is 1.5 times higher and electrode wire feed speed is 1.2 times higher. The pulsed conditions of welding at methods TIG (variants 2 and 3) and MIG (variant 6) do not provide the increase in the fatigue resistance of the welded joints. Their fatigue limits are by 5 % lower on average than those of the joints made by the corresponding methods of welding at conventional alternating current (variants 1 and 5).

Some samples, welded by the TIG method and having a minimum (about 1 mm) convexity, were fractured in weld having flaws in the form of pores and oxide inclusions. The flaws were formed in the lower root weld part and decreased greatly the fatigue life of the joint. Moreover, the test results of samples with weld defects (Figure 2) are available in principle within the region of scattering of results of testing the samples welded by the MIG method, which are typical of large (1.3 – 2.7 mm) height of the weld convexity.

The high resistance to low-cycle fatigue of samples of welded joints with defect-free welds is provided by small convexity and low values of stress concentration factors defined by a shape of the joint at the weld boundaries (see Table 2). With increase in values h/b and α_σ the resistance to a low-cycle fatigue of the joints is decreased, The change in weld convexity from $h/b = 0.8 - 0.16$ for the investigated bases of fatigue life of the joints $N = 2 \cdot 10^3 - 2 \cdot 10^4$ is accompanied by decrease in fatigue limit of the joints by 9 – 21 % (Figure 3). Here, the tensile strength of the joints is increased approximately by 3 % (Table 3).

The large weld convexity in the joints made by the MIG method is formed, unlike the TIG method, at the expense of increasing the volume of the metal deposited. This is explained by 7 times increase in wire feed speed at 3 times increase in the welding speed. In MIG welding in shielding gases Ar + He using the variant 4, the value h/b is 1.7 times decreased as compared with variant 5 due to 1.9 times decrease in the volume of the metal deposited (see Table 2). In addition, the stress concentration factor is 1.4 times decreased. However, in a pulsed-current MIG welding using variant 6 the decrease in the volume of the metal deposited to the values close to those

Table 3. Characteristics of fracture resistance of butt welded joints at static and cyclic loading

No. of variant	*Method of welding*	σ_t, *MPa*	σ_{max}, *MPa*				
			$N = 2 \cdot 10^3$	$N = 5 \cdot 10^3$	$N = 1 \cdot 10^4$		$N = 2 \cdot 10^4$
					$\bar{\sigma}_{max}$*	S_σ	
1	TIG	329.5	291.6	245.0	214.8	15.97	188.3
2	»	325.4	293.1	236.1	200.5	13.61	170.2
3	»	325.4	293.1	236.1	200.5	13.61	170.2
4	MIG	330.0	259.1	222.1	198.0	15.89	176.0
5	»	332.1	227.1	199.9	181.6	9.98	164.9
6	»	336.2	221.1	192.5	173.4	17.99	156.2

* $\bar{\sigma}_{max}$ — mean values.

obtained in TIG welding does not lead to the decrease in the weld convexity as the noticeable narrowing of its width and increase in convexity height are occurred. Correlation between the ratio h/b and factor α_σ is presented in Figure 4. Due to a significant increase in ratio h/b and stress concentration factor at the weld boundaries the maximum reduction (by 17 – 24 %) of fatigue limits of the joints made using variant 6 as compared with variant 1 is occurred.

At low values of ratio h/b of weld made with a non-consumable electrode the effect of a pulsed welding current on the characteristics of fatigue resistance is not so large as in the MIG method.

Thus, the effect of method and condition of welding on the fatigue resistance of welded butt joints is determined by changes in a shape of the convexity contour and parameters of mating the weld and parent metal which are correlated with definite values of a stress concentration factor.

Taking into account that the fatigue resistance of the butt joint is determined by the conditions of stress concentration at the weld boundaries and basing on the satisfactory correlation between the factor α_σ and parameter h/b for the given type of the joint, it is possible to predict the fatigue life of the joint by setting such welding conditions by the preset value h/b to which the fatigue limit will correspond with a certain probability.

The feasibility of using parameter h/b as an indirect criterion for evaluation of the fatigue resistance of welded joints makes it possible to clarify the approaches to evaluating the welded joint quality regulated by standards. The actual parameter h/b of weld made, according to GOST 14806–80, by single-pass welding without edge preparation of 6 mm thick plates, has scattering of values within the 0.036 – 0.158 ranges. The increased scattering of values of fatigue resistance of butt joints corresponds to this wide range of scattering of this parameter. The limit of ranges of values of parameter h/b in control of the weld convexity shape can decrease the scatter of values α_σ and, consequently, will lead to a significant decrease in scattering of values of the fatigue resistance of the joints. Moreover, the selection of results of measurements of welded joints with similar parameters h/b (see Figure 4) will indicate a frequency distribution of values α_σ close to normal.

The low values of convexity parameter h/b which were obtained in welded joints during welding with a non-consumable electrode promote the increase in resistance of the weld boundaries to a low-cycle fatigue due to decrease in the stress concentration. How-

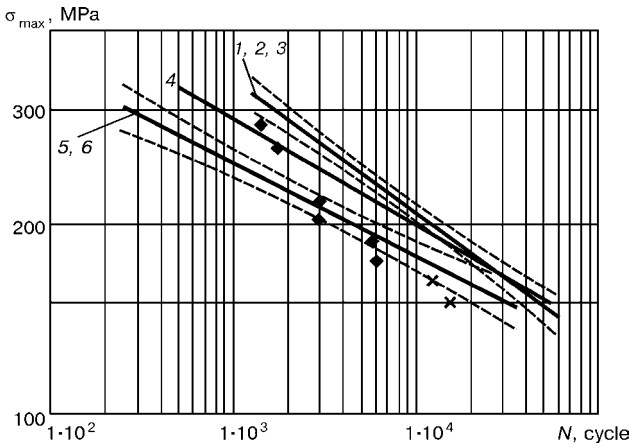

Figure 2. Fatigue curves and their confidence boundaries (95 % probability) for welded butt joints with defect-free welds of three groups of samples (variants 1 – 3 in TIG welding, variants 4 – 6 at MIG method (see designations in Figure1)), and also the results of testing samples fractured in weld having flaws: ◆ — variant 1; × — variant 2

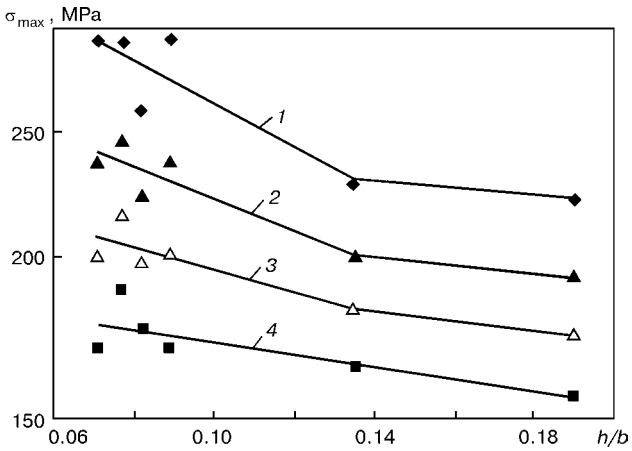

Figure 3. Relationship between the fatigue limit σ_{max} of samples of butt joint and parameter of weld convexity h/b at different test bases: *1* — $N = 2 \cdot 10^3$; *2* — $5 \cdot 10^3$; *3* — $1 \cdot 10^4$; *4* — $2 \cdot 10^4$

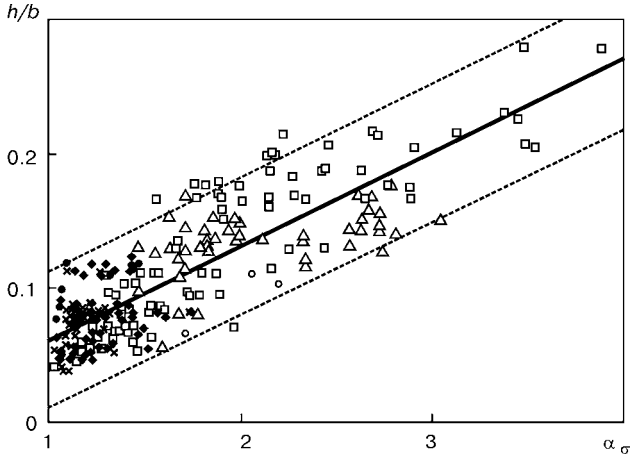

Figure 4. Relationship between the stress concentration factor α_σ at the weld boundaries and parameter of its convexity h/b in AMg6 alloy butt joints made with consumable and non-consumable electrodes (see designations in Figure 1)

ever, the decrease in convexity height leads to the increase in stress in the weld metal. Here, the probability of reducing the fatigue life of the joint in the presence of flaws up to the values typical of joints with large height of the weld convexity is increased. Therefore, the way for improvement of the fatigue resistance of butt welded joints by decreasing the weld convexity height can be in this case ineffective. The flaws which are difficult to reveal and eliminate, remain inevitably in welds even at their skilled making.

In case of use of a pulsed welding with a consumable electrode the decrease in volume of deposited metal to that obtained in TIG welding does not provide the increase in fatigue life of joints due to increase in values of convexity parameter h/b the same as in joints made by MIG welding with increased volumes of the metal deposited. The increase in height of the weld convexity directed for stress decrease in weld metal will not be a cause of deteriorating the welded joint quality if to use the auxiliary measures for improvement of the fatigue resistance of joints at the weld boundaries ([17] and oth.).

Optimum values of parameter h/b, at which high resistance of a low-cycle fatigue is attained, weld defects are minimum and satisfactory static strength of the butt welded joint is observed, are provided using method with a consumable electrode in shielding gases Ar + He at a high welding speed and minimum volume of the metal deposited.

Thus, when the welded butt joint is made it is recommended to optimize the geometry of the weld convexity contour on the basis of relation between the external parameters of convexity, stress concentrations in the zones of weld and parent metal mating and also the conditions of influence of weld flaws at static and cyclic loading.

CONCLUSIONS

1. It was established, that low- cycle fatigue resistance of samples of a butt joint is decreased with increase in a parameter of the external shape of the weld convexity which is determined by ratio of convexity height to width. This parameter has a satisfactory correlation with a stress concentration factor in the zone of weld and parent metal mating, where the fatigue cracks are initiated.

2. With decrease in weld convexity parameter h/b and a proper decrease in stress concentration factor α_σ at the weld boundaries the danger of a fatigue fracture of the welded joints due to flaws is occurred. In this case, the fatigue life of the sample is reduced to values typical of welds with large convexities made by welding with a consumable electrode using a conventional alternating or pulsed current.

3. To have the optimum shape of the weld convexity contour, providing increased fatigue resistance of 6 – 8 mm thick AMg6 alloy butt joint at minimum probability of fracture caused by flaws it is recommended to use the high-speed welding with a consumable electrode in shielding gases Ar + He at minimum volume of the metal deposited.

REFERENCES

1. Silvestrov, A.V. (1960) Fatigue strength of alloy AMg6 welded joints. *Svarochnoye Proizvodstvo*, **7**, 15 – 17.
2. Saveliev, V.N., Chizhevsky, S.V., Navrotsky, D.M. (1963) Technology of welding and strength of welded joints made from aluminium-magnesium alloys. *Series Welding, Brazing and Cutting of Metals*, Issue 5. Leningrad: LDNTP.
3. Trufyakov, V.I., Osaulenko, L.L., Koryagin, Yu.A. (1966) Stress concentration in butt joints. *Avtomaticheskaya Svarka*, **10**, 19 – 21.
4. Sanders, W.W. (1972) Fatigue behavior of aluminium alloy weldments. *WRC Bulletin*, April, **171**, 31.
5. Krüger, U. (1981) Fatigue strength of defective TIG-welded joints of thin-walled aluminium alloys. In: *Colloq. on Aluminium and its Alloys in Welded Construction*, Porto.
6. Sanders, W.W., Dey, R.H. (1983) Fatigue behavior of aluminium alloy weldments. *WRC Bulletin*, August, **286**, 21.
7. Lieurade, H.P. Fatigue testing of welded components. *IIW Doc. XIII-WG1-37–92*.
8. Asnis, A.E., Ivashchenko, G.A. (1985) *Improvement of strength of welded structures*. Kyiv: Naukova Dumka.
9. (1973) *NF A 89220*. Aluminium and aluminium alloys. Welding. Classification and control of welded joints. April, 447 – 467.
10. Lawrence, F.V., Munse, W.H., Burk, J.D. (1975) Effect of porosity on the fatigue properties of 5083 aluminium alloy weldments. *WRC Bulletin*, June, **206**, 23.
11. Labur, T.M., Ishchenko, A.Ya., Poklyatsky, A.G. (1990) Effect of inclusions of oxide film on characteristics of resistance of aluminium alloy AMg6 NPP welded joints to fracture at different temperatures. *Avtomaticheskaya Svarka*, **12**, 59 – 60.
12. Belchuk, G.A., Naletov, V.S. (1972) About some regularities of weld formation in place of weld-parent metal mating. *Svarka v Sudostroyenii*, **79**, 15 – 21.
13. Berezovsky, B.M., Stikhin, V.A. (1981) Peculiarities of formation of zone of transition from butt weld reinforcement to the parent metal. *Voprosy Svarochn. Proizvodstva*, **266**, 99 – 106.
14. Berezovsky, B.M. (1983) Wetting and spreading of weld pool at the metal surface. *Avtomaticheskaya Svarka*, **10**, 31 – 34.
15. Patskevich, I.R., Ryabov, V.R., Deev, G.F. (1991) *Surface phenomena in metal welding*. Kyiv: Naukova Dumka.
16. Makhnenko, V.I., Mosenkis, R.Yu. (1985) Calculation of stress concentration factors in welded joints with butt and fillet welds. *Avtomaticheskaya Svarka*, **8**, 7 – 19.
17. Hobbacher, A. (1991) Verbesserung der Schwingfestigkeit geschweißter Aluminium-Bauteile durch Nachbehandlung. *Aluminium*, **7/8**, 786 – 791.

CHEMICAL COMPOSITION OF AEROSOL GASEOUS CONSTITUENT IN A SHIELDED-GAS WELDING

O.G. LEVCHENKO
The E.O. Paton Electric Welding Institute, NASU, Kyiv, Ukraine

ABSTRACT

It was established that a carbon monoxide and nitrogen oxides are the main components of a gaseous constituent of the welding aerosol in mechanized solid wire welding in CO_2, in Ar + CO_2 and Ar + CO_2 + O_2 mixtures. The reduction in oxidizing ability of the shielding gas leads to the decrease in intensity of evolution of carbon monoxide and increase in nitrogen oxides. Introducing of oxygen to the shielding mixture composition reduces the evolution of the carbon monoxide at the expense of its oxidizing and increases the intensity of formation of the nitrogen oxides. The mechanisms of formation of gaseous components of the welding aerosol and relations between the intensity of their evolution and welding conditions are explained.

Key words: *mechanized welding, shielding gases, welding aerosol, toxic components, welding conditions*

The arc welding is accompanied by evolution of harmful elements of the welding aerosol, having hard and gaseous constituents, into the air. Chemical composition of a hard constituent of welding aerosol (HCWA) has been studied comprehensively and described in detail in different literature sources. However, the data about the compositions of a gaseous constituent of the welding aerosol (GCWA) are not numerous and, sometimes, contradictory. Thus, according to [1] the ozone (O_3), nitrogen oxides (NO_x) and carbon monoxide (CO) are the obligatory components of the GCWA, which are formed during the shielded-gas welding. The results of investigations of intensity of evolution of these elements using different shielding gases showed that in case of welding of steel with a consumable electrode in CO_2 they are negligible (approximately by one order lower than those in argon welding with an addition from 2 to 20 % CO_2) [2]. The recent data [3], obtained using upgraded gas analyzers, show that the mechanism of the ozone formation is complex and the intensity of its evolution depends on the method of welding, parent metal, type of welding consumables, welding current I_w, voltage U_a, arc length and also the shielding gas chemical composition. Moreover, it is noted in [3] that at different methods of welding in shielding gases the ozone formation is observed in welding with consumable and non-consumable electrodes only in inert gases, while the appearance of the carbon monoxide is typical of welding with a consumable electrode in CO_2 [4].

The present work was aimed at verification of the above-mentioned statements using generally-accepted domestic procedures, and also establishing the relationships between the intensity of formation of GCWA and HCWA during mechanized welding in different shielding gases and conditions.

Initial materials and procedures of investigations. Sampling of welding aerosols was made during the process of automatic surfacing of beads with 1.6 mm diameter wire Sv-08G2S (C — 0.11; Si — 0.5; Mn — 1.4; Cr — ≤ 0.1 wt.%) on plates from steel VSt.3 (rimmed) (C — 0.14 – 0.22; Mn — 0.4 – 0.65; Si — 0.12 – 0.3; Ni — ≤ 0.3; Cr — ≤ 0.3; Cu — ≤ 0.3; S — ≤ 0.05; P — ≤ 0.4; As — < 0.08 wt.%), using the following conditions: welding current (direct at reversed polarity) — 225 – 450 A; arc voltage — 27 – 37 V; wire feed speed — 365 – 908 m/h; welding speed — 16 m/h; electrode stickout — 25 mm. The following shielding gases were used as a gas protection: CO_2; 75 % Ar + + 25 % CO_2 and 70 % Ar + 25 % CO_2 + 5 % O_2 mixtures. The shielding gas consumption was 20 l/min.

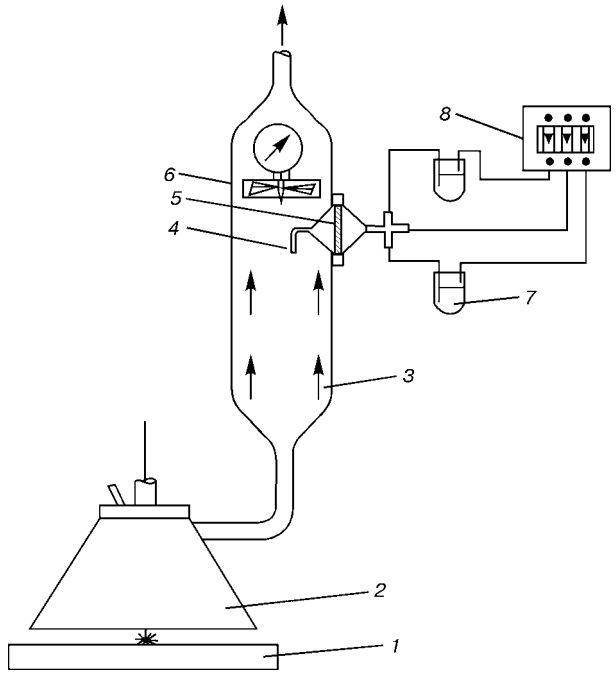

Figure 1. Sketch of a bench for GCWA sampling: *1* — parent metal; *2* — collecting nozzle; *3* — measuring-separating chamber; *4* — collecting pipe; *5* — filter; *6* — anemometor; *7* — absorbers; *8* — aspirator

Intensity of formation of GCWA components using different shielding gases*

Welding condition			CO_2	$Ar + CO_2$	$Ar + CO_2 + O_2$
I_w, A	U_a, V	v_w, m/h			
225	27	365	$\frac{1.59 \pm 0.32}{2.03 \pm 0.18}$	$\frac{0.79 \pm 0.15}{3.80 \pm 0.31}$	$\frac{0.30 \pm 0.06}{5.10 \pm 0.44}$
300	33	459	$\frac{0.89 \pm 0.19}{0.76 \pm 0.62}$	$\frac{0.29 \pm 0.07}{1.11 \pm 0.09}$	$\frac{0.17 \pm 0.43}{2.22 \pm 0.18}$
350	33	583	$\frac{0.63 \pm 0.14}{4.25 \pm 0.31}$	$\frac{0.30 \pm 0.06}{4.57 \pm 0.38}$	$\frac{0.14 \pm 0.03}{5.07 \pm 0.42}$
400	35	754	$\frac{1.52 \pm 0.34}{4.18 \pm 0.36}$	$\frac{0.58 \pm 0.12}{5.33 \pm 0.51}$	$\frac{0.16 \pm 0.03}{6.33 \pm 0.57}$
450	37	908	$\frac{1.65 \pm 0.41}{4.31 \pm 0.35}$	$\frac{0.79 \pm 0.16}{6.34 \pm 0.48}$	$\frac{0.38 \pm 0.07}{10.15 \pm 0.83}$

*In numerator the values of CO (g/min) are given, in denominator — NO_2 (mg/min).

The chemical composition and intensity of GCWA formation were determined using the generally-accepted procedures [5, 6] in a special bench (Figure 1). All the flow of aerosol was trapped using a special collecting nozzle, then it came through the measuring-separating column by a draught agitator, from which a part of flow was sampled by an aspirator into absorbers to determine the content of oxides of nitrogen and ozone. The content of carbon monoxide was examined using the GKh-4 type analyzer. The intensity of formation of HCWA was examined using procedures [6, 7]. At each welding condition 5 samples of aerosol were made.

To determine the concentrations of nitrogen oxides in the selected air volume, the method based on the reaction of interaction of nitrogen oxides with an agent of Griess-Ilosway was used [5]. The method sensitivity is 0.65 mg/m^3 that in calculation for intensity of formation of nitrogen oxides at the 0.1 l/min rate of air sampling was $6.5 \cdot 10^{-5}$ mg/min. Error in measurement did not exceed ± 15 %. The ozone content in air was determined by the method based on interaction of this element with a potassium iodine. Sensitivity of the method was 0.05 mg/m^3 (intensity of formation of nitrogen oxides is equal to $2.5 \cdot 10^{-5}$ mg/min at the 0.5 l/min rate of sampling), the error in measurement was not more than ± 25 % [5].

Results of investigations. The results of investigations (Table) showed that GCWA contains a monoxide of carbon and nitrogen oxides whose anount depends on the composition of the shielding gas and welding conditions, the ozone was not present.

During welding in mixtures Ar + CO_2 and Ar + + CO_2 + O_2 the intensity of CO formation is, respectively, 2 and 5 times lower than in case of welding in CO_2. As the source of CO formation is CO_2, dissociating as a result of arc burning [8], then with decrease in CO_2 in the shielding gas the content of CO in aerosol is decreased. The replacement of a part of CO_2 by Ar decreases the formation of a toxic carbon monoxide during welding. When the mixture Ar + + CO_2 + O_2 is used, a minimum evolution of carbon monoxide is observed due to its oxidizing at the arc high temperature:

$$2CO + O_2 \rightarrow 2CO_2. \quad (1)$$

Thus, the significant (5 times) decrease in a partial pressure of CO during welding in mixture Ar + CO_2 + + O_2 is explained by presence of argon and oxygen in it. In addition, as the ozone can form in the process of arc burning from the oxygen of air and shielding gas under the action of the ultraviolet arc radiation

$$3O_2 \leftrightarrow 2O_3, \quad (2)$$

then the reaction is possible

$$CO + O_3 \rightarrow CO_2 + O_2, \quad (3)$$

that also reduces the evolution of carbon monoxide and ozone. The above-mentioned statement is confirmed by the absence of ozone in the GCWA composition during our experiments. The results of investigations [3, 8, 9] showed that at the initial moment of welding the ozone content is high. Then it reacts with a nitrogen monoxide, forming dioxides of nitrogen and oxygen

$$O_3 + NO \rightarrow NO_2 + O_2, \quad (4)$$

and under the action of the arc radiation it decomposes into

$$O_3 \rightarrow O_2 + O. \quad (5)$$

Hence, the conclusion can be made that the absence of ozone in GCWA is explained by its fast decomposition during interaction with the carbon monoxide, nitrogen monoxide and under the action of the arc radiation. At the same time the full absence of the ozone in our experiments is explained by its decomposition in the process of sampling aerosols during ozone movement in measuring-separating column and hoses to the gas analyzer (see Figure 1). It was established in the course of other experiments on determination of the ozone content directly in the respiratory zone in CO_2 welding that its content does

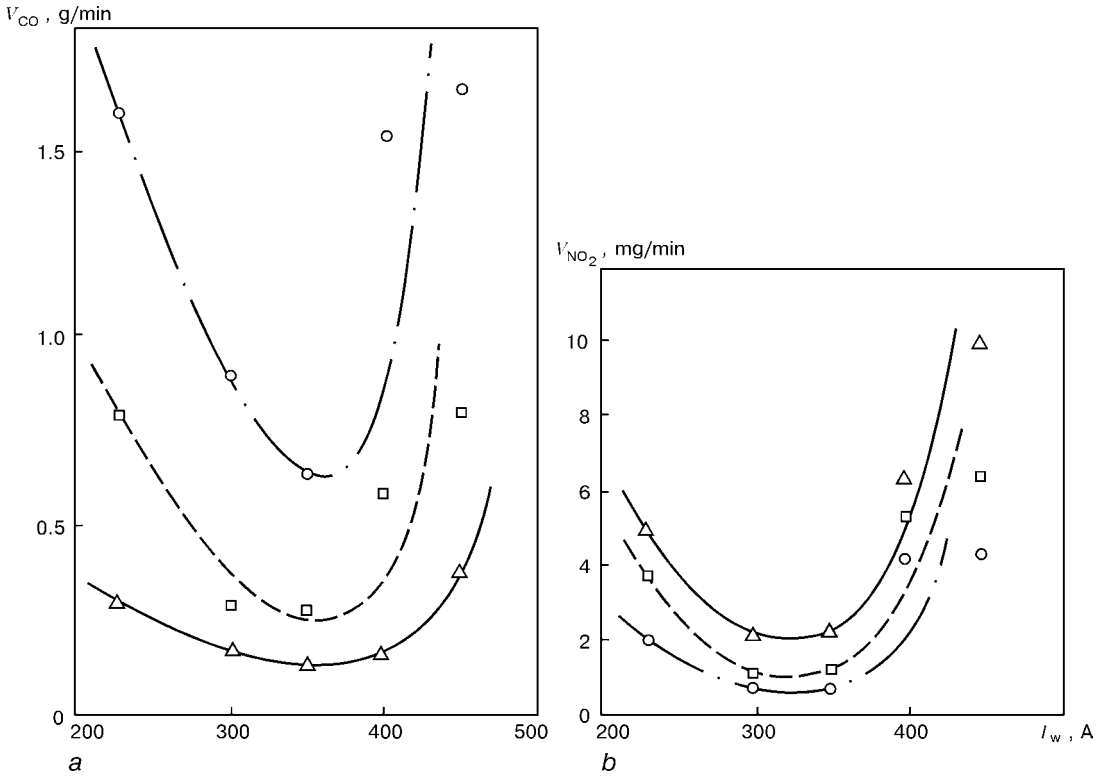

Figure 2. Relationship between the intensity of formation of carbon monoxide V_{CO} (*a*) and nitrogen dioxide V_{NO_2} (*b*) and welding current in welding with 1.6 mm diameter wire Sv-08G2S in shielding gases: ○ — CO_2; □ — Ar + CO_2; Δ — Ar + CO_2 + O_2

not exceed the limiting admissible concentration (lower than 0.1 mg/ m^3), and, sometimes, only the ozone traces are observed.

The nitrogen monoxide is formed as a result of high-temperature oxidizing of nitrogen of air surrounding the arc:

$$N_2 + O_2 \leftrightarrow 2NO. \quad (6)$$

Under the action of the ultrasonic radiation of the arc the nitrogen monoxide is oxidized by oxygen of air up to a poisonous dioxide of nitrogen [10, 11]:

$$2NO + O_2 \leftrightarrow 2NO_2. \quad (7)$$

In CO_2 welding the arc is burning in the atmosphere of this gas, therefore, the intensity of formation of nitrogen oxides is too small as compared with that of a carbon monoxide. It is, on average, by three orders lower than the intensity of formation of the carbon monoxide (see Table). During welding in mixtures Ar + CO_2 and Ar + CO_2 + O_2 the intensity of formation of nitrogen oxides is higher than that in CO_2 welding that is due to the ultraviolet radiation which becomes more intensive during welding in mixtures on the base of argon.

With the increase in the welding current the intensity of the formation of the carbon monoxide and nitrogen dioxide is reduced first to a certain value of current and then it is increased again (see Figure 2). The minimum level of intensity of the formation of these gases corresponds to the moment of the arc immersion to the parent metal [12] and to the decrease in area of its contact with the surrounding air and shielding gas. With a further increase in the welding current the arc length over the surface of the parent metal is increased and, respectively, the area of arc contact with air and shielding medium is increased.

Thus, there are definite welding conditions for HCWA [12, 13] and for GCWA, which provide the minimum level of their evolutions. So, in welding at 350 A the intensity of formation of carbon monoxide is 2 – 3 times lower than in case of using the minimum (I_w = 225 A) and maximum (I_w = 450 A) welding current.

The investigations of relationship between the intensity of HCWA formation and welding current, made at the same welding conditions that were used in determination of intensity of evolutions of GCWA components showed that relationships obtained have

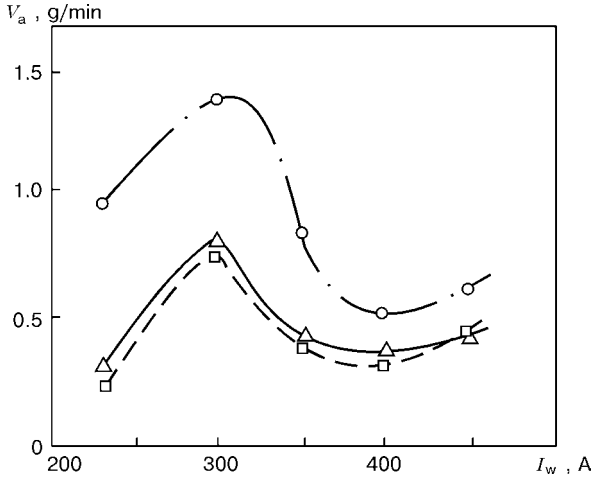

Figure 3. Relationship between the intensity V_a of HCWA formation and I_w in welding with 1.6 mm diameter wire Sv-08G2S in shielding gases (designations of Figure 2)

more complicated form as compared with that of GCWA (Figure 3), and also reflect the minimum evolution of HCWA.

CONCLUSIONS

1. It was established that in solid wire mechanized welding in CO_2, mixtures Ar + CO_2 and Ar + CO_2 + + O_2 the main components of a gaseous constituent of the welding aerosol are the carbon monoxide and nitrogen oxides.

2. Reduction of oxidizing ability of the shielding gas (introducing of argon into mixture composition) leads to the decrease in intensity of evolution of the carbon monoxide and increase in nitrogen oxide. Introducing of oxygen to the composition of a shielding mixture also reduces the evolution of carbon monoxide as a result of its oxidizing and activates the formation of nitrogen oxides.

3. Relationships between the intensity of formation of carbon monoxide and nitrogen oxides and welding current using CO_2, mixtures Ar + CO_2 and Ar + CO_2 + O_2 have a form of parabolas with a minimum that corresponds to the condition at which the arc has a maximum immersion to the parent metal.

4. These relationships should be taken into account in the selection of optimum parameters of the welding process (compositions of shielding gases and welding conditions) for improving the labour conditions of welders.

REFERENCES

1. Gorban, L.N., Krasnyuk, E.P., Faktorov, I.E. (1983) Effect of labour conditions on the health and morbidity of personnel in welding industry. In: *Coll. on Labour hygiene, Republ. Interindustry*, Issue 19, 40 – 49.
2. Sipek, L., Smars, E. Ozone and nitrogen oxides in gas-shielded arc welding. *IIW VIII-1486–89*.
3. Matusiak, J. (1999) Powstawanie ozonu przy procesach spawania i ciecia metali. *Biuletyn Institutu spawalnictwa w Cliwicach*, **5**, 142 – 147.
4. *AWS F1.3–83*. Evaluating contaminants in the welding environment. A sampling strategy guide. Miami: AWS.
5. *MU No.4945–88*. Methodical recommendations on determination of harmful substances in welding aerosol (hard phase and gases). Approv. on 22.12.88. Moscow: Minzdrav SSSR.
6. *MU No.1924–78*. Hygienic evaluation of welding consumables and methods of welding, surfacing and cutting of metals. Approv. on 29.09.78. Moscow: SSSR.
7. Pokhodnya, I.K., Shlepakov, V.N., Suprun, S.A. *et al.* (1983) *Methodology of primary sanitary-hygienic evaluation of flux-cored wires*. Kyiv: PWI.
8. Migaj, K.V. (1975) *Hygiene and safety of labour in electric and welding works in ship-building*. Leningrad: Sudostroyeniye.
9. Press, H. (1981) Formation des oxydes dazote lors du soudage aux gaz. Mesures pour la prevention datteintes a la sante. *Soudage at techniques connexes*, **516**, 307 – 212.
10. Sipek, L. Emission of gases pollutants during GTA welding of Yorcalbro Brass. *IIW VIII-1443–88*.
11. (1981) *Nitrogen oxides: Hygienic criteria of surrounding medium state*, Issue 4. Geneva: VOZ.
12. Levchenko, O.G. (1992) Effect of technological conditions of CO_2 welding of structural steels on the aerosol evolution. *Avtomaticheskaya Svarka*, **9/10**, 31 – 33.
13. Levchenko, O.G. (1998) Technological methods of reducing the level of welding aerosol formation (Review). *Svarochnoye Proizvodstvo*, **3**, 32 – 38.

STAGES OF IMPROVEMENT OF SUBMERGED-ARC WELDING TECHNOLOGY IN SHIPBUILDING (REVIEW)

V.D. GORBACH and **V.S. GOLOVCHENKO**
Central Research Institute of Shipbuilding Technology, St.-Petersburg, Russia

ABSTRACT

The paper presents the results of development and introduction of the technology of SAW of steels and structures used for ship hulls, that enabled construction of modern ships with a high quality and effectiveness.

Key words: *submerged-arc welding, welded structures, shipbuilding, developments, investigation*

Transition from riveted ship structures to all-welded structures that began in river shipbuilding in the middle of 1930s, made it possible to stop using the small-assembly method of ship hull construction and go over to the sectional method, thus allowing a considerable volume of assembly and welding operations to be transferred to the shops [1 – 3].

During this period all the welded joints were made by manual welding with arc electrodes or with ionising (chalk) coating. A considerable oxidation and nitrogen saturation of molten metal resulted in a higher strength and much lower ductility of weld metal (to $\delta \leq 3$ %) [4, 5]. This limited the applications of electric arc welding. It was not allowed for performance of butt joints on the ship hull, but found application only for welding of the framing and welding it to the ship hull skin.

Steel welding was initially introduced into river shipbuilding for the same reason [5]. Transition to sea ship hull construction was further restrained by the absence of reliable, easily weldable steels.

A serious impetus to welding introduction into shipbuilding was given by invention at the E.O. Paton Electric Welding Institute of the Academy of Sciences of Ukr.SSR of high-speed automatic SAW with wire electrode in 1939 – 1940 [6]. An essential contribution to mastering SAW also was development of OSTs-45 (SiO_2 — 38 – 44; MnO — 38 – 44; CaO — ≤ 10; MgO — ≤ 3; Al_2O_3 — ≤ 6; CaF_2 — 6 – 9; FeO — 0.5 – 2; S, P — ≤ 0.014 wt.%) fused flux in TsNIITMASh in 1941, that is still widely applied in various industries in automatic welding of steels of regular, medium and higher strength (composition of the above materials is given in the Table at the end of the article).

The concept of transition from riveting to welding in shipbuilding was implemented into practice by «Orgsudprom» Trust, established in 1939 and reorganised in 1948 into a Central Research Institute of Shipbuilding Technology (TsNIITS) that later on became a well-known major research center for development of the technology of construction of modern ships [2, 3].

In this period the welding research at TsNIITS was conducted in close interaction with the well-known welding research centers (PWI, TsNIITMASh, M.I. Kalinin LPI, «Elektrik» Factory, etc.). and other specialists in the field of shipbuilding technology [1 – 3].

In the initial period of welding development, low-carbon steels of grades St.3, St.4 and St.5 were used for ship hulls that were welded manually with electrodes of acid type. Use of higher strength low-alloyed steels was proposed for all-welded hulls of sea ships.

Introduction of sectional method of construction into shipbuilding practice enabled application of a new technology for that time — automatic arc welding. By 1937 PWI in principle developed two automatic welding processes. The first was based on application of wire with a stabilising thin coating, and the second — on the use of wire of a cruciform cross- section with a thick coating. In the same period PWI developed the first in the USSR self-propelled welding unit–tractor for automatic welding in shipbuilding. Applicability of such units in shipbuilding had not yet been proved or accepted by anyone before [6, 7].

At the same time (starting from 1946) «Orgsudprom» resumed the work begun in 1940 and interrupted by the war, on development and introduction of the technology of automatic SAW to replace manual coated-electrode welding. Already before the war, it was established that flux of OSTs-45 grade is the most suitable for automatic welding of steels St.4, St.5 and 20G. Its application provides high technological properties of the weld metal, its lowest susceptibility to porosity and the highest values of the welded joint mechanical properties. In the same period it was shown that automatic SAW is possible only in the downhand position and provides 5 – 6 times higher efficiency of welding operations, compared to manual coated-electrode welding [3, 6, 7].

These features of welding in the post-war period, on the one hand, necessitated its faster and wider introduction, and, on the other hand — investigation

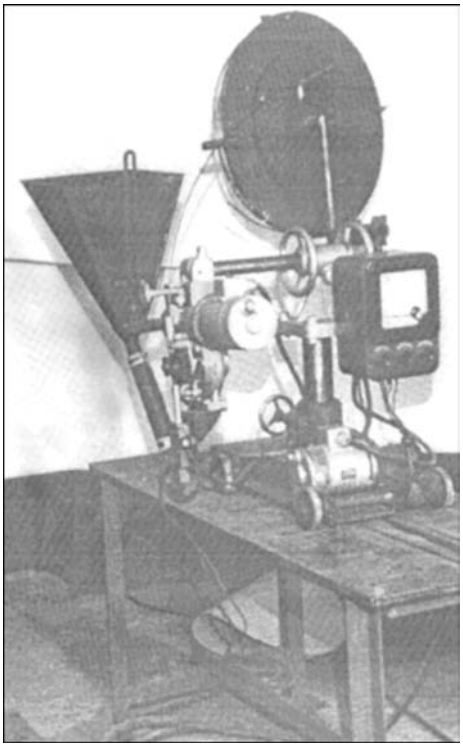

Figure 1. First automatic machine MAG-1 for SAW of butt joints on ship structures

and development of the technology of welding all ship hull steels applied at the time of grades St.3, St.4, 10KhSND, 15KhSND, 10KhSN2D, etc. 7 to 50 mm thick.

Investigation and development of the technology of automatic welding were conducted with a simultaneous retrofitting of the pilot sample of MAG-1 automatic machine (Figure 1), developed by «Orgsudprom» Trust as far back as in 1944. Batch production of this machine starting from 1946 played a decisive role in introduction of automatic SAW for butt joints of ship hull structures 7 – 50 mm thick. Technology of automatic SAW of butt joints of thin (2 – 7 mm) sheets was optimised at the same time.

Fundamental issues of automatic SAW of butt joints of the main steel grades in the downhand position, were solved by 1948 – 1951, this allowing an essential reduction of the volume of manual welding application and achieving a significant technical-economic effect [2, 3].

In 1949 – 1957 the technology of hose mechanised SAW with electrode wire of 1.6 and 2.0 mm diameter by semi-automatic machines of PSh-5 and PSh-54 type, designed by PWI, was developed and introduced for mechanising the welding of fillet, as well as short butt joints.

Special rotating «beds»-tilters were developed for partial tilting of the sections and allowing downhand welding were developed for application of mechanised SAW of butt and fillet joints when making sections with curvilinear contours. This area of welding mechanisation was not developed any further, in view of the cumbersome design of the tilters and great complexity of operations. The method of separate assembly and welding of the framing developed in 1949 – 1950 that allowed applying automatic SAW for these purposes, turned out to be a quite effective method for mechanisation of fillet welding (joining the framing to the decking). For this purpose TsNIITS developed the technology of automatic inclined-electrode SAW of fillet welds and a special automatic machine ASU-138 (Figure 2).

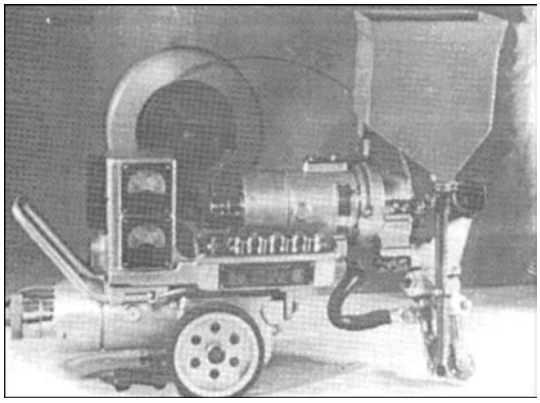

Figure 2. Automatic machine ASU-138 for inclined-electrode SAW of T-joints of ship structures

In 1948 – 1951 the main principles of automatic and mechanised welding of butt and fillet welds of ship structures were elaborated.

Further on (after 1951) SAW developed through improvement of the welding technology, welding equipment, welding consumables, methods and means of control of welding quality, and of sanitary-hygienic conditions of welding operations performance, etc.

In order to achieve a wider introduction of mechanised SAW, a procedure was accepted under which the design bureaus were to envisage the maximal possible volume of SAW already at the stage of the ship detail design, and TsNIITS studied the technical projects and issued appropriate recomendations. In order to determine the volume of mechanised welding, TsNIITS in 1949 – 1951 developed a calculation procedure, according to which the volume of mechanised welding application (or level of welding operations mechanisation) were determined as a ratio of the area of longitudinal section of the welds produced by mechanised welding processes, to the total area of the longitudinal section of the welds made by all the welding processes [2].

In 1961 – 1962 this procedure was replaced by PWI procedure, according to which the level of mechanisation of welding operations was determined as the ratio of the reduced labour consumption of welding by mechanised processes, to the total labour consumption of welding performed by all the processes.

In 1953 – 1957 a series of investigations were carried out to establish the applicability of various processes of welding butt joints with larger gaps (up to 4 mm) on a flux pad or flux-copper backing. For these purposes, a number of shipbuilding yards, based on PWI developments, built electromagnetic benches

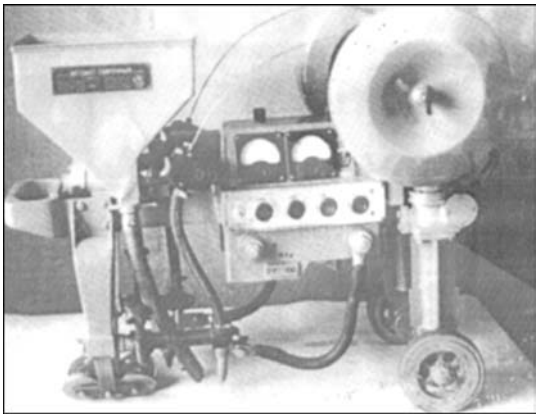

Figure 3. Automatic machine DASU-138 for twin wire SAW of T-joints from two sides simultaneously

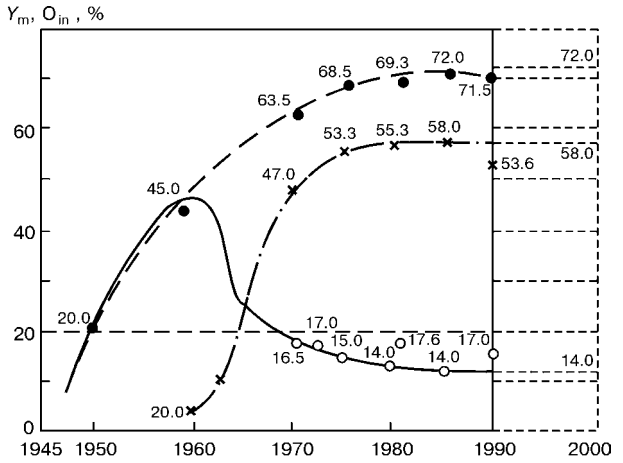

Figure 4. Dynamics of variation of the volume of introduction, O_{in}, of mechanised processes of consumable electrode electric arc welding and level of welding operations mechanisation, Y_m, in shipbuilding: ○ — SAW; ● — CO_2 welding; × — mechanisation level

and TsNIITS developed a technology of automatic SAW from both sides on flux pads of butt joints with larger gaps and square edges for sheet thickness of 2 – 20 mm and with edge preparation (for 22 – 34 mm thick sheets). The technology of automatic welding from one side with weld formation from both sides, was developed at the same time.

In view of insufficient uniformity of the welded joint quality, however, the above technologies did not become widely accepted. In order to improve the effectiveness of fillet welding, TsNIITS developed the technology and automatic machine DASU-138 (Figure 3) for simultaneous automatic inclined-electrode SAW of two welds (from two sides) of T-joints (in welding of the framing to the panels), as well as the technology of mechanised SAW of fillet spot welds on sheet structures.

In 1958 – 1959 research on welding two-layer steels (different grades of ship hull steels, clad with 10Kh18N9T (AISI 304) steel) was performed, electrodes UONI-13/NZh2 and technology of manual and automatic SAW were developed. In addition to development and improvement of the welding processes, considerable attention was given to improvement of the quality of welding consumables, welds and welded joints.

Investigation of weld susceptibility to brittle fracture demonstrated the adverse influence of the weld and HAZ metal saturation with hydrogen. Investigations of the fatigue and dynamic strength, sensitivity to ageing and corrosion resistance of welded joints were performed, that resulted in development of Ni-containing wire 08-GN for automatic SAW and of manual special-purpose electrodes, providing a weld metal resistant to corrosion and having high mechanical properties.

Limitations on the content of silicon and manganese, sulphur and phosphorous were introduced for the fluxes composition. This resulted in division of the flux into two kinds, namely large granule flux for automatic welding and fine granule flux with a more stringent limitation of phosphorous content for mechanised welding.

1949 was the start of development of the technology of automatic vertical arc (and later on also electroslag) welding of field butt joints using a welding tractor of TC-20 type with a magnetic shoe developed by PWI.

A series of investigations on optimisation of the technique and technology of welding and welding equipment, as well as on studying the properties of welded joints, allowed beginning in 1955 – 1956 the introduction of automatic vertical welding with forced formation of welds of field butt joints of the hulls in construction of large tonnage ships of the type of tankers, dry-cargo ships, refrigerators, etc. [3].

In the same period extensive research has been performed on application of the process of electroslag welding in fabrication of large-sized items of up to 80 t weight of the type of stems, rudder pins, ship shafts, etc. Electroslag welding turned out to be especially effective in fabrication of large-sized parts of cast-welded structures. It can be said that by 1960 investigations of SAW processes had been completed, and they became quite widely introduced at that time already, while the technical capabilities of mechanisation of structure welding by applying SAW processes, had been practically exhausted.

Figure 4 shows the dynamics of introduction of consumable electrode electric arc welding processes in shipbuilding.

The ability to widely apply the above technologies in production was fortified by development of the necessary welding equipment. Over a relatively short period PWI developed a family of special and all-purpose welding tractors and units (TS-11, TS-12, TS-13, TS-15, TS-17, TS-17M, IS-17MU, DTS-24, TS-32, A-433, PSh-5, PSh-54, etc.).

A considerable assistance was rendered by the staff of this Institute and its director, academician E.O.Paton to the factories of this industry in introduction of advanced welding processes, especially during its mastering in the enterprises located in the south of the country [6, 7].

Leningrad «Elektrik» Factory, and later on also VNIIESO, developed a broad range of equipment for arc and resistance welding that is extensively applied in shipbuilding factories.

By 1970 the problems of the technologies of mechanised processes of welding the shipbuilding structures had been solved. The created range of welding technologies and equipment allowed fabrication of any welded ship structures.

In construction of welded ships in this period top priority was given to the issues of improvement of welding efficiency at different stages of ship construction.

Construction of large tonnage ships and application of large-sized steel sheets for ship hulls, as well as developments in the field of integrated automation of ship hull structures fabrication, posed a number of tasks for the welding production, related to the need to develop new effective welding technologies, among which primarily is automatic one-side welding of flat panels with weld formation from two sides (without tilting the panels).

In 1969 – 1970 the technology, «Mir» automatic machine and benches for automatic welding of butt joints up to 32 mm thick on a flux-copper pad were created, and in 1973 the technology and «Brig» automatic machine for welding on a sliding copper shoe were developed [3].

For welding the framing of main orientation to the panels, in 1974 – 1976 welding-assembly units were developed that perform pressing of the framing to the panels, reverse bending in the weld area and simultaneous welding of the framing from both sides, as well as positioning of four stiffeners from two sides for their simultaneous automatic welding on by eight welding heads.

The technology of multi-head automatic SAW with AN-65 flux (PWI development) was proposed in order to improve the efficiency of welding in fabrication of flat sections in integrated mechanisation lines. The technology envisaged performance of butt joints of the panels by two welding heads from two sides making single-pass welds on a flux-copper backing or a flux pad with the welding speed of 85 – 90 m/h and of T-joints of the framing with the panel by twin-arc welding heads from two sides of the framing simultaneously with the welding speed of up to 80 m/h.

Improvement of welding technology, welding consumables and welding equipment for automatic one-side welding of flat panels without tilting them, should be regarded as major developments in this field. Backing flux AN-80P for the variant of welding on a flux-copper backing was developed in co-operation with PWI (1980).

In 1981 TsNIITS developed the technology of automatic welding from both sides of butt joints of flat panels without tilting them, which envisages downhand welding by automatic submerged-arc process, and a backing run from the reverse side in the overhead position by automatic CO_2 welding with thin wire.

An essential drawback of the technologies of automatic SAW from one side with weld formation from two sides, is production of welds from both sides with large variations by the width and height of the convexities. This is largely dependent on the fit-up operations during structure assembly.

When fit-up operations are performed, the purpose is to ensure such a gap in the joint, which eliminates the possibility of formation of a burn-through or lack-of-penetration in welding, and insufficient attention is given to the produced dimensions of structural elements of edge preparation for welding. As a result, cross-sectional areas and groove volumes to be filled in welding, respectively, vary greatly in different sections of the joint, this, in combination with variations of the welding mode, leading to significantly different geometrical dimensions of welds that often go beyond the tolerance limits.

TsNIITS performed studies to establish the admissible deviations of the gap and groove width, at which the specified weld dimensions can be provided. The rationality of development and application of automatic control of welding mode parameters to produce welds of required dimensions was established [8].

In welding, deviation from the specified values of welding current, arc voltage and welding speed towards larger or smaller values, as well as variation of gap sizes, groove angles, toes, etc. in the joint assembled for welding lead to a situation where, on the one hand, the welded joint needs a greater or smaller volume of deposited metal to fill the actual groove, and, on the other hand, the actual welding mode will provide a larger or smaller volume of the deposited metal. This results in the conditions under which the dimensions of the weld convexity after welding have inadmissible deviations from the specified values.

Therefore, the main requirement that should be met by a welding technology with program control, is provision in welding of a variable (required) volume of the deposited metal in different sections of the joint along its length, so that the dimensions of the weld convexity (or weld leg) did not go beyond the values established by the standards, despite the possible variations of the welding mode parameters and structural elements of the joints assembled for welding.

Thus, the volume of the deposited metal is the main controllable parameter of programmable technology of automatic welding that directly influences the weld quality. It follows from the above said that in order to produce welds of the required quality, it is necessary to apply the technology of consumable electrode electric arc welding and CNC welding

equipment that should meet the following requirements:

• automatic selection of welding current, arc voltage and welding speed, depending on metal thickness and joint type, according to the current standards;

• automatic maintenance during welding of the process mode, established in keeping with the standards, its correction at variation of the mains voltage, dimensions of structural elements of edge preparation in the joint, etc.;

• automatic direction of the welding arc along a specified trajectory with the required accuracy;

• automatic switching on of welding flux or shielding gas feed prior to the start of welding and its switching off after welding is over, and flux removal during welding.

Technologies of consumable electrode electric arc welding meeting the above requirements, should be called computer-controlled or CNC automatic technologies (Figure 5).

For optimising such a technology, a mock-up of CNC automatic machine of «Mir-3P» type and welding from one side of flat panels of up to 20 mm thick metal and length of 10 m with weld formation from both sides on a flux-copper backing were developed.

Panel fabrication is envisaged in the appropriate positions of the flow line. Welding of up to 1.6 mm thick joints is performed by one arc, and that of thicker joints — by two arcs simultaneously.

SAW is performed at direct current supplied from power sources of two types VDU-202 or VDU-1201 at currents of 300 – 1200 A and arc voltage of 28 – 46 V with of 2 – 5 mm electrode wire and flux OSTs-45 or AN-348.

Welding unit (moving over a gantry) belongs to suspended type with two sequentially located heads with CNC system and system of following the direction of the welding arcs movement along the butt. The first welding head in the direction of movement, is designed for welding with one wire, and the second — for welding with a split electrode.

CNC unit software allows the automatic machine to perform work in the automatic, mechanised (manual), correction and reference modes.

Program control system was evaluated by comparing the quality of weld formation with the switched on or switched off system of automatic control of the welding process.

Statistical processing of experimental results in welding the joints of 12 mm thick metal, showed that the geometrical parameters of welds performed with the switched on and switched off automatic control system, are within the tolerances, i.e. no correction of the main parameters of the welding process was required, but stabilisation of the process with program control resulted in production of smoother beads, both from the face and the reverse side, smoother transition

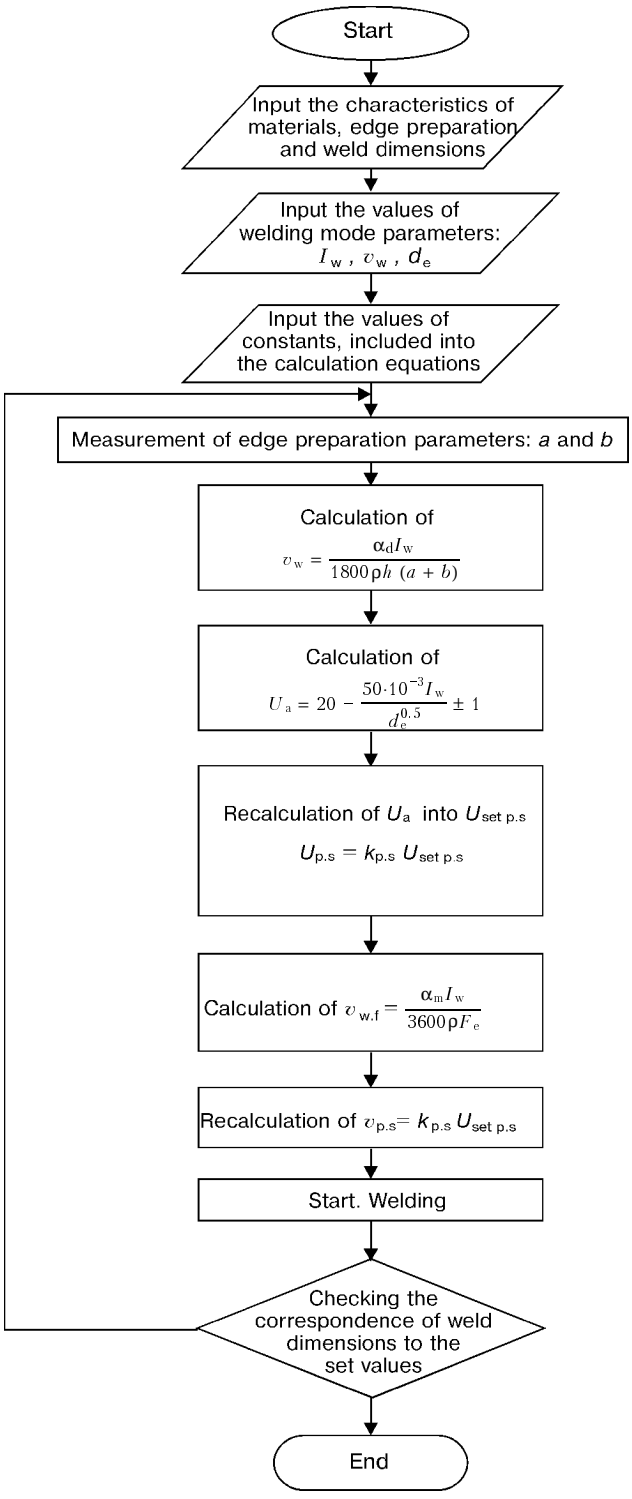

Figure 5. Block diagram of an algorithm for automatic consumable electrode SAW with CNC

from the weld to the base metal, smaller variation of the weld convexity width and height.

In twin-arc welding of joints on up to 20 mm thick metal without automatic control of the welding process, the welds are characterised by greater variation of weld convexity width and height, especially from the reverse side of the joints. Incomplete filling of groove and undercuts are found on some of the macrosections. When the system of automatic control

Material	Element content, wt.%								
	C	Mn	Si	Cr	Cu	Ni	S	P	Fe
St.3	0.14 – 0.22	0.3 – 0.6							Balance
St.4	0.2 – 0.3	0.35 – 0.65							Same
St.5	0.28 – 0.38	0.3 – 0.6							»
20G	0.17 – 0.24	0.7 – 1.0	0.17 – 0.37						»
10KhSND	≤ 0.12	0.5 – 0.8	0.8 – 1.1	0.6 – 0.9	0.4 – 0.65	0.5 – 0.8			»
15KhSND	0.12 – 0.8	0.4 – 0.7	0.4 – 0.7	0.6 – 0.9	0.2 – 0.4	0.3 – 0.6			»
10KhSN2D	≤ 0.2	0.5 – 0.8	0.8 – 1.1	0.6 – 0.9	0.2 – 0.4	1.4 – 2.0			»
08-GN	< 0.08	0.8 – 1.2				0.9 – 1.2			»
UONI-13/NZh2	≤ 0.06	1.0 – 2.0	0.5 – 1.0	18.0 – 22.0		7.5 – 10.0	< 0.018	< 0.025	

of the welding process is switched on, the above weld defects are absent.

Production trials of the above welding technology confirmed the earlier derived results.

CONCLUSIONS

1. The process of consumable electrode SAW developed by PWI, had a considerable impact on advance of science and technology in various industries.

2. Extensive application of automatic and mechanised SAW in shipbuilding allowed effective construction of high-quality modern ships and vessels with hulls made of various grades of hull steel.

3. PWI, TsNIITMASh, «Elektrik» Factory, alongside with TsNIITS, made a great creative contribution to development and improvement of the technology of SAW of hull steels and welding equipment.

REFERENCES

1. Belchuk, G.A. (1951) On history of electric arc welding development in local shipbuilding. *Transact. of LKI*, Issue 9, 15 – 23.
2. Golovchenko, V.S., Shraerman, M.R., Abramovich, V.R. *et al*. (1964) Development of welding in shipbuilding. *Sudostroyeniye. Tekhnologia Sudostroyeniya*, **5**, 40 – 43.
3. Golovchenko, V.S., Kazimirov, A.A., Matskevich, V.D. *et al*. (1981) Welding in shipbuilding. In: *Welding in the USSR*. Moscow: Nauka.
4. Vologdin, V.P. (1931) Construction of the first arc-welded launch in Dalzavod Factory in Vladivostok. In: *Coll. of Papers on Electric Arc Welding in Automotive Industry, Aircraft Construction and Shipbuilding*. Moscow: Gostekhizdat.
5. Mushchenko, D.A. (1933) Electric arc welding in river shipbuilding in the 2nd Five Year Plan period. *Morskoye Sudostroyeniye*, **6**, 18 – 21.
6. Paton, E.O. (1944) *Automatic welding in shipbuilding*. Moscow: Oborongiz.
7. Kazimorov, A.A. (1951) Automatic welding in river shipbuilding. In: *Coll. devoted to 80th anniversary of E.O. Paton*. Kyiv: AN Ukr.SSR.
8. Gorbach, V.D., Golovchenko, V.S., Stegantsev, V.P. (1999) Automatic control of the mode of SAW of steel panels. *Vestnik Tekhnologii Sudostroyeniya*, **5**, 11 – 15.

TECHNOLOGY OF LASER SURFACING AND TREATMENT OF COMPONENTS OF ROLLING STOCK WHEELSETS

I.D. KOZUBENKO[1], **V.Yu. KHASKIN**[2] and **V.D. CHERNIENKO**[2]
[1]East Siberian Rail Road, Irkutsk, Russia
[2]The E.O. Paton Electric Welding Institute, NASU, Kyiv, Ukraine

ABSTRACT

The importance of solving the problems of strengthening of roll surfaces of wheels is shown. Drawbacks of traditional repair technologies intended for reconditioning of necks of axles of railway car wheelsets are considered. The use of laser surfacing and heat treatment is suggested. Example of experimental-commercial implementation of recommended laser technologies in the Irkutsk-«Sorting» car depot (ESRR, Russia) is described.

Key words: *laser surfacing, heat treatment, restoration, strengthening, laser complex, railway transport, rolling stock components, optimization of technology*

During service of the railway transport the components of the rolling stock are changed due to wear or appearance of different kinds of troubles. This results in necessity of using technologies of diagnostics and repair. Therefore, the problem of restoration and repair of undercarriage of railway cars is actual [1].

One of subassemblies of the car undercarriage, which is operating under most complicated conditions, is a wheelset. Its axle is subjected constantly to the action of high static and dynamic loads. In addition, it undergoes additional compression stresses in points of load-carrying joints with wheels and takes shocks from rails in presence of defects at the roll surface of wheels and at junctions. Different technological violations in manufacture and treatment influence the axle serviceability. Combination of a number of factors causes the initiation of local stresses in the axle which lead, together with fatigue phenomena, to the crack initiation. The depth of a defective layer in axle necks is usually about 0.1 – 0.3 mm per diameter.

In restoration of axle necks it is necessary to grind (to bore) necks preliminary for the size which is smaller than the rated size by 0.4 – 0.5 mm per diameter and then to perform surfacing with a tolerance for a final mechanical treatment and to grind finally to the rated size. Such defects of the deposited layer, as cracks, cavities and pores are inadmissible. The hardness of the deposited layer should be *HRC* 30 – 35.

Traditionally, the car parts were restored using the methods of arc or flame welding and surfacing (manual arc, automatic and mechanized submerged arc and shielded-gas, plasma arc, gas welding, etc.) [2]. The drawbacks of the above-mentioned methods are a large (above 1 mm) tolerance for a finishing mechanical treatment and high preheating of the part to be surfaced that can influence negatively on its shape and sizes after cooling. In addition, the material of the wheelset axle (steel 60) (C — 0.57 – 0.65; Mn — 0.5 – 0.8; Si — 0.17 – 0.37 wt.%; Fe — balance) is difficult-to-weld. It is not recommended for use in arc welding and surfacing [3]. Therefore, from our point of view, it is rational to use the laser surfacing with a continuous radiation of the CO_2-laser for restoration of necks of the car axles to eliminate the mentioned drawbacks [4].

Taking into account the peculiarities of the parent metal of the railway car axles it is recommended to use the powders of Ni-based self-fluxing alloys for the laser surfacing of the necks. The technology of surfacing these materials is described in detail in [4].

At the E.O. Paton Electric Welding Institute the technology of laser surfacing of necks of the car axles was tested on the samples-simulators made from steel 60 using a filler of powder PG-SR2 (C — 0.2 – 0.5; Cr — 12.0 – 15.0; Si — 2.0 – 3.0; B — 1.5 – 2.1; Fe — up to 5.0 wt.%; Ni — balance) providing hardness of approximately *HRC* 40. The following conditions were selected: radiation power — 3.2 – 3.5 kW; surfacing speed — 64 – 72 m/h; diameter of radiation focusing spot — 2.5 – 3.0 mm; mass consumption of surfacing powder — 0.25 g/s. Experiments were also performed using other filler materials. It was established that in the deposited metal the microcracks are formed (5 – 20 μm opening width) whose number, size and periodicity of repetition depend on many factors (for example, on hardness of the layer deposited, chemical composition and granulation of the surfacing powder, nature and rate of heat dissipation). The preheating and a delayed cooling of the part being surfaced are the most efficient and simple methods of the crack prevention.

In the railway car depot Irkutsk-«Sorting» (ESRR, Russia) an experimental workshop of a laser restoration of the surfaces of axles intended for fitting bearings was created in 1966. The equipment included a laser technological installation LOK-3M (fast-flow CO_2-laser of 2.5 kW radiation power), a horizontal rotator M310504 (0.5 – 2.5 min^{-1} frequency of face

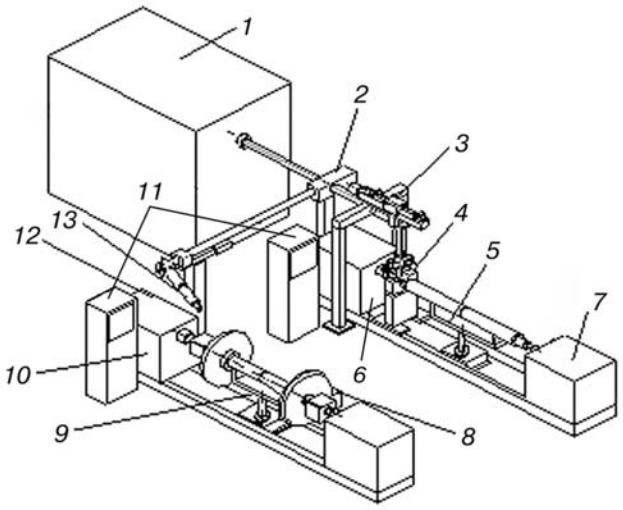

Laser technological complex for surfacing axle necks and heat treatment of roll surfaces of car wheelsets: *1* — technological laser; *2* — unit of distributing mirror; *3* — head for laser surfacing; *4* — device for auxiliary heating; *5, 9* — loading rotating devices; *6* — station of laser surfacing of axle necks; *7, 12* — rotators; *8* — device for deposition of absorbing coating; *10* — station for laser thermal strengthening of wheelsets; *11* — control cabinets; *13* — head for laser strengthening

plate rotation), circular grinding machine-tool of the 3M173 type, a specialized heating unit for heat treatment after surfacing. This workshop could restore monthly up to 360 axles which were rejected earlier to the metal scrap.

In parallel with a restoration of the car axle necks, the actual problem is the increase in a service life of the roll surfaces of wheelsets, i.e. wheel rims. However, this effect should not be accompanied by the decrease in the service life of the rails. Our investigations showed that the best results are provided using an «island» strengthening which creates hard wear-resistant areas of metal in a comparatively soft damping matrix. This strengthening can be realized by using a laser heat treatment (LHT) without fusion which is used as a finishing operation.

At the PWI the technology of LHT of steels without fusion was tested on samples-simulators, including cleaning and degreasing of the surface to be strengthened, deposition of an absorbing coating, LHT proper and removing (rinsing) of remnants of the absorbing coating. Specially-developed water-soluble polymeric coatings, for example, MTsS-510, SG-504, FS-1M are used as absorbing coatings [5]. They possess high (about 80 – 90 %) absorbability and are inexpensive, not toxic, not burning. They do not evolve fumes in laser heating and are easily deposited by a pneumatic spraying, painting by a brush or a roller. In case of using coating MTsS-510 the LHT parameters are as follows: radiation power — 3.0 – 3.2 kW; width of a hardening path — 9 mm; speed — 60 m/h. The depth of LHT path is 0.7 – 0.8 mm, the surface is not subjected to fusion. To achieve the effect of «island» strengthening at the wheel rim, fillet and a part of the flange, it is necessary to use scanning which provides the saw-shaped path of strengthening.

The strengthened samples were tested for a wear resistance by the method of a «dry» friction in a specially-designed machine using a cylinder-pin scheme. Mating bodies were manufactured from steel 45 (C — 0.45 wt.%; Fe — balance) with a next hardening to about *HRC* 55 hardness. The specific pressure was in the 10 – 16 MPa range, frequency of rotation of the test sample was 50 – 1600 min^{-1}, linear rates of friction — 1600 – 54000 m/h. The wear of samples was measured by a change in diameter using a micrometer with 0.01 mm division of scale, and also by changing the mass in weighing using scales of MTZ No.265 type (1965) with error ± 10 mg. To improve the accuracy of measurements the friction duration was extended. The test results showed that the wear resistance of the strengthened samples exceeds that of samples made from a material of a standard car wheel by 2 – 3 times.

On the basis of results and also the experience of service of a complex for restoration of axle necks (Irkutsk city) the decision was taken about the development and designing of an industrial complex for a laser restoration of axle necks and strengthening of roll surfaces of the railway car wheelsets. The Experimental Design Technological Bureau of the PWI has designed a complex (Figure), which includes a technological laser *1* of 5 kW radiation power (for example, «Pluton-5» [5]), two stations for laser treatment *6* and *10*, a system of transportation and focusing of a laser radiation, system *11* for control of stations *6* and *10*.

The complex is operating in a semi-automatic condition, i.e. loading, fixing and unloading of the parts are performed with the help of transport means of the workshop, while the other technological operations are automatic. Just before the beginning of the work the laser *1* is switched on and set for a required condition, covering preliminary the path of radiation by a gate-ticker. Further the supply and interruption of radiation are made by a mechanical displacement of the gate. The car axle, prepared for surfacing (cleaned and degreased) is mounted at the station *6*. For this purpose the device *5* is turned normal to the axis of the station, and the axle, heated in the furnace to ≈ 300 °C, is lowered by a single-rail overhead travelling crane, the device *5* is placed in the position shown in the Figure and fixed, the rotator *7* centers are put under and the axle is clamped by them. Then, the device for auxiliary heating *4* is placed near the neck to be surfaced and switched on. The axle is set into rotation, the head *3* is put into initial position, the level of the surfacing powder in the head hopper is checked (if necessary, the powder is added), the powder feeding and laser radiation are switched on and the surfacing process is started.

It should be noted that the device *4* represents a two-half reflector with vacuum-arc tubes (by 5 tubes of 2 kW capacity each), which embraces the axle neck from both sides. The upper part of the reflector is made

open to have a free access of a laser radiation and filler powder to the surface being deposited, and also to have a feasibility of visual inspection of the surfacing process. This device maintains a constant temperature of preheated neck during the whole process.

The rotating device *5* can reset equipment quickly after completion of surfacing of one neck for the surfacing of the another neck. The ready part is unloaded in a reversed sequence. The loading and unloading of the wheelsets at the station *10* is performed similarly. The difference in preparation for LHT at this station consists of deposition of an absorbing coating on the strengthening surface of the wheel using a device *8* representing a pneumatic sprayer of the absorbing coating solution and a fen for its drying. Head *13* of the station *10* has a mechanical scanner which makes it possible to produce the LHT of roll surfaces both in saw-like and spiral way.

REFERENCES

1. (1988) *TsT/4351*. Instruction on formation and maintenance of wheelsets of tractive rolling stock of railways of 1520 mm wheel track. Moscow: Transport.
2. Bogdanov, A.F., Chursin, V.G. (1985) *Service and repair of car wheelsets*. Moscow: Transport.
3. Sorokin, V.G., Volosnikova, A.V., Vyatkin, S.A. *et al.* (1989) *Handbook of grades of steels and alloys*. Moscow: Mashinostroyeniye.
4. Velichko, O.A. (1990) Laser strengthening and surfacing of idustrial products. In: *Transact. of PWI on New Processes and Equipment for Thermal and Vacuum Coating*. Kyiv: PWI.
5. Abilsiitov, G.A., Golubev, V.S., Gontar, V.G. *et al.* (1991) *Technological lasers*. Handbook. Moscow: Mashinostroyeniye.

PECULIARITIES OF FORMATION OF MACROINCLUSIONS OF OXIDE FILM IN WELD METAL OF ALUMINIUM ALLOYS (REVIEW)

A.G. POKLYATSKY
The E.O. Paton Electric Welding Institute, NASU, Kyiv, Ukraine

ABSTRACT

The effect of quality of manufacture and preparation of materials to be welded and a filler wire and also conditions of assembly and welding of joints on the appearance of macroinclusions of an oxide film in the weld metal during welding advanced aluminium alloys is considered. The regularities of formation and location of defects in weld section depending on the causes of their initiation are described. The conditions which contribute to the oxidizing processes and reduce the effectiveness of the cathode destroying of the oxide film in the zone of welding are analyzed. Peculiarities of formation of thread-like longitudinal inclusions of oxide film in the weld central part during welding Li-containing alloys are defined.

Key words: *argon-arc welding, high-strength Li-containing alloys, aluminium alloys, macroinclusions of oxide film, thread-like longitudinal oxide inclusions*

Inclusions of the oxide film are one of the defects which is most widely observed in a non-consumable arc welding of aluminium alloys [1 – 3]. The quality of manufacture and preparation of surfaces of materials welded and a filler wire, and also conditions of assembly and welding of joints influence greatly the initiation of oxide inclusions in the weld metal. The presence of laminations and discontinuities in the parent metal or its increased gas saturation can cause the appearance of macroinclusions of the oxide film in the weld metal [4]. With moving flows of the weld pool molten metal these defects can move all over its volume and remain in the weld metal in the form of coarse oxide films and pores (Figure 1, *a*).

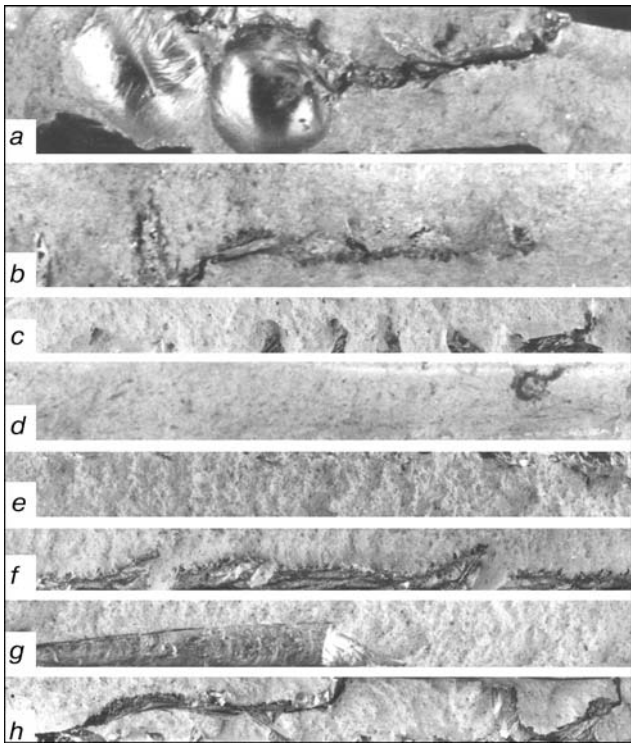

Figure 1. Inclusions of oxide film in fractures of aluminium alloy welds made by argon-arc non-consumable welding. They are caused by an increased content of gases in parent metal (*a*); organic impurities of edges to be welded (*b*); insufficient cathode destroying of initial oxide film at the edge surfaces (*c*); presence of defects (overlaps) in filler wire (*d*); higher temperature of filler melting as compared with that of parent metal (*e*); injection of air through the gap formed in the butt (*f*); arc shifting from the butt center (*g*) and several factors simultaneously (*h*)

Non-quality preparation of edges to be welded leads, as a rule, to the appearance of oxide inclusions in welds [5 – 8]. Organic impurities at the workpiece surfaces are decomposed actively during welding, thus reducing the effectiveness of the heating zone protection with an inert gas. Here, the oxygen compounds are evolved promoting the aluminium oxidizing in the welding zone. The presence of hydroxyl groups in the film composition or moisture absorbed at its surface also promote the activation of the oxidizing processes and appearance of the oxide film in the weld metal (Figure 1, *b*).

The oxide films locating at the edge surfaces are most hazardous [6]. The cathode cleaning is most effective only in the upper part of the butt. Its lower part does not experience the direct arc action. The oxide films, locating there, can be fragmented and escape to the surface only by the moving metal of the weld pool. However, due to a high specific weight of oxide as compared with that of the molten aluminium, only thin fine film inclusions can escape. Most inclusions of the oxide film are remained during the weld solidification in its lower part (Figure 1, *c*).

The probability of occurrence of oxide inclusions in the weld is increased in using the filler wire [8] and depends on the conditions of its feeding to the welding zone [5, 9]. The organic impurities and adsorbed moisture at its surface bring a large amount of oxygen compounds, thus increasing the oxidizing

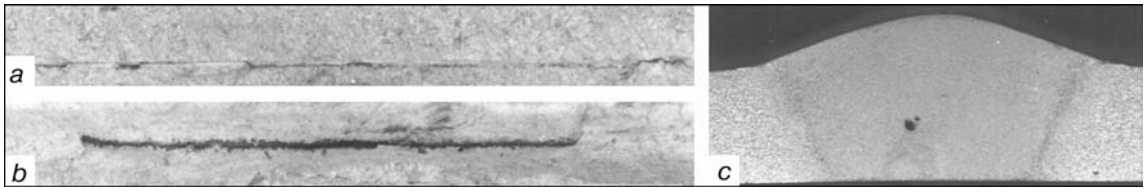

Figure 2. Extended thread-like inclusions of oxide film in fractures of welds (*a*, *b*) and in transverse macrosection (*c*) formed in argon-arc non-consumable welding of Li-containing aluminium alloys

processes in the weld pool. The filler is fed usually to the front part of the weld pool (by a slight contact of the upper cut of the edge in the butt center). Its periodic displacement from the center leads to a wandering or shifting of the arc to one edge, thus disturbing the cathode cleaning of surfaces welded and, sometimes even to the lack of fusion of the edges. This probability is increased at a high rate of feeding the small-diameter filler wire. This wire has no time in principle to be melted in the head part of the weld pool and hinders the cathode cleaning of the edges welded which are located under it. As a result of this, the separate macroinclusions of oxide film, arranged mainly in its middle and upper parts are observed (Figure 1, *d*).

Unproper selection of the filler wire composition can be a cause of the appearance of the oxide films. In case of using the composition of the filler with a melting temperature, much exceeding the temperature of the parent metal melting, the undestroyed particles of the oxide film are observed in the upper part of the weld metal (Figure 1, *e*).

The conditions of assembly and edge fixation before welding influence greatly the processes of oxidizing of arc-melted metal and a cathode cleaning of edges welded [5, 10 – 12]. Due to uncareful assembly and fixation of the components before welding and distortion of edges from heating, they are displaced and a gap is formed in the butt. This results in creation of unfavourable conditions ahead of the weld pool for the injection of atmospheric air to the edges through the gap. Therefore, the conditions are created ahead of the weld pool for growing the oxide film, including also the edge surfaces. This is promoted by the heat spreading beyond the zone of the inert gas protection. Moreover, as a result of harmonic oscillations of the molten metal it penetrates easily to the gap that leads to an intensive oxidizing of the surface of the molten metal and edges at the points of their contact.

In downward welding the molten metal flowing to the head part of the weld pool decreases the depth of arc penetration to the parent metal, thus reducing the effectiveness of the cathode cleaning of the edges. Non-destroyed oxides form the non-metallic inclusions in the weld metal, which, as a rule, are remained in the lower part of the weld due to a negligible stirring of the weld pool molten metal in a conventional argon-arc welding (Figure 1, *f*).

The presence of a large butt gap increases the probability of arc shifting to one of the edges. This results in a possible formation of oxidized areas of non-fusion in a weld root part (Figure 1, *g*). Here, it is important to provide a perfect protection of the weld zone with an inert gas [13]. The probability of occurrence of macroinclusions of oxide film in welds is increased in a violation of laminarity of shielding gas flow, at its insufficient consumption or unproper selection of sizes and shape of the shielding nozzle. The presence of a condensed moisture at the inner surfaces of pipings for the shielding gas feeding and also in a gun nozzle, as well as application of argon with a dew point above 214 K as a shielding gas can serve an additional source of oxygen [14].

The arc shifting from the butt center influences greatly the formation of inclusions in welds, leading to a non-uniform destroying of the oxide film at the edges welded and the filler wire [5]. The main causes of the arc shifting can be a non-symmetric location of electrode relative to the edges welded; a non-symmetric formation of a crown or a burning-through of the electrode edge during welding; a non-uniform or untight contact of butt edges to the forming backing (especially in thin metal welding); a non-uniform heat removal from both sides of the butt (especially in welding of dissimilar materials and those of different thickness).

It is natural that in welding of structures under the industrial conditions several factors may occur simultaneously, promoting the oxidizing of parent and filler materials, melted by arc, or hindering the effective destroying of the oxide film. This results in formation of branched inclusions of oxide film, different in shape and located almost across all the thickness of the weld metal (Figure 1, *h*).

The oxide inclusions in weld metal of the Li-containing alloys should be especially distinguished. In argon-arc welding of these alloys with a non-consumable electrode using a filler wire the typical thread-like extended oxide inclusions are formed in the weld central part (Figure 2). The causes of appearance of these defects are clarified now, but it has already become evident that the formation of inclusions is due to the use of fillers having a higher temperature of melting than that of the parent metal. This is proved by a full absence of above-mentioned defects in welding without the filler wire and also in case of using the stationary inserts (strips) of metal corresponding in chemical composition to the parent metal.

CONCLUSIONS

1. Macroinclusions of oxide film in welds during welding aluminium alloys are formed due to violation of requirements to the preparation of surfaces of edges to be welded, accuracy of assembly and welding technology.

2. It is possible to reveal the main cause of formation of non-metallic oxide inclusions in welds by their shape and location. In case of insufficiently effective cathode destroying of the oxide film they are arranged close to the upper part of the weld in the form of separate inclusions and have a dark surface, while in case of an excessive oxidizing of metal during welding they are arranged mainly in the weld root part, having a large length and light bright surface.

3. The long thread-like inclusions of oxide film, typical of Li-containing alloys are formed in welds due to insufficient cathode cleaning of the filler surface, which possesses usually higher temperature of melting as compared with that of the parent metal.

REFERENCES

1. Moiseenko, I.G., Stolbov, V.I., Turchenko, M.A. (1968) Oxide inclusions in welding alloy AMg6. *Svarochnoye Proizvodstvo*, **5**, 23 – 24.
2. Moiseenko, I.G., Lukashin, N.V. (1969) About the problem of improving the leak-tightness of AMg6 alloy welded vessels. *Ibid*., **8**, 31 – 32.
3. Lukianov, V.F., Fomin, V.N., Moiseenko, V.P. *et al*. (1970) Effect of oxide inclusions on strength of welded joints of AMg6 alloy pressure vessels. *Ibid*., **6**, 24
4. Erofeeva, M.M., Bykov, V.V., Konkevich, V.Yu. *et al*. (1989) Evaluation of feasibility of using granulated alloy of Al–Zn–Mg sustem in welded prefabrications. *Ibid*., **8**, 19 – 20.
5. Kryukovsky, V.N., Novikov, O.M., Meshkova, O.V. *et al*. (1970) Dicontinuities in weld of AMg6 alloy in presence of oxide inclusions. *Ibid*., **12**, 25 – 27.
6. Oboturov, V.I., Tolkachev, Yu.I. (1973) Some peculiarities of formation and destroying of oxide films in argon-arc welding of aluminium alloys. *Ibid*., **11**, 22 – 24.
7. Stolbov, V.I., Moiseenko, I.G., Lukashin, N.V. (1969) Effect of some technological factors on formation of oxide inclusions in AMg6 alloy welding. *Ibid*., **3**, 26 – 28.
8. Terentiev, I.M., Barutkin, F.E., Konovalov, G.S. (1965) Effect of conditions of aluminium alloy welding on weld metal density. *Ibid*., **10**, 16 – 18.
9. Terentiev, I.M., Slyusarevsky, V.V., Kalinichenko, B.G. *et al*. (1971) Effect of technological parameters of quality of weld metal of AMg6 alloy welded joints. *Ibid*., **4**, 36 – 37.
10. Sushkov, V.N., Skachkov, Yu.N., Novikov, O.M. *et al*. (1975) Susceptibility of light alloys to the formation of oxide inclusions in welding. *Ibid*., **5**, 23 – 24.
11. Skachkov, Yu.N., Novikov, O.M., Mamon, M.D. (1973) Causes of appearance of oxide films on AMg6 alloy welds. *Ibid*., **4**, 27 – 29.
12. Yusufova, Z.A. (1979) About the mechanism of destroying of oxide films in butt during argon-arc welding of aluminium alloys. *Ibid*., **10**, 25 – 26.
13. Skachkov, Yu.N., Mamaev, A.A., Novikov, O.M. (1974) Improvement of quality of AMg6 alloy welds. *Ibid*., **2**, 44.
14. Sushkov, V.N., Kryukovsky, V.N., Zhandarev, A.P. *et al*. (1976) Effect of some parameters of atmosphere of welding shop on the quality of aluminium alloy welds. *Ibid*., **6**, 27 – 29.

EXPERIENCE OF EFFECTIVE COMPUTERIZED DESIGN OF ASSEMBLY-WELDING JIGS

S.V. MEDVEDEV and **D.P. KUNKEVICH**
Institute of Engineering Cybernetics, NASB, Minsk, Belarus

ABSTRACT

Structure and functional capabilities of INSVAR system of CAD of assembly-welding jigs are considered. Examples are given of jigs designed by computerized methods for fitting agricultural machinery with welded structures. Multivariant design allowed the quality of engineering solutions of the jigs to be improved, and the labour consumption in their construction to be reduced almost two times.

Key words: *information technologies, assembly-welding jigs, design automation, part fabrication technology*

New information technologies of design, modeling and production rapidly penetrate into the processes of welding and allied technologies [1]. A number of specialists regard them as the very basis for industrial renovation and maintaining a high level of product competitiveness [2].

The Principal Welding Engineer Department of «Mogilevliftmash» Factory was faced with the task of providing in as short time as possible the required jigs for production of the main load-carrying structures of an agricultural machine. By preliminary estimates, development of devices and benches by the traditional methods would have taken a group of designers 4 to 6 months with participation of a qualified technologist. This time being unacceptable, a decision was taken to apply the technology of CAD of assembly-welding jigs (AWJ) developed in the Institute of Engineering Cybernetics of the NAS of Belarus [3].

At present, AWJ CAD has been brought to the level of a developed software system INSVAR (Russian abbreviation for Tool Kit of Welding Engineer), functioning in IBM PC Pentium II in Windows'95 (98) operating system supported by Auto-CAD v.14 graphics system. The drawings generated by a PC are taken to the peripheral graphic devices of the type of HP6L laser printer and HP450C jet plotter. Figure 1 is a generalized block-diagram of INSVAR system.

In the general case, «Item» block provides entering of the initial geometrical information on the parts of the welded structure being fitted, as well as control assembly of welded assembly elements (WAE) in nominal dimensions. Assembly of parts with deviation of dimensions from the nominal values is also possible for evaluation of the gaps in butts of welded joints. Also used is the information from «Technology» block on the welded structure breakdown into process assemblies of the welded structure, position of assemblies and parts in assembly-welding, and modes of weld performance.

«Statement of work» block enables the engineer-technologist to set forth his requirements to the developed device, giving the following data:

- AWJ type (stationary, rotating or non-rotating);
- type of loading devices drive (manual, mechanical, pneumatic, magnetic, electromagnetic, hydraulic, combined);
- type of AWJ body (plate, frame, beam, frame-beam);
- requirements to weld accessibility for the welding tool (good, satisfactory);
- need to analyze the stress-strain state of WAE in AWJ, allowing for the results of CAD of the latter.

The information on the types (typesizes) of the used tilters, rotators, manipulators, welders' tables and other devices, with which the developed device is fitted, is entered into the «Device operating envi-

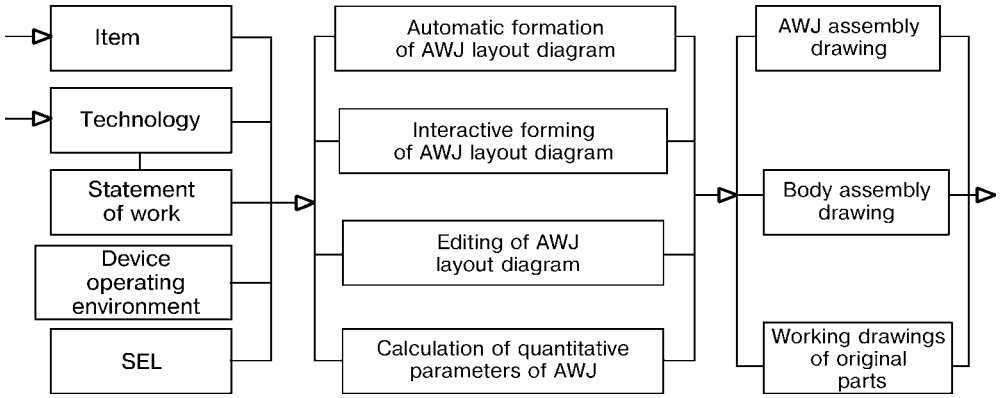

Figure 1. Block-diagram of INSVAR system for CAD of assembly-welding process jigs

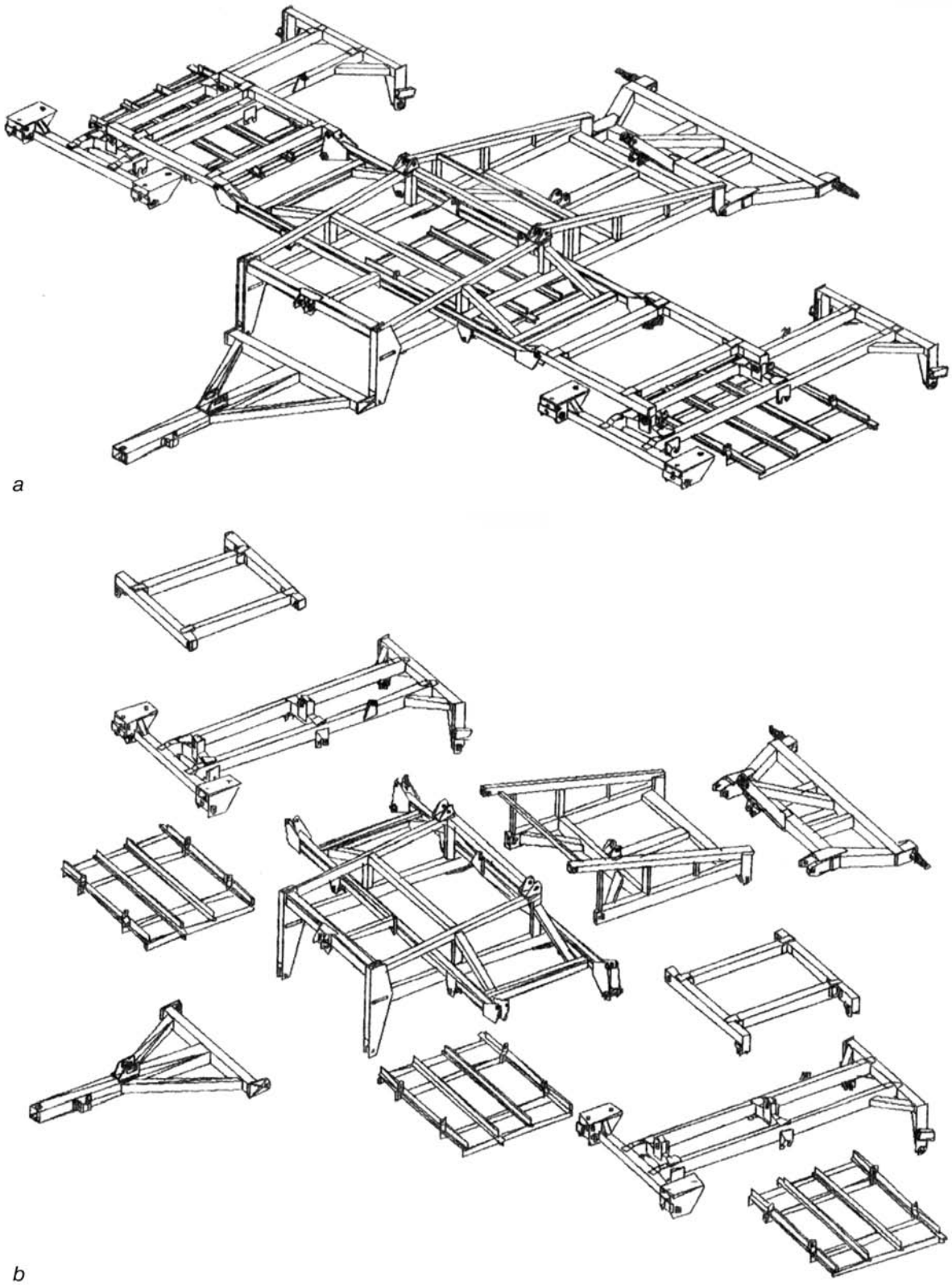

Figure 2. Fitted welded structures: *a* — working position; *b* — assembly sequence

ronment» block. Also indicated is the type of profiles (channel bar, rectangular tube) available in the factory, for making the body of the device, jig or bench.

Over just a month and a half period, the INSVAR system has been used to construct three-dimensional computer models of assembly units and technological assemblies for the welded elements of the item (Figure 2) and develop variants of device and bench designs (Figure 3). The rational variant agreed upon with the engineer-technologist has been brought to the stage of assembly and working drawings. Making the jig elements by such computer-developed drawings using the factory tool stock, demonstrated the high quality of the documentation and practical ab-

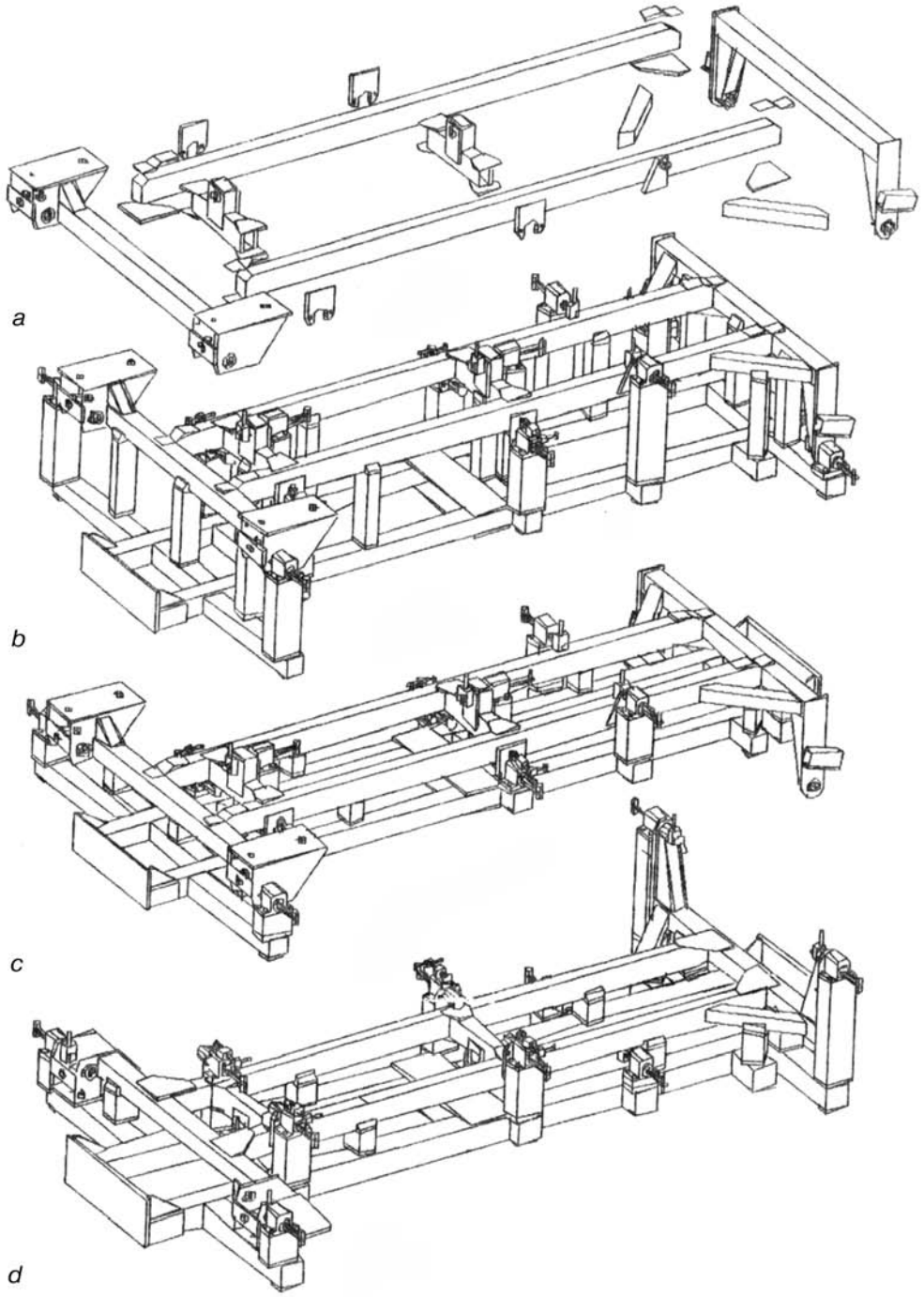

Figure 3. Schematic of welded structure assembly (*a*) and variants of design embodiment of assembly-welding bench with a relatively high (*b*), preferable position of the center of gravity of WAE – AWJ (*c*) and changed position of WAE in welding (*d*)

sence of any errors when reproducing the welded structure geometrical dimensions in the base elements and bodies of the benches.

The total scope of drawings was ≈ 200 sheets of A1 format, generated by one design engineer in one computer with «modest» technical characteristics (clock frequency of 166 MHz, on-line storage of 32 Mb, HDD — 4Gb). By our estimates, the labour consumption for design was reduced by almost two times. However, the main positive features of AWJ CAD are found in other aspects.

Firstly, when three-dimensional models of parts were constructed from plane projection drawings, control assembly was performed and design deficiencies were removed. The breakdown of the main WAE into technological assemblies, was also determined more precisely at this stage.

Secondly, the same basic schematic was used to design several variants of the devices, this being practically impossible with the traditional procedure in view of the lack of time. A number of quantitative characteristics for each design variant have also been determined: AWJ weight; production area occupied by AWJ; surface area protected from molten metal spatter; unification factor of the device components; coefficient of effectiveness of heat removal from the

welds into the body elements of the device; consumption of standard stock (channel bar, rectangular tubes) for making the AWJ body; three-dimensional coordinates of the position of the center of gravity of the installed WAE, the developed AWJ, as well as WAE–AWJ system; tentative labour consumption and cost of assembly-welding fixture fabrication under the conditions of a particular factory.

The variants were jointly co-ordinated by the AWJ designer and the technologist, who developed the statement of work for the design. The preferable variant was used to evaluate the accessibility of the welds for the welding torch, as well as the convenience of welding performance using computerized dummies of welders.

Thirdly, on rather large benches (25 – 45 rests and clamps around the WAE), the main time saving and quality improvement consist in that the co-ordinates of all the fastener holes of the rests and the clamps are recalculated for the device body automatically and are provided in the form of tables, designed for the coordinate-setting operator of the drilling-boring machine.

The structural element library (SEL) of the system includes more than 700 entries of different rests, locks, pins, and clamps (screw, lever, bayonet, pneumatic and magnetic). Of the latter, the screw clamps were used in the devices and benches, in view of the small production program. Using the same basic schematic without any retrofitting the system can design a variant of the device with pneumatic clamps of the type, size and force specified by the user. SEL is open for entering new ingenious designs of assembly-welding fixture and non-standard equipment. To satisfy the needs of customized and small-scale production, this block incorporates the main elements from the range of all-purpose assembly devices for welding with 12 mm slot.

The engineer-designer of welding jigs is required to efficiently «base» the welded structure, having first co-ordinated with the technologist the assembly-welding sequence and rational position of the item in welding in the jigs. The preliminary variant of AWJ three-dimensional model is formed in the automatic mode, taking into account the information received from the «Statement of work» block.

Visual assessment of the design variant, alongside with its quantitative characteristics can be followed by the change of the design as regards the types and sizes of the structural elements, types of bodies and respective materials.

To produce a co-ordinated rational variant of AWJ, assembly drawings of AWJ with the specification are generated in the automatic mode, as well as of the device body on several sheets with appended tables of fastener hole co-ordinates on the body.

The experience of such an effective computer-aided design of the welding jigs in a short production time once more confirmed the effectiveness of the developed methods of interactive-algorithmic synthesis of the objects of technological preparation for welding production. In our opinion, the technology of CAD of welding jigs can meet the requirements to AWJ both for the robotic [4] and for the traditional technological processes.

In further work we believe it is rational, it addition to improvement of design algorithms and programs, to provide the capabilities for analysis and evaluation of the stress-strain state of WAE in the device [5], as well as a gradual transition from the traditional forms of process documents to the graphic forms [6].

CONCLUSIONS

1. Multivariant CAD of process jigs and benches for frame welded structures has provided a real shortening of the development period two times and essentially improved the quality of the documentation.

2. Currently, there is a need for development and introduction of computer systems that combine the capabilities of design of assembly-welding processes, as well as of the jigs and non-standard process equipment.

REFERENCES

1. Makhnenko, V.I. (1994) Computerization of engineering activity in welding and related technologies. *Svarochnoye Proizvodstvo*, **5**, 31 – 34.
2. Davydov, Yu.V., Zlygarev, V.A., Koncheev, L.K. (1998) Information technologies — a basis for renovation in the Russian industry. *Inform. Tekhnologii v Proektirovanii i Proizvodstve*, **1**, 55 – 59.
3. Medvedev, S.V., Rakovich, A.G. (1997) CAD of assembly-welding jigs. *Avtomaticheskaya Svarka*, **7**, 33 – 38.
4. Korshenko, E.A., Zvorykin, N.O., Gaevsky, O.A. (1998) Experience of integrated production-technological solution for assembly and robotic welding of a three-dimensional structure. *Ibid.*, **6**, 11 – 15.
5. Kiselev, S.N., Aksenov, Yu.N., Smirnov, V.Yu. *et al.* (1995) Program-procedural support and analysis of stress-strain state of complex welded structures. *Svarochnoye Proizvodstvo*, **3**, 26 – 30.
6. Medvedev, S.V. (1998) Generation of welding process documents. *Ibid.*, **5**, 37 – 40.

IMPROVEMENT OF TRANSFORMERS FOR MANUAL ARC WELDING

I.I. ZARUBA, V.V. ANDREEV and **V.V. DYMENKO**
The E.O. Paton Electric Welding Institute, NASU, Kyiv, Ukraine

ABSTRACT

The advantages of thyristor control of welding transformers are considered. It is demonstrated that pulse stabilization of arcing in a thyristor-controlled transformer greatly expands its welding-technological capabilities and applications. A transformer of this type developed in PWI provides a smooth adjustment of the operational mode, «hot» and «cold» start, welding current modulation with an adjustable frequency. It can be used in AC and DC electrode welding.

Key words: *arc welding, welding transformer, welding generator, thyristor regulation, welding current modulation, arcing stabilization device, technological properties of welding power sources, metal spatter*

The earlier anticipated wide and fast ousting of traditional arc welding power sources by inverter rectifiers actually took longer and did not become an all-embracing process. This is true not only for our country, but also for other industrialized countries of the West. In this paper we do not analyze the causes for this phenomenon, not do we have any doubt about a number of advantages of inverter welding power sources, and the prospects for their practical application. We will just indicate that the simplicity and reliability of a welding power source in many applications remain, and, probably, will still remain for a long time some of its main quality characteristics and the base for selection of its type. With the currently available components, the inverter power sources have a limitation on current. For powerful welding rectifiers with the rated current $I_r > 1000$ A, application of traditional circuit solutions is preferable for reliability and cost-effectiveness reasons. There is no doubt, also, that introduction of inverter power sources was a kind of challenge for the regular welding transformers and rectifiers, quite acutely raising the issue of their future. This «challenge» gave an impetus to improvement of the traditional welding power sources. A good example of it are a number of PWI developments for improvement of transformers for consumable and non-consumable electrode arc welding.

It is known that welding transformers still belong to the most widely accepted power sources for arc welding. The simplicity and reliability of their design, as well as their servicing, maneuverability, rather high efficiency, good technological properties quite often make them beyond comparison with other kinds of similar equipment. Among the technological advantages of welding transformer application, primarily, is the absence of magnetic blow that often becomes an almost unconquerable «vice» of DC arc welding. Also valuable is the process of the item cleaning from oxide films in AC non-consumable electrode welding of aluminium and its alloys in inert gases and mixtures.

Insufficient arcing stability at 50 Hz is now successfully overcome by applying the arcing stabilizers (AS) — pulse generators that provide a reliable re-ignition of the arc at polarity reversal in welding [1]. Availability of the modern semi-conductor elements allowed AS to be brought to a high degree of perfection — they are comparatively inexpensive and small-sized, and fit easily into the casing of any transformer [2]. When the welding transformer operates in an open-circuit mode, AS automatically switches off. In view of these advantages, the transformers with AS in terms of their welding-technological capabilities can completely substitute the welding rectifiers in welding with coated electrodes of practically any grades, both for alternating and direct current. AS application allowed the effective value of open-circuit voltage $U_{o.-c}$ in welding transformers to be reduced to 45 V. Consumption of active materials used for transformer fabrication, its weight and overall dimensions were reduced and its efficiency was improved [2].

As shown by experiments [3], in welding with AS $U_{o.-c}$ value of the welding transformer can be reduced to 36 V. In this case, however, not just its amplitude value U_{max} is reduced, but also the rate of rise of the instantaneous voltage to the level of ignition voltage, which cannot be regarded as favourable in terms of improvement of the process stability. In addition, with a set rated current the external volt-ampere characteristic becomes stiffer, short-circuit current rises, angle of phase shift between $U_{o.-c}$ and I_w becomes smaller, this being also undesirable, both in terms of stable arcing and for technological considerations (for instance, metal spatter becomes more intensive).

Improvement of welding transformers is related to transition from the mechanical and electromechanical regulation of the operational mode to semi-conductor or electronic control. One of the major advantages of such a control, is the operating speed. This enables expansion of the range of technological tasks, also in terms of dosed heat input into the weld pool, as well as purposeful impact on metal transfer.

Known are welding transformers with the devices for thyristor control of the operating mode, the so-called thyristorised transformers that operate by the principle of phase regulation of current. The controller consists of two thyristors, in anti-parallel connection and a system of phase-pulse control. However, TDFZh-1002, 2002 type transformers designed as such a circuit, generate intermittent current in the secondary (welding) circuit, this being highly undesirable in terms of the process stability. Nonetheless, in SAW with powerful hidden arcs, when the molten metal pool reliably insulated from the environment, has a great heat inertia, a quite stable process is achieved, despite a periodical interruption of the current in the circuit. This, however, is practically unachievable in welding with less powerful open arcs (with coated electrodes or gas shielding).

In this case we have to resort to the method of the so-called periodical powering of the arc from an auxiliary low-power source. Despite the different variants of periodical powering [4], the essence of all these methods is reduced to filling the pauses in thyristor control by small current that maintains the normal welding process. It is known that in order to maintain the arcing in coated-electrode manual arc welding it is sufficient for the value of current in the pauses to be in the range of 10 – 15 A.

Use of periodical powering can also promote a lowering of $U_{o.-c}$ of the main welding transformer. In this case, however, one should not ignore such an important factor as electrode metal transfer in the discharge gap. Violation of the stability of AC welding process is related not so much to current polarity reversal, as to the moment of the drop separation during its half-period. Especially dangerous are large drops, separating from the electrode during the dip of the welding current sinusoid. Such drops can deionize the arc column so much that after polarity reversal it will not re-ignite, and the process will be interrupted [5].

Taking it into account, PWI developed AS that feed into the discharge gap an energy pulse not only at polarity reversal, but also at any moment of the arc extinction, as a result of its elongation, an abrupt drop of current or for other reasons. These measures provide a quite high stability of the process in a broad range of welding modes. Testing confirmed the rationality of applying such AS in phase regulation of the transformer current.

Experiments showed that large drops fall into the molten metal pool predominantly at the end of a half-period during the current sinusoid dip, when electromagnetic forces are decreased to a minimum and the forces of gravity and surface tension prevail. Metal transfer is quite often accompanied by short circuits of the discharge gap [6], that being extremely unfavourable for the thyristor-controlled transformers. If switching on of the thyristor key at polarity reversal and power source transition to the operating mode coincides with short circuiting of the arc gap, the current in the circuit is abruptly increased, causing an explosion of the bridge between the drop and the molten metal pool. The drop is ejected beyond the weld. Metal losses are abruptly increased — spatter may exceed 30 – 35 %, this being absolutely inadmissible for technological reasons. In this case, one should try to make the current minimal during the bridge explosion, as far as possible. At short circuiting caused by metal transfer, the pilot current mode should be on for a longer time, and switching to the operating mode should only be performed after the molten bridge breaking up. This algorithm should form the basis of the circuit of thyristor commutator control.

Thus, in development of thyristor transformers with AS two additional requirements are introduced that must be satisfied by the control system:

- AS switching on and energy pulse feeding into the discharge gap for the arc reignition must be performed not only at polarity reversal, but also at any other arcing interruptions during welding;
- at short circuiting due to metal transfer as large drops during the current sinusoid dip, thyristors switching to the operating mode should be delayed up to explosion of the bridge between the electrode and the molten metal pool in the pilot arc mode.

It is natural that thyristor control allows performance of a whole number of other adjustments that may be required for various technological processes. They expand the welding-technological capabilities of the transformer, even though they are optional features.

The external volt-ampere static characteristic of a thyristor-controlled power source with periodical powering has two branches. One of them corresponds to the main power transformer and has a rather low open-circuit voltage (45 – 50 V) and a rather high short-circuit current $I_{sh.-c} = (1.5 - 1.8)I_r$. The second corresponds to operation of an auxiliary transformer that can be made in the form of an individual component or additional winding of the main power transformer with $I_{sh.-c} = (0.1 - 0.3)I_r$. For both branches the total open-circuit voltage is equal to 70 – 80 V.

When auxiliary transformer is designed as a separate component, the primary windings of the main and auxiliary transformer are connected to the same phases of the power mains. The secondary winding of the main transformer is connected in series with a chain that consists of the secondary winding of the auxiliary transformer and a thyristor controller connected to it in parallel. The electrode and the item are connected to the secondary circuit output. Thus, the main power transformer provides the assigned welding mode, and the auxiliary transformer operates in a time interval when the power commutator is closed, and keeps the pilot arc running.

In the variant of pilot arc powering from the auxiliary winding of the main transformer, the current level is determined by the parameters of this winding and is limited either by the throttle, or by the resistor.

Proceeding from the results of calculations and experiments it is found that in terms of optimizing

the weight of the entire power source, the first variant of the thyristor transformer design is preferable at $I_r \geq 250$ A, and the second — at $I_r < 250$ A.

Figure 1 shows the so-called phase trajectory of current — $di/dt = f(i)$ dependence for the power source with the volt-ampere characteristic changing during each half-period. The external branches of this phase trajectory (curves *1*) correspond to arcing in the working mode, and the inner branches (curves *2*) — to pilot arc running. In the second case di/dt varies only slightly at the start and end of each half-period.

PWI developed thyristor-controlled welding transformers that have extensive functional capabilities. Among them are smooth (local and remote) adjustment of welding current in one range, pulse stabilization of arcing, welding current modulation, «hot» and «cold» starts. Such process multifunctionality is provided by the electronic control unit that incorporates special algorithms. They are used to issue to the appropriate components of the control unit the commands for performance of a particular function. These algorithms are implemented as feedbacks by current and voltage of the arc, as well as by the mains voltage. Let us consider in greater detail the operation of the control unit of a new thyristor-controlled transformer.

Stabilization of AC arc running is provided by an energy pulse that comes to the arc gap in each half-period, when the instantaneous value of open-circuit voltage reaches the level of arcing voltage. The algorithm of time $\theta_{p.f}$ of such a pulse feeding will be expressed as follows:

$$\theta_{p.f} = \arcsin (U_a/U_{max} + \pi n),$$

where U_a is the arcing voltage; U_{max} is the amplitude value of open-circuit voltage, and n is the number of current half-periods.

Stabilizing pulses come to the discharge gap, irrespective of its condition at a given moment (whether it is open, shorted by a drop of transferred metal or whether the arc is running). When the discharge gap is closed by a drop of molten metal, the control unit generates a «ban» for opening the power thyristors until the bridge has separated completely at a small current from the auxiliary power source. After the short circuit, the power thyristors open, and the working current is restored. Such a measure, as was noted above, promotes a lowering of metal spatter.

Welding current adjustment is performed by changing the angle of opening of the power thyristors: when they are completely open, the current is maximal, and when they are completely closed, it is minimal. In the latter case, it is determined by the initial parameters of the power and auxiliary transformers.

Welding current modulation is performed by alternative switching on the main (pulse current) and auxiliary (pause current) transformers. The values of these currents are set in advance. The duration of the pause and the pulse varies between 0.05 – 1.00 s.

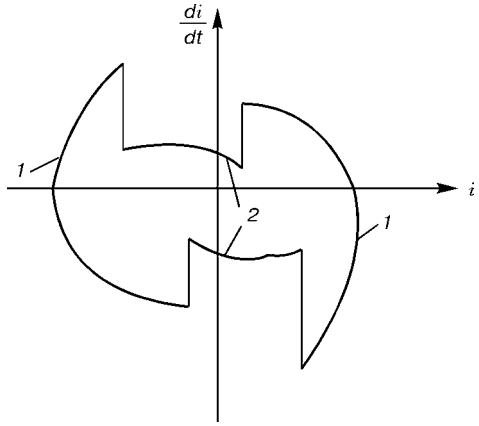

Figure 1. Graph of $di/dt = f(i)$ dependence for one current period ($f = 50$ Hz)

Current rise up to the rated value at the start of coated-electrode metal-arc welding for a reliable initial ignition of the arc — the so-called hot start — is provided by a complete opening of the thyristors for 5 – 10 periods of 50 Hz current when the electrode touches the item at the start of welding.

Current lowering to the minimal value (about 10 – 70 A) at the start of non-consumable electrode welding to avoid burning through the item or electrode erosion because of the initial ignition of the arc at the moment of short circuiting of the electrode to the item — «cold» start — is performed by switching on the pilot arc current for 5 – 10 periods with subsequent transition to the set current from the main transformer.

It should be borne in mind that coated-electrode welding in all positions in space, except for the downhand position, is conducted practically with a kind of current modulation. It is performed at the expense of mechanical moving of the arc away from the weld by the welder. The arc becomes longer, whereas the current decreases and runs outside the molten metal pool. The latter cools down slightly and does not flow from a vertical or inclined plane of the item. In this case, part of the arc energy is practically wasted, as it is spent for heating the HAZ metal. In addition, the molten metal of the pool periodically remains unprotected, thus promoting deterioration of the weld quality. In case of welding current modulation due to thyristor control, the arc stays above the molten metal pool all the time, thus providing its protection also during the weld cooling when the welding current is reduced. Such a modulation improves the weld quality, saves the power, even though it requires the welder to have certain skills that are acquired rather quickly.

The functional capabilities of the developed thyristor-controlled transformers guarantee a high-quality manual arc welding with coated electrodes of any grades both for alternating and direct current. Such a power source provides consumable electrode welding of not only the carbon, but also some stainless steels, cast iron, as well as non-consumable electrode welding of stainless steels, aluminium and its alloys in argon.

Process testing of the developed transformer was conducted to GOST 25616–83, while arcing stability

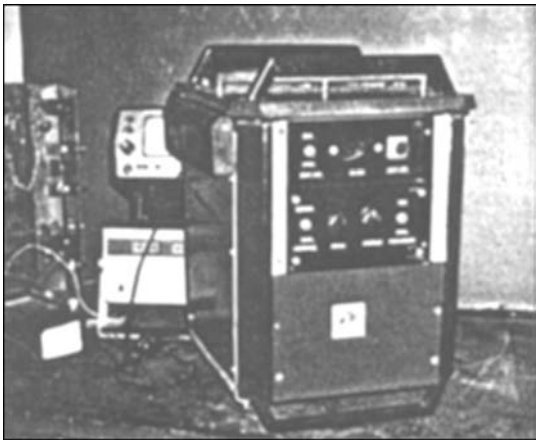

Figure 2. Mock-up of UDS-251 U2

was evaluated further by other methods. Two grades of coated electrodes were mostly used: UONI-13/45 (C — 0.06 – 0.12; Si — 0.2 – 0.3; Mn — 0.6 – 0.9; Cr — up to 0.15; Ni — up to 0.3; S — up to 0.03; P — up to 0.35 wt.%) as a typical representative of electrodes with calcium fluoride coating (for direct current) and MP-3 (C — 0.06 – 0.1; Si — up to 0.15; Mn — 0.4 – 0.6; Cr — up to 0.1; Ni — up to 0.25; S — up to 0.04; P — up to 0.04 wt.%) with a rutile coating (for alternating current), as well as others, for instance, VI-10-6 (C — 0.15 – 0.22; Si — 0.15 – 0.35; Mn — 0.4 – 0.7; Cr — 0.8 – 1.1; S — up to 0.03; P — up to 0.03; Mo — 0.15 – 0.3 wt.%), OZL-8 (C — 0.09; Si — 0.5 – 1.1; Mn — 1.0 – 2.0; Cr — 19.0 – 21.0; Ni — 7.8 – 9.8; S — up to 0.02; P — 0.03 wt.%), etc. Welding in the same modes using a batch-produced welding generator PSO-300 was performed for comparison.

It is found that the welds made with the developed thyristor transformer, practically do not differ from those made at direct current supplied by PSO-300 generator. A new transformer provides a high stability of the process of welding with electrodes both for alternating and for direct current, not being in any way inferior to the welding generator by this characteristic [7, 8].

A mock-up of one of the new transformers with thyristor control of current, namely of UDS-251 U2, is shown in Figure 2.

Specification of UDS-251 U2

Mains:	
voltage, V	380
frequency, Hz	50
Rated welding current at relative duty cycle of 20 %, A	250
Range of welding current adjustment, A	50 – 275
Total open-circuit voltage, V	70 ± 4
Open-circuit voltage of welding winding, V, not more than	50
Rated working voltage, V	30
Efficiency at rated current, %, not more than	75
Power factor	0.7
Rated power consumption, kW	14.3
Frequency of pulses stabilizing the arcing, Hz	100
Weight, kg, not more than	45
Overall dimensions, cm, not more than	45 × 35 × 47

By the results of production trials UDS-251 U2 unit can be recommended for quantity production.

REFERENCES

1. Zaruba, I.I., Dymenko, V.V. (1982) Double-control stabilizers of AC arc. *Avtomaticheskaya Svarka*, **5**, 43 – 46.
2. Zaruba, I.I., Dymenko, V.V., Bolotko, V.I. (1989) Welding transformers with arcing stabilizers. *Ibid.*, **10**, 46 – 51.
3. Pentegov, I.V., Dymenko, V.V., Sklifos, V.V. (1994) Welding power sources with a pulsed arc ignition. *Ibid.*, **7**, 36 – 39.
4. (1986) *Equipment for arc welding.* Reference book. Ed. by V.V. Smirnov. Leningrad: Energoatomizdat.
5. Zaruba, I.I., Dymenko, V.V. (1983) Influence of drop transfer of metal on stability of AC welding arc. *Avtomaticheskaya Svarka*, **12**, 14 – 20.
6. Zaruba, I.I., Dymenko, V.V., Bargamen, V.P. (1973) AC welding in CO_2. *Ibid.*, **10**, 64 – 68.
7. Zaruba, I.I., Andreev, V.V., Dymenko, V.V. (1982) Einige Wege zur Verbesserung des MAG-Schweiβprozesses. *ZIS Mitteilungen*, **6**, 592 – 601.
8. Zaruba, I.I., Andreev, V.V. (1998) Ways of improvement of thyristorized power sources. *Svarshchik*, **2**, 20 – 21.

RESIDUAL STRESSES IN EXPLOSION TREATED WELDED JOINTS

V.G. PETUSHKOV and **V.A. TITOV**
The E.O. Paton Electric Welding Institute, NASU, Kyiv, Ukraine

ABSTRACT

General principles of formation of residual stresses and strains in welded joints as a result of their local explosion treatment are considered in terms of the elasto-plastic theory. Recommendations on optimization of explosion loading parameters are given. It is shown that results of the treatment do not depend upon the presence and value of initial residual stresses in weld metal.

Key words: *explosion treatment, residual welding stresses, stress relaxation, deformation diagram, Hugoniot curve, shock wave*

Physical model of the mechanism of relieving residual stresses (RS) by local explosion treatment, suggested in [1, 2], allows a satisfactory description of the experimental data on the effect of such treatment on the load-carrying capacity of welded joints [3]. This model is based on the concept of formation of the biaxial stress-strain trace (SST) in a short range of explosion caused by relaxation of tangential stresses and selective deformation of metal behind the front of non-unidimensional shock wave flows. The quantitative estimation of values of stresses and strains in SST in a unidimensional approximation, including those induced by its so-called secondary relaxation [2], as well as shock compression pressures required for formation of an efficient SST with preset stress components is described in [2, 4, 5]. In [1, 6] the relief of RS is attributed to interaction of the fields of stresses in SST and residual stresses, leading to establishment of a new equilibrium state in a weldment as a whole.

Consider schematically the sequence of events in interaction of SST with the stressed metal of a welded joint using a combined $\sigma(\varepsilon)$ diagram [7]. It is of interest to dwell separately on a version of explosion loading which creates uniaxial strains along the y axis, which coincides with a direction of propagation of a plane shock wave, and on a practically more important version of treatment which induces non-inidimensional wave flows.

To simplify discussions, we will use a flat three-rod simulator of a welded joint, in which the central rod is loaded by initial tensile RS σ_{x1} and the end rods are loaded by balanced compressive RS σ_{x2}. The shock wave front is parallel to the plane of the central rod. Initial RS and strains in the rods are shown in Figure 1 by points A and B, and the specific potential energy of elastic strain of the system is delineated by the area of triangle OAC.

Loading of the central rod by the plane shock wave with pressure σ_y at the front ($\sigma_y > 0$ for the compressive wave), which satisfies condition $\sigma_y/\sigma_d > 1 - \nu/(1 - 2\nu)$, where σ_d is the dynamic yield stress, and ν is the Poisson's ratio, induces SST of an instantaneous intensity in it. In this case the rod transforms into a state the representative points of which are located in length AP_0 (Figure 1). It is expressed by equation $\varepsilon = \varepsilon_1 = \text{const}$, while ordinates of σ_x for points of the instantaneous states are determined by the value of pressure in a wave and by the Hugoniot curve of metal [1]. At $\sigma_x < \sigma_{y.s}$ SST relaxes at an alternating strain rate until an equilibrium or some intermediate state (e.g. corresponding to point F in Figure 1) is achieved within a time period required for propagation of the disturbance introduced into the system by formation of SST to the end rods.

Approximate estimation of the time of relaxation of the instantaneous SST to reach the equilibrium state [2] can be made, for example, on the basis of the known data on dependence of the velocity of mobile dislocations upon the applied stresses. Velocity V of the mobile dislocations in crystals of alloy Fe +

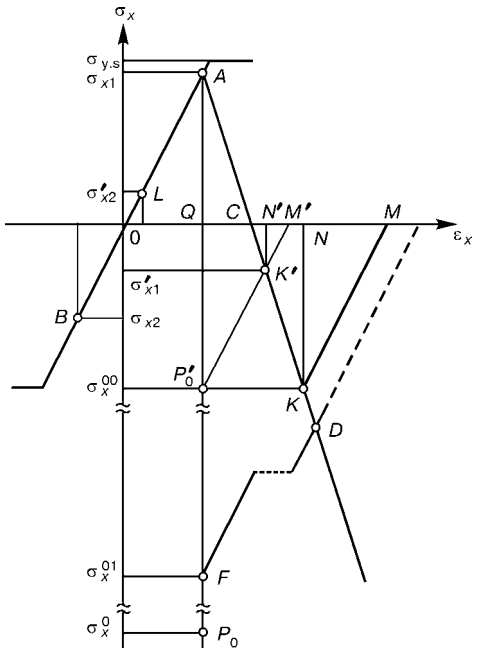

Figure 1. Interaction of SST formed under conditions of uniaxial strain at loading and unloading with the stressed metal

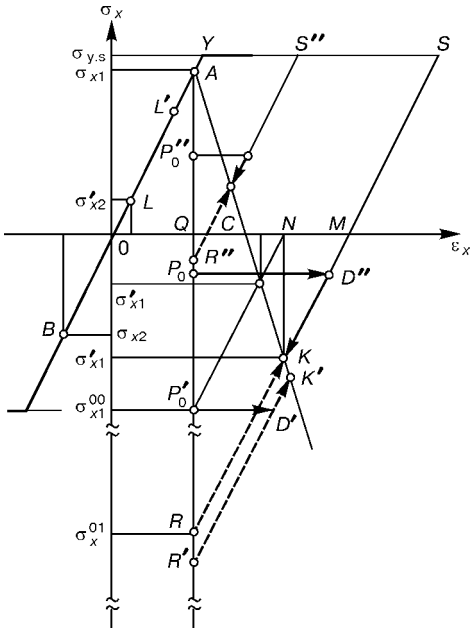

Figure 2. Interaction of the effective SST with the stressed metal (σ_x^{01} — RS in SST of the instantaneous intensity)

3.25 % Si with the *bcc* lattice at a shear stress of about 150 MPa is $4 \cdot 10^{-2}$ cm/s [8]. By setting the typical values of the Burgers vector at $b \cong 2.5 \cdot 10^{-8}$ cm and the mobile dislocation density (upper estimate) at $\rho_0 = 10^{10}$ cm^{-2}, we find that during the process of relaxation of the instantaneous SST one might expect realization of the strain rate at $\dot{\gamma} = \rho b V \cong 10$ s^{-1}, which corresponds to the dynamic viscosity coefficient equal to $\mu_\sigma \cong 10^6$ Pa·s [9]. Therefore, the characteristic time of relaxation of SST equals about $\mu_\sigma / E \approx 5$ μs. This estimation is rough, and first of all because of the absence of reliable data on density and velocity of the mobile dislocations. Supposedly, for the class of materials under consideration, at substantially high stresses $\sigma_x = \sigma_d \cong 3\sigma_{y.s}$ the characteristic time of relaxation of the instantaneous SST is shorter at least by an order of magnitude and, thus, equals fractions of a microsecond or several microseconds [10].

As interaction of SST with RS in the short and long explosion ranges of welded joints occurs at a rate equal to the velocity of elastic waves, i.e. within the microsecond time ranges, one might expect that starting from a certain time moment after formation of SST the processes of its relaxation and balancing with the RS field in a welded joint will take place simultaneously.

By conditionally separating these processes in time, one might suppose that since the moment of beginning of interaction of SST with the RS field the establishment of a new equilibrium of the system shows up as a combined deformation of the rods along straight lines *FD* and *BA* (Figure 1). In this case, if in the state of the established equilibrium $\sigma(D) >> \sigma_{y.s}$, the relaxation process continues along straight line *DA* to point *K*, where $\sigma(K) = \sigma_1$. At stresses of $\sigma_x \le \sigma_{y.s}$ in SST (e.g. point P_0' corresponding to $\sigma_x = \sigma_{y.s}$) the stage of the secondary relaxation is absent and the system is transformed into a new state of equilibrium by elastic deformation of the respective rods along lines $P_0'K'$ and *BL* to form the resulting tensile RS σ_{x2}' in the end rods and compressive RS σ_{x1}' in the central rod, the specific potential energy of the system being delineated by the area of triangle $CK'M'$.

In the actual cases of local explosion loading of welded joints, which induces non-unidimensional wave configurations in metal, a substantial contribution to the effect of redistribution of RS is made by plastic strains resulting both from relaxation of stresses in formation of SST and from peculiarities of the field of mass velocities behind the front of the non-unidimensional shock waves, where there is a possibility for a plastic flow (spread) of metal to occur in a short explosion range along and across the detonation propagation direction [6]. Therefore, the state of metal in the trace formed in this case can be represented, depending upon the instantaneous intensity of SST, completeness of its secondary relaxation and value of the formed plastic strains, by points D_i (Figure 2), abscissas of which are $\varepsilon(D_i) > \varepsilon(A) = \varepsilon_{x1}$ and ordinates depend upon the intensity and geometry of loading.

Figure 2 shows three particular cases of interaction of SST of a different intensity in the three-rod simulator of a welded joint: $\sigma_x < \sigma_{x1} < \sigma_{y.s}$ (point D''), $\sigma_x < \sigma_{y.s}$ (point D) and $\sigma_x > \sigma_{y.s}$ (point D'). For example, when the σ_x component of SST, which coincides with the direction of action of tensile RS σ_{x1}, is lower than $\sigma_{y.s}$, and plastic deformation accompanying its formation is equal to the P_0D length, the system is balanced by way of deformation of the central rod along straight line *DK* and of the end rod — along line $L'L$, so that points *K* and *L* correspond to the final stresses and strains of the rods.

Based on the use of the concept of an effective SST with a reduced effectiveness of $\sigma_x^0 = \alpha' \sigma_{y.s}$ [2, 7], where α' is the coefficient of reduction, the lines of a combined deformation of the rods in the system are *RK* and *BL*, respectively. In this case RS in the rods decrease by their absolute values and change their signs, while the potential energy of the system is proportional to triangle *CKM*. This situation can also be represented as follows: the central (tensioned) rod is instantaneously withdrawn from the system and replaced by the other one, having a larger length and in a different stressed state [1, 7]. The latter can change depending upon the specific conditions of loading of the rod. But unlike the initial rod, this rod is as a rule compressed, which, in combination with its plastic strains, is responsible for the beneficial effect of the relief of RS by explosion treatment.

Assume that in a general case $\sigma_x / \sigma_{y.s} = r' = \alpha' - 1$. Then, on the basis of analysis made in [7], we find that, for example, at $r = 1.6$, $f = 2/3$ and $k = 0.75$ (f is the ratio of areas of the zones affected by the initial compressive and tensile RS and $k = \sigma_{x1}/\sigma_{x2}$), the system as a whole will be elongated approximately

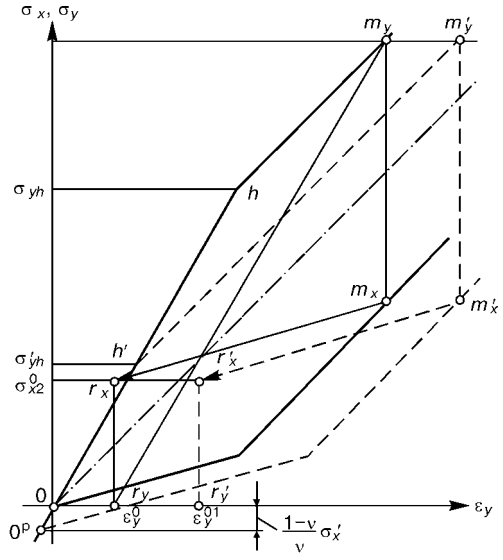

Figure 3. Hugoniot curve $\sigma - \varepsilon_y$ plotted to illustrate the effect of RS on the state of metal in the SST zone

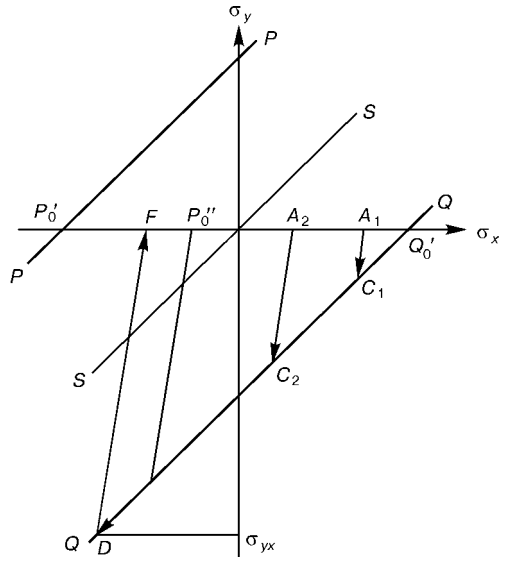

Figure 4. Lines of the representative points of the stressed state in the plane of main stresses for metal with different RS loaded by the plane shock wave

by 0.9 ($\sigma_{y.s}/E$) and the final RS in the system will change their sign. The limiting state σ'_{x1} is not always indicated. Often it may suffice to have the final values of RS to be close to zero, for which the intensity of loading should meet condition of $r' = fk$ or $\sigma_x^0 = \sigma_{x2}$ (Figure 2). It may be well to interpret the process under consideration visually and in such a way that under the effect of explosion the central rod is just deformed along the *AYS* line, acquiring plastic deformation *YS*. Further combined deformation of the rods occurs along the *YL* and *SK* lengths and leads to the same final stressed state of the system.

Consider now how the value of stresses and strains in SST is affected by the presence of the initial RS. In this case the equations describing an elastic behaviour of metal on coordinates σ_x and σ_y have the following form [1, 2]:

$$\sigma_y = \frac{1-\nu}{\nu}(\sigma_x + \sigma'_x), \quad \sigma_y = \sigma_d + \sigma_x + \sigma'_x. \qquad (1)$$

Here σ'_x is the initial longitudinal tensile RS, wherefrom it follows that at the moment of beginning of the flow:

$$\sigma_{yh}^p = \sigma_{yh} + \frac{1-\nu}{\nu}\sigma'_x, \quad \sigma_{xh}^p = \sigma_{xh} + \frac{1-\nu}{\nu}\sigma'_x, \qquad (2)$$

where σ_{xh} and σ_{yh} are the main stresses at a point corresponding to the Hugoniot yield stress at the absence of the initial stressed state and σ_{xh}^p and σ_{yh}^p are the same at the presence of the latter.

Allowing for relationships of the theory of shock waves in metals [1], the following expressions can be derived for the plasticity region:

$$\sigma_y^p = K\varepsilon_y \pm \frac{2}{3}\left(\sigma_d - 2\frac{\mu}{\lambda}\sigma'_x\right), \quad \sigma_x^p = K\varepsilon_y \mp \frac{1}{3}\left(\sigma_d - 2\frac{\mu}{\lambda}\sigma'_x\right), \qquad (3)$$

where K, μ and λ are the Lame's constants and σ_x^p and σ_y^p are the main stresses at the wave front at the presence of the initial RS in metal.

If metal with and without the initial RS is loaded to the same pressure, the strain in a direction of propagation of the wave under loading will change by a value of $\varepsilon_y^p - \varepsilon_y = -\sigma'_x/E$, as a result of which the residual uniaxial strain will be as follows:

$$\varepsilon_y^{0p} = \varepsilon_y^0 - \sigma'_x/E.$$

The relationships obtained show that at the presence of initial RS in the metal its behaviour, when loaded by a plane shock wave, can be described in the coordinate system the origin of which is translated to point 0^p (Figure 3), the coordinates of the latter being as follows $\frac{1-\nu}{\nu}\sigma'_x$, $\frac{\sigma'_x}{E}$.

Figure 3 shows the Hugoniot curve plotted for cases of $\frac{1-\nu}{\nu}\sigma'_x$ and $\sigma_x = 0$.

By using the relationships derived, it can be shown that $\sigma_x^{0p} = (\sigma_y/\sigma_{yh}) - \sigma_d = \sigma_x^0$. This allows a conclusion that the value of the intensity of SST does not depend upon the value and sign of the initial RS. The presence of the latter leads only to a change in an instantaneous residual strain (Figure 3). And if we take into consideration the existence of a stage of relaxation of SST ($\varepsilon_y^{00} \to \varepsilon_y^{00} + \varepsilon_{yh}^{00}$ [2]), we can conclude that the state of the metal in a relaxed SST does not depend upon its initial stressed state, providing that $\sigma'_x < 0$ (tensile RS) and $0 < \sigma'_x < 2\lambda/3K$ (compressive RS).

Figure 4 shows lines of loading of the metal which has different RS. It can be seen from this Figure that if the shock compression pressure σ_y is sufficient for the stressed metal to transform to the yield state, its instantaneous state will be characterized by point F, whose position does not depend upon abscissa of point A_i. This conclusion is proved by results of the experimental studies of stresses and strains in the SST zone metal [6]. Note that the correction made by the second term in formulae (3) for steel St.3 (C — 0.14 – 0.22;

Mn — 0.3 – 0.6 wt.%; Fe — balance) at σ'_x = = 300 MPa is not in excess of about 0.5 %.

REFERENCES

1. Petushkov, V.G., Fadeenko, Yu.I. (1980) Explosion treatment of welded joints. *Fizika Goreniya i Vzryva*, **5**, 64 – 68.
2. Grishaenko, A.I., Petushkov, V.G. (1996) Residual stress-strain state of metal after local explosion loading. *Avtomaticheskaya Svarka*, **9**, 9 – 14.
3. Kudinov, V.M., Petushkov, V.G. (1984) Increase of load-carrying capacity of welded metal structures by a local explosion treatment. In: *Proc. of the 8th Int. Conf. on High Energy Rate Fabrication*, San Antonio, June 17 – 21. New York: ASME.
4. Petushkov, V.G., Fadeenko, Yu.I., Kudinov, V.M. (1981) Physical mechanism of explosion treatment of welded joints. In: *Proc. of the 8th Int. Colloq. on Explosions and Reactive Systems*, Minsk, Aug. 24 – 28. Minsk: S.I.
5. Davydenko, A.V., Petushkov, V.G. (1983) Redistribution of arbitrary system of internal stresses in a normal incident shock wave. *Zhurnal Prikladnoj Mekhaniki i Tekhn. Fiziki*, **2**, 98 – 102.
6. Petushkov, V.G., Fadeenko, Yu.I., Kudinov, V.M. (1982) Relief of residual stresses in welds by explosion. In: *Proc. of 11th Conf. on Explosion Treatment of Materials*, Novosibirsk, Sept. 8 – 10. Novosibirsk: SO AN SSSR.
7. Petushkov, V.G., Pashchin, A.N. (1975) Evaluation of the efficiency of decreasing welding stresses by applying an external load. *Avtomaticheskaya Svarka*, **7**, 19 – 23.
8. Krasovsky, Ya.A. (1977) *Physical principles of strength*. Kyiv: Naukova Dumka.
9. Deribas, A.A. (1980) *Physics of explosion strengthening and welding*. Novosibirsk: Nauka.
10. Mogilevsky, M.A. (1969) *Peculiarities of the mechanism of deformation of metals under plane shock wave loading*. Synopsis of Thesis for the Cand. Sci. (Phys.-Math.) Degree. Novosibirsk.

EFFECT OF Fe–C ALLOY IN COATING OF ILMENITE ELECTRODES ON REDUCTION PROCESSES DURING WELDING

N.G. EFIMENKO and **N.A. KALIN**
Ukrainian Engineering-Pedagogical Academy, Kharkov, Ukraine

ABSTRACT

Calculation formulae are suggested and the amount of silicon, titanium and aluminium being reduced from a slag in deoxidizing of ilmenite type electrodes with Fe–C alloy is defined. It is shown that TiO_2 can serve an additional oxidizer of carbon in parallel with Fe–O. The use of alloy Fe–C in ilmenite type electrodes does not lead to a significant increase in content of silicon and aluminium in the deposited metal.

Key words: *reduction, oxidizing, oxides, carbon, ilmenite, electrodes, cast iron powder, deposited metal*

The ilmenite concentrate $FeO{\cdot}TiO_2$ is a main slag-forming component of electrode coatings of an ilmenite type, containing also alumosilicates, carbonates, ferromanganese and organic substances. When carbon in the form of Fe–C alloy is used as a deoxidizer in parallel with a ferromanganese, the reduction of iron, manganese, silicon, titanium and aluminium from their oxides, available in a slag, will be thermodynamically feasible [1, 2].

The present work is aimed at the investigation of reactions of reduction of silicon, titanium and aluminium in welding with electrodes of an ilmenite type containing Fe–C alloy in the form of a cast iron powder as a deoxidizer.

The experimental electrodes manufactured by the method of extrusion on 4 mm diameter wire Sv-08A (C — 0.1; Si — 0.03; Mn — 0.35 – 0.65 wt.%; Fe — balance) were investigated. Here, the coefficient of coating weight was 0.47. The mass content of components introduced into the coating was as follows, %: ilmenite concentrate — 45; ferromanganese — 18; cast iron powder — within 0 – 15. The multilayer surfacing for conductance of chemical analysis of the deposited metal was made at DCRP (160 – 180 A) in accordance with GOST 94–66.

Table 1. Formulae of calculation of contents of silicon, titanium and aluminium being equilibrium with carbon

Reaction of interaction	*Constant of reaction equilibrium*	*Formula of calculation of content of reduced element in deposited metal*
$(SiO_2) + 2[C] = [Si] + 2\{CO\}$	$\lg K_{Si-C} = -29024/T + 16.1$	$[Si] = K_{Si-C}\,[C]^2 = 1.176[C]^2$
$(TiO_2) + 2[C] = [Ti] + 2\{CO\}$	$\lg K_{Ti-C} = -32014/T + 15.95$	$[Ti] = K_{Ti-C}\,[C]^2 = 1.184[C]^2$
$(TiO) + [C] = [Ti] + \{CO\}$	$\lg K_{Ti-C} = -16815/T + 8.70$	$[Ti] = K_{Ti-C}\,[C] = 0.25[C]$
$1/3(Ti_2O_3) + 5/3[C] = [Ti] + 5/3\{CO\}$	$\lg K_{Ti-C} = -27587/T + 13.22$	$[Ti] = K_{Ti-C}\,[C]^{5/3} = 0.0095[C]^{5/3}$
$1/2(Ti_2O_3) + 3/2[C] = [Ti] + 3/2\{CO\}$	$\lg K_{Ti-C} = -25572/T + 12.19$	$[Ti] = K_{Ti-C}\,[C]^{3/2} = 0.0115[C]^{3/2}$
$(FeO{\cdot}TiO_2) + 3[C] = [Ti] + Fe + 3\{CO\}$	$\lg K_{Ti-C} = -35895/T + 19.43$	$[Ti] = K_{Ti-C}\,[C]^3 = 0.392[C]^3$
$1/2(Al_2O_3) + 3/2[C] = [Al] + 3/2\{CO\}$	$\lg K_{Al-C} = -30106/T + 13.46$	$[Al] = K_{Al-C}\,[C]^{3/2} = 0.00068[C]^{3/2}$

Table 2. Mass content of elements, reduced from oxides at [C] = 0.12 %, in deposited metal, %

Reduced element	SiO_2	TiO_2	TiO	Ti_3O_5	Ti_2O_3	$FeO{\cdot}TiO_2$	Al_2O_3
Si	0.02	–	–	–	–	–	–
Ti	–	$2.65{\cdot}10^{-4}$	0.03	$2.77{\cdot}10^{-4}$	$4.76{\cdot}10^{-4}$	$6.77{\cdot}10^{-4}$	–
Al	–	–	–	–	–	–	$2.81{\cdot}10^{-5}$

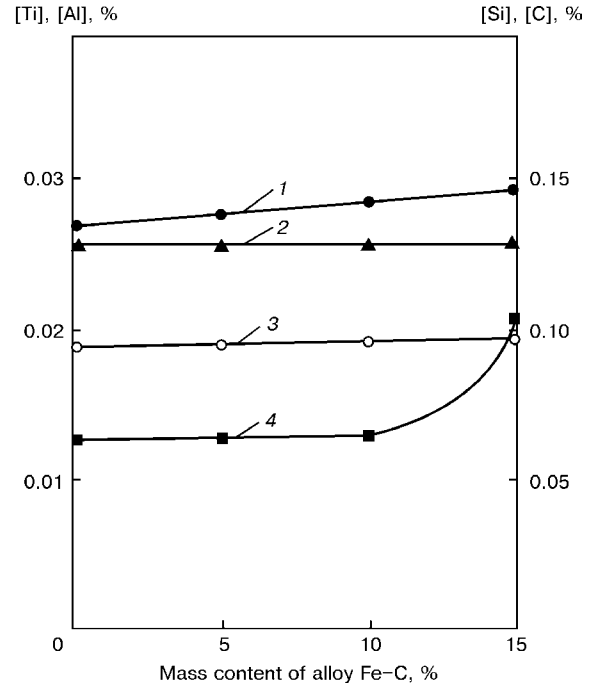

Relationship between the content of titanium (*1*), aluminium (*2*), silicon (*3*) and carbon (*4*) in the deposited metal and the amount of alloy Fe–C in coating of electrodes

It is shown in [2] that silicon, titanium and aluminium are reduced from oxides in contact with a molten alloy Fe–C according to the following reaction:

$$(MeO) + [C] = [Me] + \{CO\}.$$

Titanium forms a series of oxides (TiO, Ti_2O_3, Ti_3O_5, TiO_2), which form in turn ilmenite $FeO{\cdot}TiO_2$ with iron oxides [3]. It is known [4] that TiO_2 in welding arc can dissociate to TiO and Ti_2O_3 as most stable at high temperatures.

The formulae of calculation of contents of reduced elements being equilibrium with carbon depending on the temperature were deduced on the basis of thermodynamic calculations of reactions of reduction of oxides of silicon, titanium and aluminium dissolved in alloy Fe–C with carbon (Table 1).

Taking into account that the mass content of carbon [C] in the deposited metal should not exceed 0.12 % the calculation of content of reduced elements was made (Table 2). Here, the data of [2, 3, 5] were used. The temperature of weld metal solidification was taken equal to 1810 K.

As is seen from Table 2, the reduction of titanium from TiO forming in dissociation of TiO_2 in welding arc, will be most probable. The probability of reduction of titanium from other oxides and ilmenite is too low. The reduction of silicon from SiO_2 provides a small growth in content of [Si] that cannot influence greatly the change of mechanical properties of the deposited metal and its susceptibility to the pore formation. The reduction of aluminium is also negligible and do not influence significantly on the welding-technological properties of electrodes. The reduction of titanium to 0.03 % in the deposited metal influences favourably on the refining of structure of the latter and increase of its mechanical properties.

To check the calculation method, the chemical analysis of metal produced by surfacing with experimental electrodes was made. Its results are given in Figure. It was established in this case that the reduction of silicon and aluminium with carbon within the given range of [C] content is not occurred in principle, unlike the observed reduction of titanium which coincides very closely with calculated data.

Thus, when the alloy Fe–C is used in electrodes of an ilmenite type as a deoxidizer in amounts which provide the mass content of [C] of not more than 0.12 % there is no hazard of the silicon-reduction process, deteriorating the welding-technological properties of the ilmenite type electrodes. The reduction of aluminium is also negligible and can be not taken into account. The titanium reduction is possible mainly by reaction of reduction TiO formed as a result of dissociation of TiO_2 from the ilmenite. Thus, TiO_2 can serve an additional oxidizer of carbon in parallel with FeO that is necessary to take into account during development of the ilmenite type electrodes which are deoxidized with alloy Fe–C.

CONCLUSIONS

1. Calculation formulae are obtained for determination of amount of reduced silicon, titanium and aluminium depending on the content of carbon in the deposited metal.

2. It is established that in electrodes of ilmenite type the TiO_2 can serve an additional oxidizer of carbon in parallel with FeO.

3. The use of alloy Fe–C as a deoxidizer at the condition of providing the mass content of [C] of not more than 0.12 % does not lead to the increase in content of silicon and aluminium above the admissible level.

4. The validity of the calculation method was proved experimentally and the data about the amounts of reduced elements in welding with experimental electrodes were obtained.

REFERENCES

1. Efimenko, N.G., Kalin, N.A. (1978) Oxidizing ability of rare-earth elements as compared with known deoxidizers. *Svarochnoye Proizvodstvo*, **10**, 1 – 2.
2. Efimenko, N.G., Kalin, N.A. (2000) Thermodynamic analysis of redox processes with carbon participation during fusion welding. *Avtomaticheskaya Svarka*, **7**, 18 – 21.
3. Kulikov, I.S. (1975) *Deoxidizing of metals*. Moscow: Metallurgia.
4. Potapov, N.N., Volobuev, Yu.S. (1981) Peculiarities of oxidizing of metal with titanium dioxide in submerged-arc welding and surfacing. *Avtomaticheskaya Svarka*, **2**, 22 – 26.
5. Medzhibozhsky, M.Ya. (1986) *Fundamentals of thermodynamics and kinetics of steelmaking processes*. Kyiv-Donetsk: Vysshaya Shkola.